Chemical Controls on the Biotic and Abiotic Release of Chromium and Vanadium

By

Fatai O. Balogun

A dissertation accepted and approved in partial fulfillment of the

requirements for the degree of

Doctor of Philosophy

in Earth Sciences

Dissertation Committee:

Dr. James Watkins, Chair

Dr. Matthew Polizzotto, Advisor

Dr. Qusheng Jin, Core Member

Dr. Owen Duckworth, Core Member

Dr. Lucas Silva, Institutional Representative

University of Oregon

Fall 2023

DISSERTATION ABSTRACT

Fatai Balogun

Doctor of Philosophy in Earth Sciences

Title: Chemical Controls on the Biotic and Abiotic Release of Chromium and Vanadium

Contamination of ground and well water by Cr and V from anthropogenic and geogenic sources has gained considerable attention over the last few decades due to environmental and public health concerns. The specific threat of Cr and V contamination is dictated by their redox speciation. In the natural environment, redox active phases such as ubiquitous Iron and manganese (oxyhydr)oxides are known to modulate mechanisms responsible for the mobility and bioavailability of Cr and V. Also, Cr and V availability is dependent on the reactivity of natural organic matter, which may serve as a major reductant of oxidized species, sorbent, and facilitator of mineral dissolution. Despite this knowledge, the specific constraints on the mechanisms of Cr and V oxidation, release, and retention by different organic carbon types, Fe and, Mn(oxyhydr)oxides in model and natural systems are not well understood.

Accordingly, the objectives of this work were to (1) gain a more detailed mechanistic understanding of how organic carbon proxies and Mn-oxide influence Cr oxidation and release; (2) determine the host phases for Cr and V in aquifer materials and quantify their adsorption capacities; (3) determine the impact of organic matter and Mn-oxide proxies on the biotic and abiotic release of Cr and V in aquifer materials. Our experiments showed that aliphatic citric acid produced 8.5 times less Cr(VI) than aromatic gallic acid. In chemically variable saprolites, the affinity for V was 8 – 11 times greater than for Cr. Amorphous phases were inferred to be the major host phases for Cr and V. Lastly, organic carbon abiotically release Cr and V from solid host phases, while Mn-oxide influenced the release of Cr and V only in Redlair saprolite. This work underscores the need to integrate organic carbon types and mineralogical controls into predictive models for redox sensitive metal dynamics and environmental availability.

This dissertation includes previously published and unpublished coauthored material.

NAME OF AUTHOR: Fatai Balogun

GRADUATE AND UNDERGRADUATE SCHOOLS ATTENDED:

University of Oregon, Eugene
Georgia State University, Atlanta, GA.
Obafemi Awolowo University, Ile-Ife, Nigeria.

DEGREES AWARDED:

Doctor of Philosophy, Earth Sciences, 2023, University of Oregon Eugene, OR
Master of Science, Geosciences, 2017, Georgia State University, Atlanta, GA
Bachelor of Science, Geology, 2012, Obafemi Awolowo University, Ile-Ife, Nigeria

AREAS OF SPECIAL INTEREST:

Environmental Geochemistry

Natural and Occupational Radiation Detection

Materials Characterization

PROFESSIONAL EXPERIENCE:

Graduate Teaching and Research Fellow, University of Oregon, 2018 – present
Soil and Water Laboratory

Environmental Intern, Georgia Environmental Protection Division, Land Protection
Branch, June – August 2018

Graduate Teaching and Research Assistant, Georgia State University, 2015 – 2017
Hominin Sites and Paleolakes Drilling Research Laboratory

GRANTS, AWARDS, AND HONORS:

Grants in Aid of Research, Sigma XI The scientific Research Honor Society, 2022

BAYER Encompass Scholar, Soil Science Society of America, 2021

Graduate Student Research Grant, Geological Society of America, 2021 & 2022

Margaret Thayer Graduate Student Research Grant, University of Oregon, 2021 & 2022

Third place for Soil Chemistry student oral presentation award, Soil Science Society of America, 2020.

Student Travel Grant, American Geophysical Union, 2020

Emeritus Tribute Faculty Award, University of Oregon, 2020

First place for Soil Chemistry student poster presentation award, Soil Science Society of America, 2019

Weiser Scholarship for Outstanding Scholastic achievements, University of Oregon, 2019

Promising Scholar Award, University of Oregon, 2018.

Outstanding graduate research award; Environmental and Engineering Geology Division of the Geological Society of America, 2017.

PUBLICATIONS:

Balogun, F. O., Aiken, M., Namayndeh, A., Duckworth, O. W., & Polizzotto, M.L. (2023). Dissolved organic carbon diminishes managanese oxide-driven oxidation of chromium. *Chemosphere*. https://doi.org/10.1016/j.chemosphere.2023.140424.

Peel, H. R., **Balogun, F. O.**, Bowers, C. A., Miller, C. T., Obeidy, C. S., Polizzotto, M. L., Tashnia, S. U., Vinson, D. S., & Duckworth, O. W. (2022). Towards Understanding Factors Affecting Arsenic, Chromium, and Vanadium Mobility in the Subsurface. *Water (Switzerland)*, *14*(22), 1–27. https://doi.org/10.3390/w14223687

Tubosun I., Tchokossa, P., **Balogun, F.O.,** Okunlola, G.A., Owoade, L.A., & Adesanmi, C. A. (2014). Measurement of Radiation Exposure Due to Natural Radionuclides in Gemstone Mining Area in Olode, Ibadan South Western Nigeria. *British Journal of Applied Science & Technology*, *4*(18), 2620–2630. https://doi.org/10.9734/bjast/2014/8619

ACKNOWLEDGMENTS

Looking back at the last decade since I finished my bachelor's degree, I can hardly recognize myself due to the tremendous opportunity I have been given to grow both as a human being and as a scientist. I have been fortunate and blessed to meet and work with incredible people over the last few years, many of which contributed to the success of this work.

I'm grateful for Dr. Matthew Polizzotto's kindness, guidance, and support and for believing in my ability to successfully complete this work. His ability to motivate and mentor in moments of overwhelming self-doubt is unparalleled. I thank Matt for his patience and investment in my development as a human and a scientist. The training and unconditional support I received under his tutelage is a model worth emulating.

It would be remise not to thank my M.S. degree mentor Dr. Nadine Kabengi who recognized my potential, cultivated discipline in me and fostered my interest in soil chemistry. Her guidance and support over my two and a half years stint a Georgia State University opened my eyes to the world of possibilities the field of soil chemistry has to offer.

I strongly believe much of this project would not have been possible with the help of my "winter soldiers" Chelsea Obeidy and Markus "buddy boo baby boy" Koeneke. They are some of the kindest and most helpful people I have worked with. Their passion, curiosity, and sustained love for science kept me going on the darkest day. In addition, I would also like to thank our present and past lab members – August Harrell, Sarah Webber, Dr. Fusheng Sun, Gabbie Lafayette, Jason John, Katie Fisher, and Charlotte Klein for their help over the last half a decade.

I would like to thank all the members of my dissertation committee (Drs. Jim Watkins, Qusheng Jin, and Lucas Silva) who were always available at the shortest notice to assist with various aspects of my work. Dr. Owen Duckworth was crucial in the successful completion of this work. I appreciate his humor, and all the time and effort he invested into my work and training.

A healthy work-life balance and environment makes a lot of difference in successfully completing any task in any work of life. I appreciate friends and colleagues

who supported me in various aspects of my personal life and work (Drs. Doyin Adeyilola,, Lottie Ling, Adrian Broz, Kellum Tate-Jones, Miranda Aiken, Macon Abernathy, Alireza Namayandeh, Alandra Lopez, and Seun Fadugba, Hannah Peel, Helena Machado, Gordon Bowman, Gbenga Okunlola, and everyone in my cohort). I would also like to say a big thank you to Dr. Chris Russo and Jesse Muratli of the Keck laboratory at Oregon State University (OSU) as well as Ryan Davis and Erik Nelson at Stanford Synchrotron Radiation Lightsource (SSRL) for their kindness and help with elemental analysis over the years.

My Fiancée Adeola Afolabi has been immense in her support over the course of my research work. Through thick and thin she has always been my source of inspiration and support; much of my mental well-being which has allowed me to complete this dissertation was because of her unwavering support and prayers.

DEDICATION

This work is dedicated to my parents, Prof., and Mrs. F.A. Balogun

TABLE OF CONTENTS

LIST OF FIGURES

15

LIST OF TABLES

CHAPTER I
INTRODUCTION

In recent decades, growing concerns have emerged regarding the environmental and human health risks posed by natural occurrences of toxic metal(loids). One of the most significant issues is the widespread exposure to inorganic arsenic (As), with over 150 million people worldwide estimated to be exposed to levels greater than the 10 µg/L maximum contaminant level (MCL) set by United states Environmental Protection Agency (USEPA). This constitutes the largest mass poisoning event in history.(Ravenscroft et al., 2009) In addition to As, other associated metal(loids) such as chromium (Cr), vanadium (V), Antimony (Sb), manganese, and (Mn) have gained prominence in recent times due to their public health implications.(Coyte & Vengosh, 2020; Gillispie et al., 2019; Gillispie et al., 2016; Vengosh et al., 2016)

In the United States, at least 7 million people across 31 cities may be exposed to the threat of hexavalent chromium in their drinking water.(Sutton, 2010) Very limited information exists on the prevalence of V in drinking water. However, due to the emergence of high concentrations of V in well water from the North Carolina Piedmont, the North Carolina Department of Health, and Human Services (NCDHHS) have set an advisory level of 0.3 µg/L for V. Cr and V are particularly of concern due to their similar redox profiles, indicating a common release mechanism into groundwater.

The primary route of exposure to these contaminants is usually through drinking water, and release into the environment could either be from human-made (anthropogenic) or natural (geogenic) sources. The most common anthropogenic sources are from industrial applications such as energy and steel production, leather tanneries, fossil fuel production, etc. Chromium and vanadium are one of the most prevalent contaminants in coal fly ash from power generating stations.(Zeneli et al., 2022) The presence of arsenic in superfund sites may complicate site remediation and create challenges for the utilization of groundwater in areas with naturally high concentrations of other contaminants.(Frohne et al., 2015; Gillispie, et al., 2016) For example, due to the complex redox chemistry of As, efforts to sequester it from the aqueous phase may

concomitantly release chromium and vanadium at sites where these contaminants co-occur due to their similar redox chemistry.

In addition to the co-occurrence of Cr and V with other metal(loids), several cofounding factors such as the Iron (Fe) and Mn(oxyhydr)oxides, microorganisms, and organic matter may antagonistically influence the release and retention in the natural environment. Several studies have attempted to unravel the complexities involved in the fate and transport of Cr and V in model, controlled systems(Abernathy et al., 2022; Hausladen & Fendorf, 2017; McClain et al., 2017; Pan et al., 2019; Vessey & Lindsay, 2020), however, these systems do not entirely replicate the natural environments complexity due to the multitude of interacting variables. Our current understanding is that Mn-oxide are capable of participating in redox reactions, releasing Cr and V, however, reactions involving organic carbon could modify these dynamics.

Therefore, there is a critical need to understand how these variables conspire to release Cr and V in both model and natural multicomponent systems. The mechanistic knowledge acquired from such studies will enable us to identify and predict conditions that cause mobilization of Cr and V from near surface geologic materials into deep groundwater aquifer, thus compromising the groundwater and threatening human health. In addition, these studies could help to improve management and remediation strategies of complex legacy waste sites with harmful levels of other redox sensitive elements, while also providing valuable data for developing mechanistic models.

This research is divided into two main parts. The first part focuses on the influence of organic matter and Mn-oxide proxies on Cr release in a model Cr-Mn oxide-organic acid multicomponent system. The second part focuses on the interplay of Fe, and Mn(oxyhydr)oxides, and organic acids in the release and retention of Cr and V in the natural environment, or more specifically, the chemically variable geogenic materials from the geologically diverse North Carolina (NC) piedmont. These efforts contribute to our understanding of contaminant cycling and can help guide land management strategies in natural Cr and V "hotspots," which are common in metasedimentary and metavolcanic tectonic settings.

Dissertation Research

The specific objectives of my research are to: (1) gain a more detailed mechanistic understanding of how ubiquitous inputs such organic carbon proxies and Mn-oxide influence Cr oxidation and release; (2) determine the host phases for Cr and V in naturally distinct geologic materials weathered from different tectonic settings, and quantify their adsorption capacities; (3) determine the impact of organic matter and Mn-oxide proxies on the biotic and abiotic release of Cr and V in near surface natural geologic materials - a process that has largely been reported to be biotically-mediated.

To achieve these objectives, I first synthesized chromium hydroxide, a Cr-bearing mineral with limited solubility for use in batch experiments and added it to the Mn-oxide while varying the concentrations of low molecular weight organic acids (LMWOAs), citric and gallic acid. This allowed for the direct quantification of impact of organic carbon types on Mn-oxide induced Cr(VI) generation. I also extended the findings of this model system to natural materials by collecting saprolite materials from two geologically distinct saprolites in the North Carolina Piedmont. Throughout the experiments, I gathered aqueous Cr, V, Mn, Fe, and As elemental concentration data from batch isotherm, kinetic, aerobic and anaerobic experiments, in conjunction with solid phase speciation data from synchrotron-based X-ray adsorption spectroscopy (XAS). The data collected allowed for the determination of possible mechanisms controlling the fate and transport of Cr and V in multicomponent model and natural systems. The objectives, findings, and significance of each project in this dissertation are described below.

The goal of Chapter (II) is to show that the interactions of Cr-bearing minerals with Mn oxide in the presence of natural organic matter proxies could influence the Cr(VI) generation differently. Here, the mechanism of Cr(III) oxidation by mixed valence Mn oxide in the presence of citric and gallic acids, two natural organic matter (NOM) constituents commonly found in the soil environment was evaluated. We hypothesized that aromatic organic acid would limit Mn-oxide driven oxidation of Cr. Batch incubation experiments showed that each organic acid enhanced solubilization of Cr(III) and Mn over controls without organic addition but increasing organic acid concentration decreased production of Cr(VI), with approximately 8.5 times less Cr(VI)

produced in the citric acid than gallic acid experiments. Geochemical modeling revealed that in the citric acid experiments, unprotonated Cr(III)-citrate was the dominant organo-metallic complex in solution, while $(CrOH)^{2+}$ distribution positively correlated with concentrations of Cr(VI) produced. X-ray absorption spectroscopy showed that negligible Cr(VI) was present in solid-phase reaction products, regardless of treatment. This study achieved our goal of understanding the oxidation mechanism in this complex multivariable system by showing that organic carbon functional groups especially those with multiple carboxyl groups rather than aromatics as earlier hypothesized, are effective in limiting Mn-oxide-driven oxidation of Cr(III) to Cr(VI). Collectively, these results illustrate how NOM can abiotically modify expected chemical pathways driving Cr cycling, and such mechanistic information should be better integrated into models predicting Cr redox dynamics and availability in the environment. Chapter (II) is titled "Dissolved organic carbon diminishes manganese oxide-driven oxidation of chromium" and published in Elsevier journal *Chemosphere*. It is coauthored by Miranda Aiken, Alireza Namayandeh, Owen Duckworth, and Matthew Polizzotto.

Chapter (III) is about a set of laboratory and spectroscopic studies designed to characterize two mineralogically and geologically distinct saprolites from Union and Gaston counties (Redlair Observatory), NC with natural abundances of Cr, V, Mn, and Fe. The goal of this study was to understand how differences in saprolite chemical compositions influence the release and retention of Cr and V. Our specific objectives were to quantify the saprolites adsorption capacities, determine contaminant host phases, and kinetics of Cr and V adsorption. We hypothesized that higher amorphous Fe phases would increase sorption capacities and act as host phases for Cr and V. A major finding of this study was that although our saprolites have capacities to adsorb both Cr and V, adsorption capacities of both saprolites for V was ~10 time greater than for Cr. Our observations from XAS data also showed a significant proportion of added Cr(VI) was immobilized as $Cr(OH)_3$ precipitates, while V was associated with clay mineral and Fe(oxyhydr)oxide surfaces; with Fe(III)-humic substances complex also playing an important role in V retention . Data from our Fe (X-ray Absorption Near Edge Spectroscopy) XANES showed small amounts of Fe(II) which may have served as reductant for the added Cr. Evidence from citrate bicarbonate dithionite (CBD)

extractions inferred that although the bulk of the native Cr (15 – 40%) and V (42 – 53%) in both saprolites appears to be structurally incorporated in the crystal latices of Fe-bearing minerals. The fate and transport of Cr and V is ultimately controlled by structural incorporation and adsorption on to amorphous phases. Chromium- and V-loaded samples highlighted that amorphous phases and ionically bound species were the dominant phase controlling Cr and V transport, especially in Union County saprolite. The importance of amorphous phases was also gleaned from our kinetic experiments where the rates of adsorption of Cr and V onto Union County saprolites was ~ 2 and 2.4 times respectively greater than for Redlair observatory samples. Chemical extractions showed the ratio of amorphous Fe in Union County and Redlair saprolites is 4:1 thus partially supporting our hypothesis. Additionally, data from micro-X-ray fluorescence (μ-XRF) analysis showed good associations between Fe, Cr and V with correlation coefficients ranging from 0.61 – 0.94 for both saprolites. These findings achieved our objectives of understanding how differences in mineralogy of geologic materials dictate the transformations, release, and retention of Cr and V in the natural environment.

After constraining the factors responsible for the release and retention of Cr and V, the last chapter of this dissertation (Chapter IV) focuses on the impact of proxies of natural chemical inputs i.e., LMWOA (citric acid) and Mn-oxide (birnessite) on mobilizing Cr and V in our saprolites. Since we established amorphous Fe oxide, clay, and to a lesser extent, crystalline Fe-bearing minerals play key roles in contaminant transport, we hypothesized that influx of labile organic carbon and preexisting natural or anthropogenic Mn-oxide may influence their capabilities to mobilize Cr and V under environmentally relevant conditions. Therefore, a major goal of this chapter was to quantify the biotic and abiotic release of Cr and V due to organic carbon and Mn-oxide inputs in order to predict the potential for Cr and V release from near surface geologic media. We hypothesized that introduction of LMWOA or Mn oxides to aquifer materials would enhance Cr and V release from natural aquifer materials by enhancing microbial stimulation, promoting abiotic dissolution of Cr and V host phases, or poising redox conditions at states conducive to Cr and V mobilization. We determined that irrespective of the original composition of the primary rock material, Cr and V may have similar release profiles, hence may occur in groundwater. A major finding from this study was

that co-cycling of Cr, V and, Fe was mostly abiotically driven by organic carbon induced dissolution reactions. Another finding was that surprisingly Mn-oxide did not release Cr and V in the Union County saprolites, but up to 0.2 mg/kg (~18 ppb Cr), presumably Cr(VI), was released in the Redlair saprolite. Although there is little support for our hypothesis on microbially and Mn-oxide driven release of Cr and V, these results achieved our final objective by corroborating the result of our model experiments showing that the cycling of Cr and V in natural samples may also be abiotically induced by organic carbon and Mn-oxide.

REFERENCES

Abernathy, M. J., Schaefer, M. V., Ramirez, R., Garniwan, A., Lee, I., Zaera, F., Polizzotto, M. L., & Ying, S. C. (2022). Vanadate Retention by Iron and Manganese Oxides. *ACS Earth and Space Chemistry*, *6*(8), 2041–2052. https://doi.org/10.1021/acsearthspacechem.2c00116

Coyte, R. M., & Vengosh, A. (2020). Factors Controlling the Risks of Co-occurrence of the Redox-Sensitive Elements of Arsenic, Chromium, Vanadium, and Uranium in Groundwater from the Eastern United States. *Environmental Science and Technology*, *54*(7), 4367–4375. https://doi.org/10.1021/acs.est.9b06471

Frohne, T., Diaz-Bone, R. A., Du Laing, G., & Rinklebe, J. (2015). Impact of systematic change of redox potential on the leaching of Ba, Cr, Sr, and V from a riverine soil into water. *Journal of Soils and Sediments*, *15*(3), 623–633. https://doi.org/10.1007/s11368-014-1036-8

Gillispie, E. C., Andujar, E., & Polizzotto, M. L. (2016). Chemical controls on abiotic and biotic release of geogenic arsenic from Pleistocene aquifer sediments to groundwater. *Environmental Science: Processes and Impacts*, *18*(8), 1090–1103. https://doi.org/10.1039/c6em00359a

Gillispie, E. C., Austin, R. E., Rivera, N. A., Bolich, R., Duckworth, O. W., Bradley, P., Amoozegar, A., Hesterberg, D., & Polizzotto, M. L. (2016). Soil Weathering as an Engine for Manganese Contamination of Well Water. *Environmental Science and Technology*, *50*(18), 9963–9971. https://doi.org/10.1021/acs.est.6b01686

Gillispie, E. C., Taylor, S. E., Qafoku, N. P., & Hochella, M. F. (2019). Impact of iron and manganese nano-metal-oxides on contaminant interaction and fortification potential in

agricultural systems-a review. *Environmental Chemistry*, *16*(6), 377–390. https://doi.org/10.1071/EN19063

Hausladen, D. M., & Fendorf, S. (2017). Hexavalent chromium generation within naturally structured soils and sediments. *Environmental Science and Technology*, *51*(4), 2058–2067. https://doi.org/10.1021/acs.est.6b04039

L. Zeneli, M. Daci-Ajvazi, A. Sekovanic, J. Jurasovic, D. B. (2022). The Effects of Chromium and Vanadium on Biomarkers of Carbohydrate and Lipid Metabolism in Workers Exposed to Coal Fly Ash. *Xenobiotics*, *12*, 307–316.

McClain, C. N., Fendorf, S., Webb, S. M., & Maher, K. (2017). Quantifying Cr(VI) Production and Export from Serpentine Soil of the California Coast Range. *Environmental Science and Technology*, *51*(1), 141–149. https://doi.org/10.1021/acs.est.6b03484

Pan, C., Liu, H., Catalano, J. G., Wang, Z., Qian, A., & Giammar, D. E. (2019). Understanding the Roles of Dissolution and Diffusion in Cr(OH) 3 Oxidation by Î-MnO 2. *ACS Earth and Space Chemistry*, *3*(3), 357–365. https://doi.org/10.1021/acsearthspacechem.8b00129

Ravenscroft, P., Brammer, H., & Richards, K. (2009). Arsenic Pollution. In *Arsenic Pollution*. Wiley.

Sutton, R. (2010). Chromium-6 in U.S. Tap Water. *Enviroenmental Working Group*, *4*, 68–70.

Vengosh, A., Coyte, R., Karr, J., Harkness, J. S., Kondash, A. J., Ruhl, L. S., Merola, R. B., & Dywer, G. S. (2016). Origin of Hexavalent Chromium in Drinking Water Wells from the Piedmont Aquifers of North Carolina. *Environmental Science and Technology Letters*, *3*(12), 409–414. https://doi.org/10.1021/acs.estlett.6b00342

Vessey, C. J., & Lindsay, M. B. J. (2020). Aqueous Vanadate Removal by Iron(II)-Bearing Phases under Anoxic Conditions. *Environmental Science and Technology*, *54*(7), 4006–4015. https://doi.org/10.1021/acs.est.9b06250

CHAPTER II.

DISSOLVED ORGANIC CARBON DIMINISHES MANGANESE OXIDE-DRIVEN OXIDATION OF CHROMIUM

1. **INTRODUCTION**

Chromium (Cr) is a global threat to drinking-water quality, and in the United States alone, over 74 million people drink toxic-Cr-laden water (Sutton, 2010). Anthropogenic activities such as legacy mining, leather tanning and agricultural activities are commonly responsible for elevated concentrations of Cr in the environment (Duckworth et al., 2014; Whitaker et al., 2018). However, weathering of Cr-rich ultramafic rocks may also lead to Cr contamination of soil and groundwater (D. M. Hausladen & Fendorf, 2017). Understanding the processes controlling Cr toxicity and mobility in the environment is crucial for assessing potential Cr sources and reaction pathways that threaten human and environmental health.

The specific risks of Cr contamination are dependent on Cr's oxidation state, which influences its toxicity and mobility in natural waters (Landrot et al., 2012). Chromium(III) is relatively non-toxic and immobile, whereas Cr(VI) is mobile and a known carcinogen (Jardine et al., 1999). In geologic materials, Cr(III) is usually present as $FeCr_2O_4$, Cr_2O_3, and $Cr(OH)_3$ (Apte et al., 2006; Chrysochoou et al., 2016; Oze et al., 2007), but manganese oxides, which are strong and ubiquitous oxidants in near-surface systems, can oxidize Cr from Cr(III) to Cr(VI) (Fendorf, 1995; Landrot et al., 2012; Oze et al., 2007; Pan et al., 2019). Redox reactions involving Cr are influenced by a host of competing processes involving Fe-oxide phases, metal reducing bacteria, and natural organic matter (NOM) (McClain et al., 2017), (N. Chen et al., 2013). In particular, the NOM in soils can serve as an easily accessible electron donor for biotically mediated reduction of Fe(III) to Fe(II) and concomitant reduction of Cr(VI) by some Fe reducing bacteria (Ginder-Vogel et al., 2005; D. Hausladen et al., 2019; D. M. Hausladen & Fendorf, 2017). In environmental systems, organic matter has also been reported to engage in ligand-promoted dissolution of solid phases, releasing Cr (Saad, Wang, et al., 2017; Schenkeveld & Kraemer, 2018), although the extent of Cr oxidation by Mn oxides within these systems has remained

elusive (D. M. Hausladen & Fendorf, 2017). Chromium(VI) reduction has been observed in the presence of bulk natural organic matter (N. Chen et al., 2013; Gu & Chen, 2003; Hori et al., 2015), but in general, mechanistic controls on Cr redox dynamics in complex Cr-Mn-NOM systems are poorly constrained. Quantifying interactions involving these environmental components is essential for predicting the fate and transport of Cr within the subsurface.

Our present study aims to provide insights into the interactions of Cr-bearing minerals with Mn oxide and NOM proxies. The research objectives were to (1) elucidate mechanisms of Cr oxidation in the presence of manganese oxides and organic carbon (OC); and (2) identify final Mn- and Cr-bearing reaction products. We specifically investigated the impacts of citric (CA) and gallic (GA) acids, two low molecular weight organic acids (LMWOAs), which are abundant in the environment and have respective carboxyl and phenolic moieties that are good proxies for reactive NOM functional groups (Caregnato et al., 2008; Giannakopoulos et al., 2005), on Cr redox dynamics in the presence of Mn-oxides. Overall, our findings reveal that CA and GA enhance the solubility of $Cr(OH)_3$ and Mn-oxides but diminish the production of Cr(VI). This work underscores the need for developing more robust multicomponent frameworks for predicting oxidation and mobility of Cr in natural environmental systems.

2. MATERIALS AND METHODS

2.1. Materials

Solutions for all experiments were prepared using >18.2 MΩ cm double deionized (DDI) water. All reagents were high purity and provided by Fisher Scientific. Manganese oxides (73.1% Mn_2O_3 and 26.9% MnO_2-Pyrolusite) was purchased from US Research Nanomaterials, Inc. Citric and gallic acids are low molecular weight organic acids (LMWOA) that are analogues of natural organic matter, and they were chosen for this study based on differences in their chemical structures and chelating abilities.

2.2. Mineral Synthesis and Characterization

Chromium hydroxide [$Cr(III)(OH)_3$] was used as an environmentally representative Cr-bearing mineral, due to its reactivity and limited solubility (Apte et al., 2006). The compound was synthesized according to Duckworth et al. (Duckworth et al., 2014). Twenty-four grams of $Cr(H_2O)_6Cl_3$ were dissolved in 1 L of > 18.2 MΩ cm DDI water and stirred with a magnetic stir

bar to produce a dark green solution in a 2 L Erlenmeyer flask. One-hundred-forty mL of 2 N NH_3OH was added to the solution to produce a light blue gelatinous precipitate. After 3 hours, the supernatant was decanted from the suspension, and 50-mL aliquots were centrifuged at 4200 rpm for 10 minutes and washed three times with DDI water. The precipitate was air dried and stored in the freezer.

Manganese oxide and chromium hydroxide were characterized by X-ray diffraction (XRD) and scanning electron microscopy (SEM). X-ray diffraction patterns were collected using a Rigaku benchtop X-ray diffractometer with a diffracted beam monochromator for Cu Kα radiation. The patterns for $Cr(OH)_3$ and Mn oxide were collected by scanning from 3˚ to 90˚ and 5 to 80˚ 2θ, respectively (Figs. S1A and S1B). The characteristic reflection peaks (d-value) were matched with the International Center for Diffraction Data (ICDD) database and respective crystalline phases were identified. The morphology of the $Cr(OH)_3$ and MnO_2 samples was further confirmed through SEM microscopy using a Hitachi TM3000 desktop microscope (Figs. S1C and S1D).

2.3.   Batch Experiments

Two-week mixed batch experiments were conducted at pH 5 in 5 mM NaCl, with the background electrolyte chosen because Na^+ and Cl^- do not interfere with the chemistry of Cr(III) oxidation (Pan et al., 2019). Equal mass (0.05 g) of $Cr(OH)_3$ and MnO_2 (1.18 molar ratio of Cr:Mn) and 200 mL of either citric or gallic acid with four concentrations ranging from 0.5 – 10 mM were added to twelve 250 mL plastic amber colored batch reactors. Five mM NaCl prepared in DDI water was used as 0 mM treatment for OC-free controls. Also, control experiments to test the influence of each component in the reaction were set up in 250 mL bottles under similar conditions with or without 5 mM citric or gallic acid. Solution pH was adjusted to 5 ± 0.1 throughout the experiments and before each sampling time by the addition of HCl or NaOH; this pH was chosen as representative of the lower limit of pH of natural waters at which $Cr(OH)_3$ dissolution could occur. The set up was covered with aluminum foil to control the influence of photooxidation. For the primary citric and gallic acid experiments, samples were taken at 8, 24, 48, 96, 168, and 336 hours after the experiment onset, and a separate pilot experiment for Cr(VI) determination in GA was sampled at 2, 4, 6, 8, 24 and 48 hours. Samples were filtered with 0.22 µm polyethersulfone (PES) syringe filters and analyzed for total Cr ($[Cr]_T$), dissolved Cr(VI),

total Mn ($[Mn]_T$), and OC concentration. All experiments except the GA pilot experiment were done in triplicate.

2.4. Aqueous-Phase Analysis

Total dissolved Cr and Mn were measured by Inductively Coupled Plasma-Optical Emission spectroscopy (ICP-OES; Spectros Arcos II) at the Oregon State University **Keck Collaboratory for Plasma Spectrometry**. The instrument detection limit for both Cr and Mn was 0.75 µg/L. Dissolved Cr(VI) was quantified using the diphenyl carbazide (DPC) method modified after EPA 218.6 rev 3.3 section 7.8 (Zaffiro et al., 2011) or ion chromatography-inductively coupled plasma-mass spectrometry (IC-ICP-MS). For the colorimetric method, after color development due to the reaction of diphenyl carbazide with Cr(VI), the concentration of dissolved Cr(VI) was determined spectrophotometrically using a Shimadzu 1280 UV-VIS spectrophotometer. The detection limit for this method was 0.043 µM (5 µg/L).

The DPC method was unsuccessful in quantifying Cr(VI) in gallic acid treatments due to chemical interference from the reaction between GA and $Cr(OH)_3$. Therefore, we employed the use of (IC-ICP-MS) according to EPA Method 218.7 (Zaffiro et al., 2011) to quantify Cr(VI) in the GA experiments. Treatments from GA concentrations 0.5 and 1 mM yielded reproducible Cr(VI) data, At 5 mM GA, Cr(VI) concentrations drifted slightly upon dilution, but Cr(VI) concentrations were consistently low and reproducible. The detection limit for this method was 0.01 µg/L. Dissolved organic carbon in aqueous-phase samples was measured with an On-line TOC-V CSH total organic carbon analyzer. The detection limit for the equipment was 10 µg C/L.

2.5. Solid-Phase Analysis

To determine the speciation and proportions of Cr in the final reaction products, Cr K-edge X-ray absorption near-edge structure (XANES) spectra were collected at beamline 4-3 at the Stanford Synchrotron Radiation Lightsource (SSRL). Reaction products were diluted with BN_3, loaded onto acrylic sample holders, and sealed with Kapton tape (with the non-adhesive part of the Kapton in contact with sample). All Cr spectra were collected at room temperature. Chromium fluorescence spectra were collected using a vortex detector, equipped with soller slits

and a V filter. A double-crystal Si(111) LN-cooled monochromator was used for energy selection. Chromium K-edge XANES spectra were collected from 5758 to 6244 eV for CA incubations and 5800 to 6186 eV for GA incubations. Three spectra were collected for each sample to assess the effect of beam damage, which was not evident in the scans. The spectra were averaged to improve signal-to-noise ratio, calibrated, baseline corrected and normalized according to the approaches described by Kelly et al. (Kelly et al., 2015) using the IFEFFIT program in the ATHENA software (Ravel & Newville, 2005). Estimates of the percentage of Cr in the sample were made using linear combination-least square fitting (LC-LSF). This procedure was done using two model compounds, $Cr(OH)_3$ and $K_2Cr_2O_4$, in order to determine proportions of Cr(III) and Cr(VI) in the reaction products. Chromium spectra were fit from 5987-6012 eV.

3. RESULTS

3.1. Influence of Citric Acid on Metal Solubilization

Citric acid had a marked impact on chromium solubilization within our mixed-system experiments, with increasing CA concentration leading to increasing release of Cr to solution (Fig. 1A). Systems without CA had final dissolved Cr concentrations of 103 μM, representing ~4% of the total Cr initially added to the system as $Cr(OH)_3$. In contrast, treatments of 10 mM CA led to dissolved Cr concentrations of 865 μM, ~38% of the total Cr in the system. Similar dissolved Cr concentrations were recorded for the Mn-free control with 5 mM CA (Fig. 2A). Across all treatments, Cr solubilization proceeded rapidly during the first 8 hours of the incubation, when 44 – 77% of the total Cr release to solution occurred. Chromium release slowed from 8-48 hours, after which release remained relatively modest for the remainder of the experiments.

Contrarily, above a threshold of 0.5 mM, CA had a negative effect on Cr(VI) production in our mixed-system experiments, with increasing CA concentrations leading to a decrease in dissolved Cr(VI) concentrations (Fig. 1B). Experiments without CA had final dissolved Cr(VI) concentrations of 0.8 μM, corresponding to ~1% of dissolved Cr released in the system. Treatment of 0.5 mM CA produced the highest dissolved Cr(VI) concentration of 11.6 μM, ~0.5% of dissolved Cr in the system. All other CA treatments led to dissolved Cr(VI) <<0.5% of total dissolved Cr. In control experiments without $Cr(OH)_3$, Cr(VI) was below the detection

limit. Across all treatments, 85 – 100% of aqueous Cr(VI) produced in the system occurred during the first 8 hours of the incubations; subsequently, chromium oxidation progressed slowly from 8 – 48 hours, after which Cr(VI) production ceased. The unusually high Cr(VI) concentration observed after 336 hours of incubation in the 5 mM CA treatment is attributed as an outlier sample, with a large span of measured Cr(VI) concentrations in experimental replicates.

The release of Mn from Mn-oxide was also dependent on CA concentration. Increasing CA concentration led to a corresponding increase in Mn concentration in solution (Fig. 1C). Incubations without CA solubilized ~2.8% of the total Mn initially added into the batch system as MnO_2. At the highest CA loading, ~100% of the Mn introduced into the system was solubilized. This was in concert with Mn concentrations released in the Cr-free control experiments with 5 mM CA (Fig. 2B). Solubilization was initially fast across all treatment levels, with 45-79% of Mn release occurring within the first 8 hours and concentrations remaining steady after 48 hours.

Control experiments highlighted the importance of CA in metal solubilization, with CA enhancing Cr release to solution, even in Mn-free experiments (Fig. 2A). Manganese-and-OC-free, OC-free, and manganese-free controls released ~3, 4 and 39% of initial Cr added to the system, respectively. Manganese was not detected in the Mn-free and Mn- and OC-free controls. Similarly, Cr-and OC-free controls, OC-free, and Cr-free controls showed that CA had a profound impact on Mn solubilization (Fig. 2B). The presence of CA increased Mn solubilization while its absence limited Mn release to solution. In total, the Cr-and-OC-free, OC-free, and Cr-free controls released ~2, 3 and 100 % of the initial Mn added in solution. In all controls, the majority of Mn release occurred during the initial 8 hours of the reaction. Chromium was not detected in the Cr-free and Cr-and OC-free sets of controls.

Across all citric acid experiments, OC concentrations somewhat declined over time, by ~12% in the 0.5 and 1 mM CA treatments, by ~33% in the 5 mM CA treatment and by ~20% in the 10 mM CA treatment after 336 h of incubation (Figs. S2A and S3). Though not tested, declining OC concentrations could be attributed to CA sorption to mineral surfaces and/or mineralization of CA with concomitant reduction of Mn(IV) or Cr(VI).
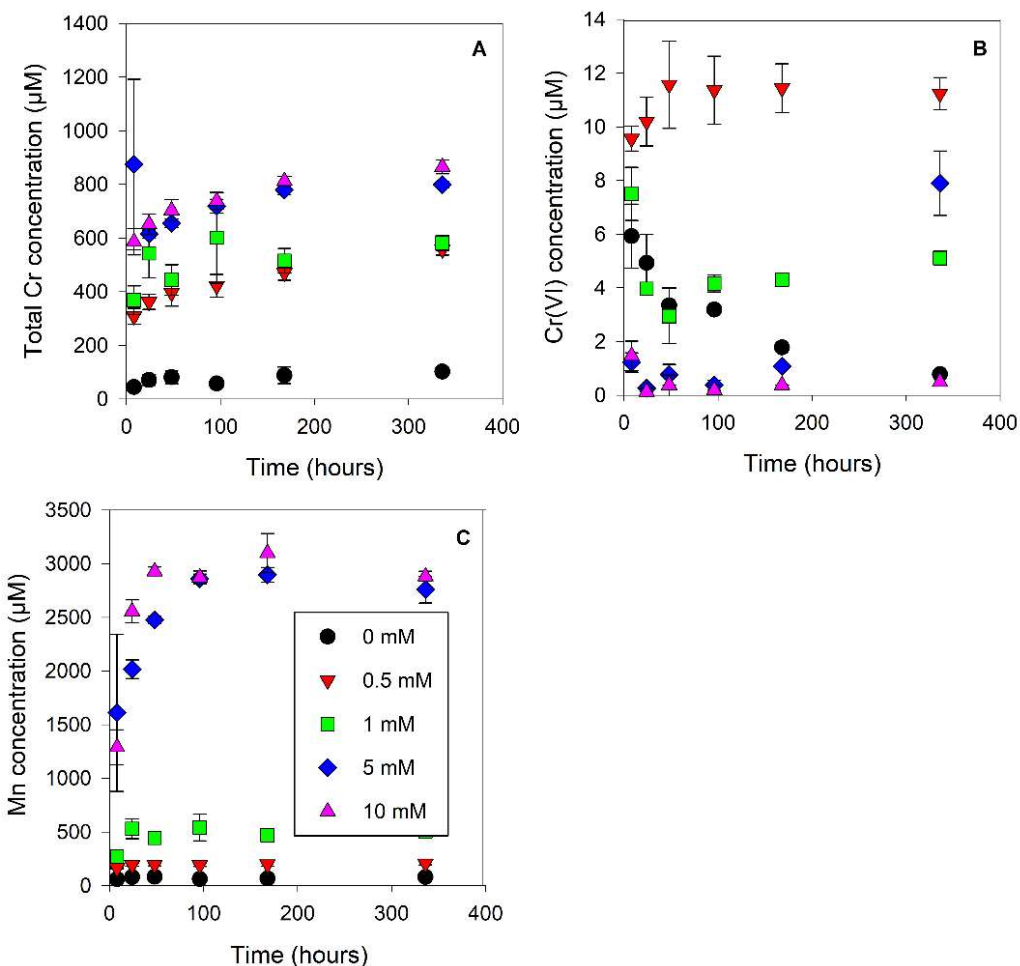
Figure 1. Dissolved concentrations of A) total Cr, B) Cr(VI) and C) total Mn over time, following incubation with varying citric acid concentrations (0 – 10 mM). Error bars represent standard error of replicates.
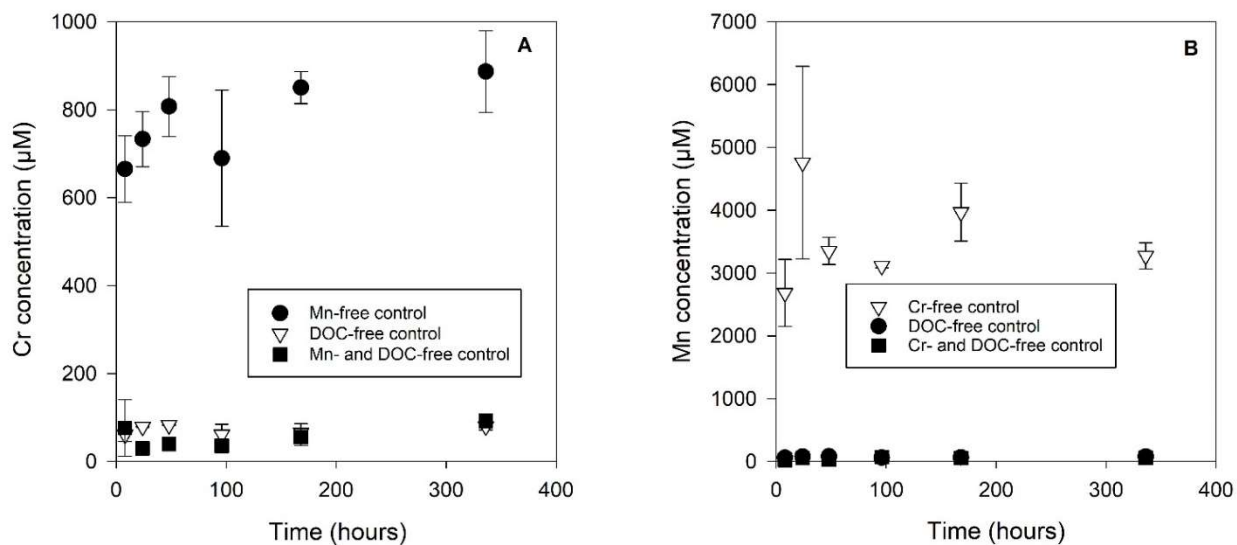
Figure 2. Dissolved concentrations of A) total Cr and B) total Mn in citric acid control experiments. 5 mM citric acid was used in Mn-free and Cr-free control experiments. Error bars represent standard error of replicates.

3.2.   Redox Dynamics with Citric Acid Additions

Citric acid had a profound effect on Cr(VI) production in our batch system, with increasing CA concentration leading to an exponential decrease in the dissolved Cr(VI):$[Cr]_T$ molar ratio (Fig. 3A) with time. Molar ratios in the OC-free treatments were highest, with a Cr(VI):$[Cr]_T$ ratio of ~0.13 recorded after 8 hours. Across other treatments, molar ratios decreased rapidly, and the lowest stoichiometric values were recorded during the final stages of the incubation period for the 10 mM CA treatments, when Cr(VI):$[Cr]_T$ was <<0.01.

Stoichiometric ratios of Cr(VI) and dissolved Mn in the batch system also generally decreased with increasing time and CA concentrations (Fig. 3B). The highest Cr(VI):$[Mn]_T$ molar ratio for OC-free incubation was ~0.10. Molar ratios decreased exponentially across CA concentration gradient, with the Cr(VI):$[Mn]_T$ ratio varying from <0.01 to ~0.06. The highest and lowest molar ratios were recorded at the initial and final stages of all CA incubations, respectively.
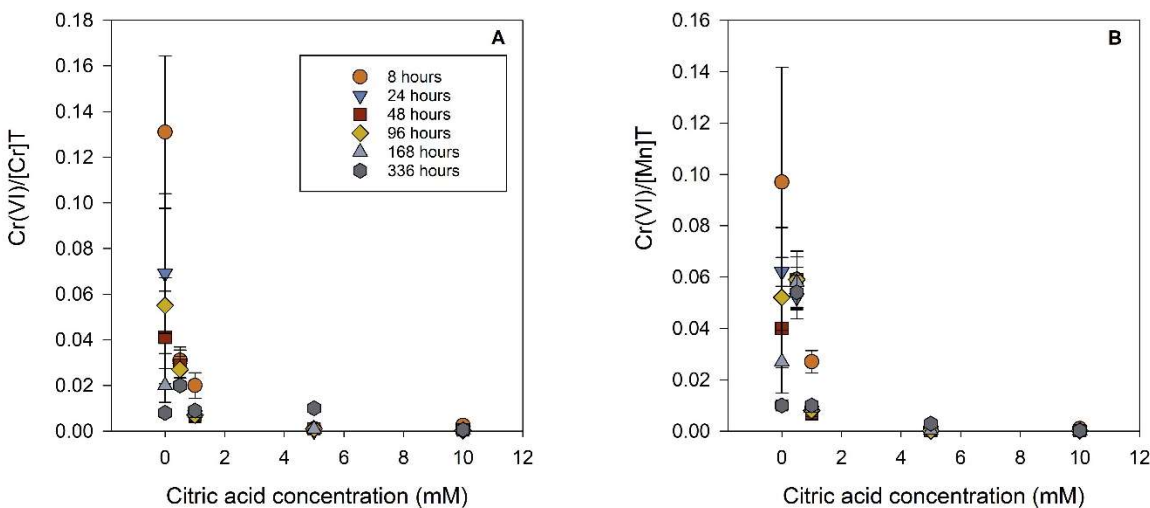
Figure 3. A) Molar ratio of dissolved Cr(VI) and total Cr produced from different initial citric acid concentrations for 8 – 336 h time points in mixed batch experiments. B) Molar ratio of dissolved Cr(VI) and total Mn produced from different initial citric acid concentrations for 8 – 336 h time points in mixed batch experiments. Error bars represent standard error of replicates.

Chromium K-edge XANES spectra and fits of final CA reaction products did not show any relationship between CA concentration and solid-phase Cr oxidation state (Fig. S4A). Fits with pure mineral standards revealed that at least 97% of the solid-phase Cr at the end of the reaction was Cr(III) (Table S1). All Cr K-edge XANES spectra exhibited a broad white line. The pre-edge region of the Cr XANES spectra showed two inconspicuous peaks with similar relative intensities; the first peak was at 5990 eV, and the second occurred at 5993 eV in all samples. Although weak, the peak at 5993 eV was attributed to the 1s to 3d-4p hybrid orbital transformation indicative of electron excitation and oxidation of Cr(III) to Cr(VI) (Fandeur et al., 2009).

3.3.   Influence of Gallic Acid on Total Cr, Cr(VI) and Mn

Batch incubations conducted with gallic acid showed it influenced metal solubilization, with increasing GA concentration promoting the release of Cr in our ternary system (Fig. 4A). Gallic acid-free experiments solubilized ~2% of the initial Cr added to the system, roughly equivalent to the independent OC-free control tested for the separate CA experiment. In contrast to the CA treatment, 10 mM GA treatments solubilized less Cr, with ~24% of initial Cr added as $Cr(OH)_3$ being released. The Mn-free controls released ~25% of dissolved Cr, which was lower than Cr mobilized in the comparable CA experiments (Fig 5A). Across all GA treatments, 22 – 70% of total Cr released into solution occurred in the first 8 hours. Chromium release continued steadily in higher GA concentration experiments, whereas Cr concentrations reached maximum by 100 hours in the lower GA incubations.

Similar to CA treatments, increasing GA concentrations (0.5 – 5 mM) in our incubations had an adverse effect on Cr(VI) generation (Fig. 4B). From 8 – 48 hours, GA-free experiments produced similar concentrations of Cr(VI) as in the CA-free treatments. In our series of treatments, incubations with 0.5 mM GA produced the highest dissolved Cr(VI) concentration of 97 μM. This value is ~4% of the initial Cr added as $Cr(OH)_3$ in the system and roughly 8.5 times the Cr(VI) produced in 0.5 mM CA treatments. Across other GA treatments, the highest dissolved Cr(VI) produced was 0.17 – 3.9% of Cr added in the system. These values are 4-9 times the Cr(VI) produced in the comparable CA treatments.

Gallic acid had a positive effect on Mn solubilization in our system, with increasing GA leading to a corresponding increase in released Mn (Fig. 4C). Gallic-acid-free treatments

solubilized ~2% of Mn added as Mn-oxide, a comparable value to the CA-free treatments. Final dissolved Mn released in Cr-free control experiments was ~95% (Fig. 5B). Across GA treatments, Mn solubilization proceeded rapidly, especially at high GA concentrations. After 8 hours, ~27 – 99% of Mn added as Mn-oxide was solubilized, indicating faster Mn release than observed in the CA treatments. In contrast to the CA treatments, GA incubations released Mn instantaneously from Mn-oxide.

Dissolved organic carbon concentrations remained steady over time in all GA experiments (Figs. S2B and S5).
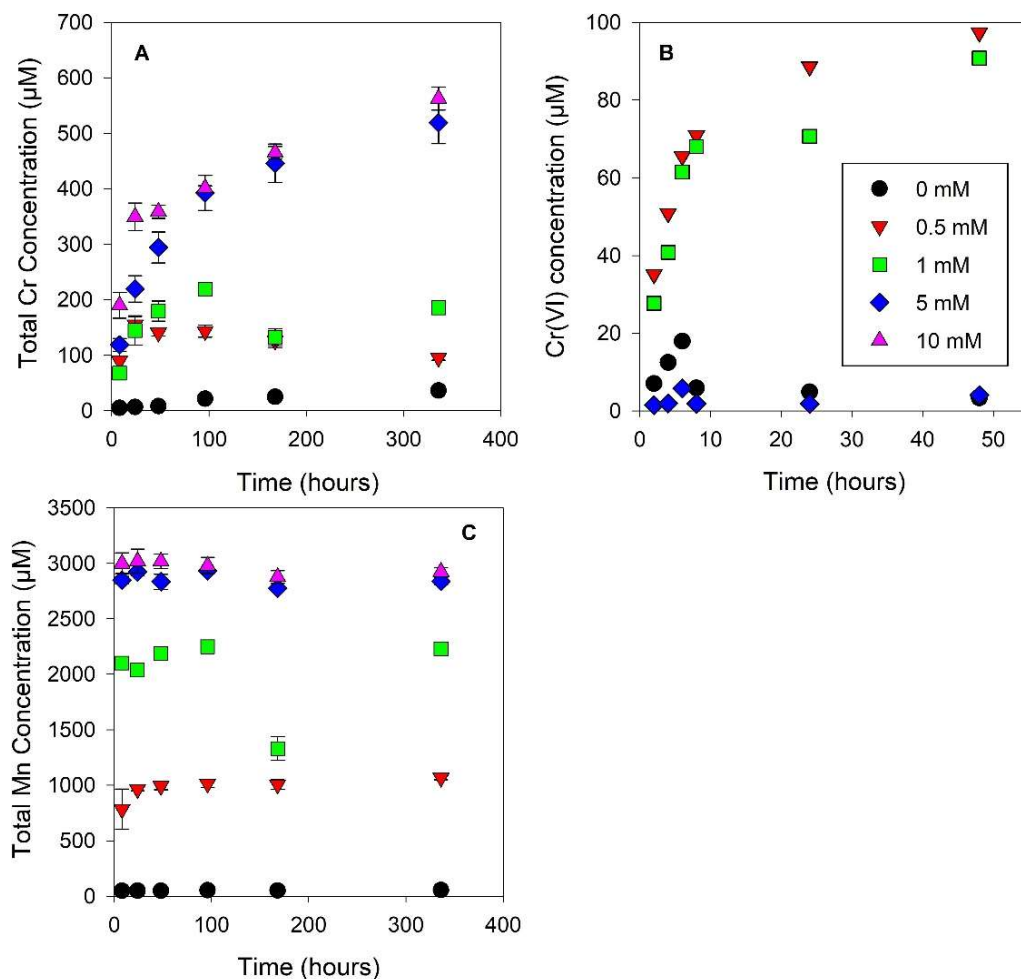
Figure 4. Dissolved concentrations of A) total Cr, B) Cr(VI) and C) total Mn over time, following incubation with up to 10 mM gallic acid. Note that in B), only 48 hours of data were collected and gallic acid concentrations were 0 – 5 mM (see Methods); chemical interferences hindered Cr(VI) quantification in 10 mM GA treatments. Error bars represent standard error of replicates.
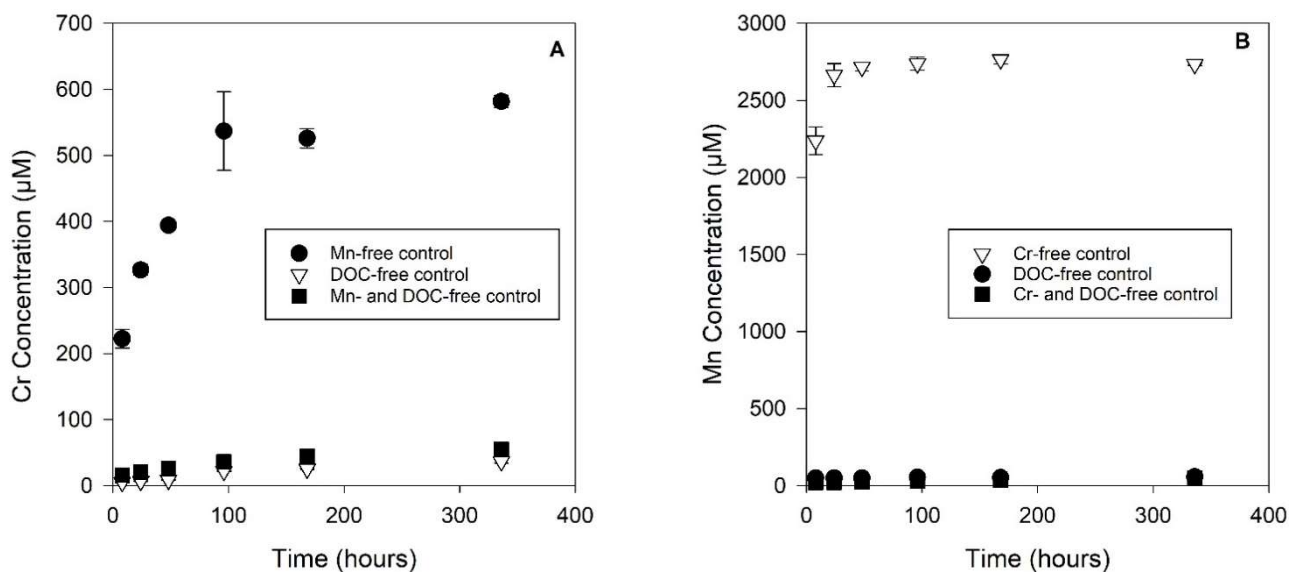
Figure 5. Dissolved concentrations of A) total Cr and B) total Mn in gallic acid control experiments. 5 mM gallic acid was used in Mn-free and Cr-free control experiments. Error bars represent standard error of replicates.

3.4.   Redox Dynamics with Gallic Acid Additions

Gallic acid had a significant effect on the relationships between dissolved Cr(VI), dissolved Cr and Mn concentrations (Fig S6). Across GA treatments, Cr(VI):$[Cr]_T$ ratios were high during the first 8 hours, with 0.5 mM treatments having a molar ratio ~25 times than what was observed in the CA treatments (Fig. S6A). Ratios of Cr(VI):$[Cr]_T$ decreased substantially in other treatments, with molar ratios being the lowest in the 5 mM GA treatments at the 48-hour time point.

Gallic acid also influenced ratios of dissolved Cr(VI) and dissolved Mn, and ratios decreased with increasing GA concentrations (Fig. S6B). Across treatments, molar ratios of Cr(VI):$[Mn]_T$ were highest with 0.5 mM GA. Similar to the CA treatments, the Cr(VI):$[Mn]_T$ molar ratios decreased with increasing GA concentration, but overall, ratios were slightly higher in the GA treatments than in the CA treatments.

Chromium K-edge XANES spectra and fits of GA solid-phase incubation products did not show a direct impact of GA on Cr(III) oxidation (Fig. S4B). Fitting experimental data with pure Cr mineral standards revealed that at least 98.8% of the solid-phase Cr in the final reaction product was Cr(III) (Table S2). The Cr pre-edge did not indicate the presence of appreciable Cr(VI) in the samples.

4. DISCUSSION

4.1.   Dissolution of Cr(OH)$_3$ and MnO$_2$ in the Presence of Citric and Gallic Acids

Prior studies have shown the importance of Mn-oxides in solubilizing and oxidizing Cr within the subsurface (K. Chen et al., 2021; D. Hausladen et al., 2019; Oze et al., 2007; Tang et al., 2014); here our data reveal that OC greatly modifies the extent of those processes. Citric acid is an organic carbon compound of environmental importance, and it represents hydroxyl and carboxyl moieties of humic substances, which are ubiquitous in natural systems. Citric acid is an α-hydroxy acid with 1 hydroxyl group and 3 carboxyl groups, which makes it suitable to engage in mineral ligand-promoted dissolution (Kabir-ud-Din et al., 2000). Our work shows that dissolution of Cr(OH)$_3$ is CA-concentration dependent at pH 5. These findings are consistent with observations of ligand-promoted dissolution increasing the availability of Cr, either as Cr(III) and/or soluble Cr(III)-citrate, in solution (Carbonaro et al., 2008), (Liu et al., 2018; Palmer & Wittbrodt, 1991). Our results also show that CA participates in the dissolution of Mn-oxide, increasing the availability of Mn in solution (Jiang et al., 2019).

Ligand-promoted dissolution of Cr(OH)$_3$ and Mn-oxide was also observed with GA. Gallic acid is a (3,4,5)-trihydroxybenzoic acid, with three hydroxyl groups and an aromatic phenolic functional group that can be easily oxidized to quinones, hydrogen peroxide and semiquinones (Eslami et al., 2010), (Z. F. Chen et al., 2015). Our results indicate that although GA participates in ligand-promoted dissolution of Cr and Mn, the extent is slightly different than for CA. Since CA has more carboxyl groups than GA, this could be responsible for the increased Cr solubilization rates observed in CA treatments (Jiang et al., 2019). The fast dissolution rate of Mn in GA treatments may be attributed to the ability of GA to form less stable Mn complexes that dissociate in solution.

4.2   Chromium (VI) Production in the Presence of Citric and Gallic Acid

Although CA and GA enhance Cr and Mn dissolution, oxidation of Cr(III) to Cr(VI) is limited by these organic acids. The chemistry of the organic ligands dictates their coordination ability with different dissolved and surface-bound transition elements. The ability of carboxylic acids to form stable organo-metallic complexes increases with number of binding sites (Smith & Martell, 1987). Citric acid has three carboxyl groups which can from strong and stable 5-

membered-chelate ring complexes with metals (Lee et al., 2007), (Jiang et al., 2019). On the other hand, GA has one carboxyl and three hydroxyl functional groups which can be oxidized to a quinone in redox reactions (Elovitz & Fish, 1995), (Nakayasu et al., 1999). The higher number of carboxyl groups in CA makes it a better chelator in comparison to GA.

Prior studies have shown that LMWOA such as CA and GA participate in ligand complexation and chelation of Cr(III), thereby inhibiting Cr oxidation (Jon Petter Gustafsson et al., 2014; Saad, Sun, et al., 2017; Sun et al., 2019). This has also been shown to be organic-acid-concentration dependent (Jean-Soro et al., 2012). Results from our batch incubation studies demonstrate that the chelating strength of CA and GA to Cr limit the oxidative abilities of Mn-oxide on Cr. For each OC type, metal-ligand complexation and chelation increased with increasing OC concentration, hence the decrease in Cr(VI) production.

To better understand these relationships, we modeled Cr(III), Mn(II) and citrate reactions using Visual MINTEQ (J P Gustafsson, 2011). Limited stability data are available for Cr(III)-ligand complexes (Saad, Sun, et al., 2017), but the stability constant of the unprotonated Cr(III)-citrate complex was previously modeled to be approximately 8.18(Gabriel et al., 2007). Using this value, our modeling results show that the unprotonated Cr(III)-citrate complex (CrL, with L = $C_6H_5O_7^{3-}$) was the dominant Cr-bearing species and the most stable complex under our experimental conditions, representing ~60% of the aqueous Cr where CA was added (Fig. S7A). The deprotonated species CrL was followed in abundance by other Cr-citrate complexes, such as $CrLH^+$, $CrLH_{-1}$, CrL_2H_{-1} and $CrLH_{-2}$, underscoring the importance of metal-ligand complexation protecting Cr(III) and thereby limiting Cr oxidation. For any initial citrate concentration, simulations using experimental data showed that the production of Cr(VI) was directly related to the proportion of $CrOH^{2+}$ in solution (Fig. S7B), suggesting that oxidized Cr is related to the Cr not complexed with citrate in solution. Under acidic conditions, other hydroxyl species of dissolved Cr(III) such as $Cr_2(OH)_4^+$ and $Cr_3(OH)_6^+$ have been reported to be abundant in soil solution (Choppala et al., 2018; Kotasâ & Stasicka, 2000). Therefore, these additional species could have played a minor role in contributing to Cr oxidation in our model system.

Existing stability constant data for gallic-acid-Cr(III) complexes are sparse, but in general, the stability of transition metals with the GA ligand varies as a function of ionic size and the hydrolysis constants of the coordinating cation (Fazary et al., 2011). Transition metals with smaller ionic sizes form more stable complexes according to the Irving Williams order (Hussain

et al., 2012). Although both CA and GA are strong chelating agents, given that the ionic radius of Cr(III) is about 0.615 Å and the gallic acid ligand is more prone to oxidation, GA-Cr(III) complexes are expected to be less stable than Cr(III)-CA complexes. Therefore, more Cr(III) was likely available for oxidation to Cr(VI) in the GA treatments than in the CA treatments.

4.3.   Mechanisms of Cr Redox Dynamics in Cr-Mn Oxide-OC Multicomponent System

Our aqueous-phase data show that metal dissolution and redox reactions in the presence of CA and GA are influenced by OC chemistry and concentration. As shown in Figures 1 and 4, $[Cr]_T$ and $[Mn]_T$ solubilized from CA and GA experiments increased with increasing organic carbon concentration, underscoring the importance of OC in ligand-promoted dissolution. However, there was a concomitant decrease in Cr(VI) production, indicating not all Cr(III) in solution was available for oxidation. This suggests an array of solution-based and surface processes, including redox reactions, chelation of solubilized Cr and Mn, and passivation of Cr(OH)$_3$ and/or Mn-oxide surfaces (Fendorf et al, 1992; Fendorf, 1995; Fischel et al., 2015; Pan et al., 2019; Varadharajan et al., 2017).

Chromium oxidation occurs through the dissolution of Cr(OH)$_3$ and diffusion of Cr(III) to Mn-oxide surfaces, but organic carbon impacts these processes. Data from CA incubation modeling showed that across all OC treatments, the formation of Cr(III)-ligand complexes suppressed the amount of CrOH^{2+} available for oxidation (Fig. S7). Similarly, the reaction between Mn-oxide and CA generates Mn(II)-citrate complexes, which could engage in redox reactions with Cr(VI) (Kabir-ud-Din et al., 2000). At higher CA concentration, Mn (presumably Mn(II)) available to complex with citrate increases substantially (Fig. S8), thereby providing more Mn(II)-citrate for Cr(VI) reduction, observations consistent with the findings of prior studies (Dai et al., 2009; Kwak et al., 2018; LI et al., 2007)(Sarkar et al., 2013). It is also likely that at higher OC concentration, Mn-oxide and CA reacted preferentially, depleting Mn-oxide and reducing the rate of Cr oxidation (Dai et al., 2009; Yang et al., 2014).

Based on the collective observations from experimental data and modeling of aqueous and solid-phase analyses, we can propose a mechanism of Cr oxidation in our system. We suggest a reaction scheme where OC initiates Cr(OH)$_3$ and Mn-oxide dissolution, releasing Cr(III) and Mn in solution. As the reaction progresses, OC forms organometallic complexes with at least 50% of Cr(III) and Mn(II), chelating and protecting it against oxidation (Fig. S7 and S8).

During the initial stages of the reaction, especially at low OC concentration, rapid oxidation of unchelated Cr(III) species takes place on Mn-oxide surfaces, afterwards, Cr(VI) was released into solution; the absence of significant Cr(VI) in our Cr K-edge XANES LCFs of final reaction products (Fig. S4) suggests Cr(VI) was released into solution after oxidation of Cr(III) on Mn-oxide surface. With increasing aqueous Cr(III) as incubation time and OC concentration increases, there may be formation of $Cr(OH)_3 \cdot nH_2O$ precipitate leading to passivation on Mn-oxide surface, shutting off Cr oxidation; however, from our data, it is difficult to establish the contribution of these phenomena to the proposed mechanism of Cr(VI) production.

4.4. Limitations and Opportunities for Future Work

Our data demonstrate how the specific interplay among aqueous and solid-phase chemical constituents in soils govern Cr(VI) production and mobilization. Although we specifically investigated the impacts of DOC form and concentration on these processes, changes to other chemical species and minerals from those in our system could further influence the potential for Cr cycling. For instance, studies have shown that δ-MnO_2 may have differing reactivity and crystallinities in comparison to mixed valence Mn-oxides used in this study; natural systems comprise numerous types of Mn-oxides, each with different solubilities and reactivities, and the specific mineralogy for a given location would have profound effects on contaminant transport. Moreover, our data show rapid reduction of Mn-oxide and gradual solubilization of Cr by organic carbon in control experiments, which suggests that with the solid-phases investigated our Mn oxides had higher solubilities and reactivities over the initial Cr solids, and that may also have influenced the observed reactions presented here. Finally, our study only addresses reactions at pH 5 due to the limited solubility of $Cr(OH)_3$ at higher pH values, but the pH of natural waters typically varies from 5-9. Further studies are needed to quantify how multicomponent-system reactions may proceed under other environmentally relevant conditions.

In the light of these limitations, future work is also needed to unravel kinetics of reactions and elucidate interactions between δ-MnO_2 and $Cr(OH)_3$ at different organic carbon concentrations over shorter temporal scales. The present study underscores the need for applying advanced characterization techniques – such as scanning electron microscopy (SEM), Fourier transform infrared spectroscopy (FTIR), quick XAS (Q-XAS), and nuclear magnetic resonance

(NMR) – to reveal short-time morphological and chemical property changes in solid- and aqueous-phase reaction products, thus improving our mechanistic understanding of these confounding geochemical processes.

5. CONCLUSIONS

Understanding the reactions involving Cr-bearing minerals, Mn oxides and OC has important implications for assessing and predicting toxic Cr(VI) generation in the environment. In this study, we investigated the combined effects of Mn-oxide, citric acid and gallic acid on Cr-bearing mineral solubility and production of Cr(VI). Citric and gallic acids have moieties that model components of humic substances, which are ubiquitous and highly reactive in the natural environment. Our study shows that these organic acids influence Cr dissolution and redox dynamics via ligand-promoted solubilization and subsequent oxidation of free Cr These processes need to be taken into consideration to better predict the threat of natural Cr(VI) contamination, which thus far, has largely been considered to be controlled mainly by Mn-oxide-induced Cr oxidation. Our work shows that organic acids can regulate Cr(III) solubilization and redox reactions, and their influence on Cr and Mn solubility and redox chemistry needs to be incorporated into models predicting Cr mobility and toxicity in the environment. Future work could couple advanced materials characterization techniques with mechanistic studies to explore the reactivities of different Mn-oxide types on Cr redox dynamics in the presence of organic carbon.

ASSOCIATED CONTENT

Supporting Information. A pdf file of Supporting Information is available free of charge. Data in the file include Cr XANES linear combination fit (LCF) results for citric acid incubations (Table S1), Cr XANES LLCF results for gallic acid incubations (Table S2), XRD and SEM images of Cr(OH)$_3$ and Mn-oxides (Fig S1), OC concentrations over time in citric and gallic experiments (Fig S2), OC concentrations over time in citric acid experimental controls (Fig S3), Cr XANES LCFs for citric and gallic acid reaction products (Fig S4), OC concentrations over time in gallic acid experimental controls (Fig S5), dissolved Cr(VI) to total Cr and Mn ratios as a function of gallic acid concentration (Fig S6), modeled proportions of Cr(III) citrate complexes

and $CrOH^{2+}$ at various citric acid concentration after 168 hours (Fig S7), modeled proportions of Mn(II)-citrate to total Mn in solution (Fig S8).

AUTHOR INFORMATION

* Corresponding Author: Matthew Polizzotto - Phone: (541) 346 5217; email: mpolizzo@uoregon.com

Present Address

Department of Earth Sciences, Cascade Hall, 100, 1272 University of Oregon, Eugene, Oregon 97403, United States

Author Contributions

The manuscript was written through contributions of all authors. All authors have given approval to the final version of the manuscript.

Notes

The Authors declare no competing financial interests.

REFERENCES

Apte, A. D., Tare, V., & Bose, P. (2006). Extent of oxidation of Cr(III) to Cr(VI) under various conditions pertaining to natural environment. *Journal of Hazardous Materials*, *128*(2–3), 164–174. https://doi.org/10.1016/j.jhazmat.2005.07.057

Carbonaro, R. F., Gray, B. N., Whitehead, C. F., & Stone, A. T. (2008). Carboxylate-containing chelating agent interactions with amorphous chromium hydroxide: Adsorption and dissolution. *Geochimica et Cosmochimica Acta*, *72*(13), 3241–3257. https://doi.org/10.1016/j.gca.2008.04.010

Caregnato, P., David Gara, P. M., Bosio, G. N., Gonzalez, M. C., Russo, N., Michelini, M. D. C., & Mártire, D. O. (2008). Theoretical and experimental investigation on the oxidation of gallic acid by sulfate radical anions. *Journal of Physical Chemistry A*, *112*(6), 1188–1194. https://doi.org/10.1021/jp075464z

Chen, K., Bocknek, L., Manning, B., & Morales, M. (2021). *Oxidation of Cr(III) to Cr(VI) and Production of Mn(II) by Synthetic Manganese(IV) Oxide*. *11*, 443. https://doi.org/10.3390/cryst11040443

Chen, N., Lan, Y., Wang, B., & Mao, J. (2013). Reduction of Cr (VI) by organic acids in the presence of Al (III). *Journal of Hazardous Materials*, *260*, 150–156. https://doi.org/10.1016/j.jhazmat.2013.05.010

Chen, Z. F., Zhao, Y. S., & Li, Q. (2015). Characteristics and kinetics of hexavalent chromium reduction by gallic acid in aqueous solutions. *Water Science and Technology*, *71*(11), 1694–1700. https://doi.org/10.2166/wst.2015.157

Choppala, G., Kunhikrishnan, A., Seshadri, B., Park, J. H., Bush, R., & Bolan, N. (2018). Comparative sorption of chromium species as influenced by pH, surface charge and organic matter content in contaminated soils. *Journal of Geochemical Exploration*, *184*, 255–260. https://doi.org/10.1016/j.gexplo.2016.07.012

Chrysochoou, M., Theologou, E., Bompoti, N., Dermatas, D., & Panagiotakis, I. (2016). Occurrence, Origin and Transformation Processes of Geogenic Chromium in Soils and Sediments. In *Current Pollution Reports* (Vol. 2, Issue 4, pp. 224–235). Springer.

https://doi.org/10.1007/s40726-016-0044-2

Dai, R., Liu, J., Yu, C., Sun, R., Lan, Y., & Mao, J. D. (2009). A comparative study of oxidation of Cr(III) in aqueous ions, complex ions and insoluble compounds by manganese-bearing mineral (birnessite). *Chemosphere*, *76*(4), 536–541. https://doi.org/10.1016/j.chemosphere.2009.03.009

Duckworth, O. W., Akafia, M. M., Andrews, M. Y., & Bargar, J. R. (2014). Siderophore-promoted dissolution of chromium from hydroxide minerals. *Environmental Sciences: Processes and Impacts*, *16*(6), 1348–1359. https://doi.org/10.1039/c3em00717k

Elovitz, M. S., & Fish, W. (1995). Redox Interactions of Cr(VI) and Substituted Phenols: Products and Mechanism. *Environmental Science and Technology*, *29*(8), 1933–1943. https://doi.org/10.1021/es00008a010

Eslami, A. C., Pasanphan, W., Wagner, B. A., & Buettner, G. R. (2010). Free radicals produced by the oxidation of gallic acid: An electron paramagnetic resonance study. *Chemistry Central Journal*, *4*(1), 1–4. https://doi.org/10.1186/1752-153X-4-15

Fandeur, D., Juillot, F., Morin, G., Livi, L., Cognigni, A., Webb, S. M., Ambrosi, J. P., Fritsch, E., Guyot, F., & Brown, G. E. (2009). XANES evidence for oxidation of Cr(III) to Cr(VI) by Mn-oxides in a lateritic regolith developed on serpentinized ultramafic rocks of New Caledonia. *Environmental Science and Technology*, *43*(19), 7384–7390. https://doi.org/10.1021/es900498r

Fazary, A. E., Hernowo, E., Angkawijaya, A. E., Chou, T. C., Lin, C. H., Taha, M., & Ju, Y. H. (2011). Complex formation between ferric(III), chromium(III), and cupric(II) metal ions and (O,N) and (O,O) donor ligands with biological relevance in aqueous solution. *Journal of Solution Chemistry*, *40*(12), 1965–1986. https://doi.org/10.1007/s10953-011-9768-1

Fendorf et al. (1992). Inhibitory Mechanisms of Cr(lll) Oxidation by .delta.MnO2. *Journal of Colloid and Interface Science*, *153*(1), 37–54.

Fendorf, S. E. (1995). Surface reactions of chromium in soils and waters. *Geoderma*, *67*(1–2), 55–71. https://doi.org/10.1016/0016-7061(94)00062-F

Fischel, J. S., Fischel, M. H., & Sparks, D. L. (2015). Advances in understanding reactivity of manganese oxides with arsenic and chromium in environmental systems. *ACS Symposium Series*, *1197*, 1–27. https://doi.org/10.1021/bk-2015-1197.ch001

Gabriel, C., Raptopoulou, C. P., Terzis, A., Tangoulis, V., Mateescu, C., & Salifoglou, A. (2007). pH-specific synthesis and spectroscopic, structural, and magnetic studies of a chromium(III)-citrate species. Aqueous solution speciation of the binary chromium(III)-citrate system. *Inorganic Chemistry*, *46*(8), 2998–3009. https://doi.org/10.1021/ic061480j

Giannakopoulos, E., Christoforidis, K. C., Tsipis, A., Jerzykiewicz, M., & Deligiannakis, Y. (2005). Influence of Pb(II) on the radical properties of humic substances and model compounds. *Journal of Physical Chemistry A*, *109*(10), 2223–2232. https://doi.org/10.1021/jp045121q

Ginder-Vogel, M., Borch, T., Mayes, M. A., Jardine, P. M., & Fendorf, S. (2005). Chromate reduction and retention processes within arid subsurface environments. *Environmental Science and Technology*, *39*(20), 7833–7839. https://doi.org/10.1021/es050535y

Gu, B., & Chen, J. (2003). Enhanced microbial reduction of Cr(VI) and U(VI) by different natural organic matter fractions. *Geochimica et Cosmochimica Acta*, *67*(19), 3575–3582. https://doi.org/10.1016/S0016-7037(03)00162-5

Gustafsson, J P. (2011). Visual MINTEQ 3.1 user guide. *Department of Land and Water Recources, Stockholm, Sweden*, 1–73.

Gustafsson, Jon Petter, Persson, I., Oromieh, A. G., Van Schaik, J. W. J., Sjöstedt, C., & Kleja, D. B. (2014). Chromium(III) complexation to natural organic matter: Mechanisms and modeling. *Environmental Science and Technology*, *48*(3), 1753–1761. https://doi.org/10.1021/es404557e

Hausladen, D., Fakhreddine, S., & Fendorf, S. (2019). Governing constraints of chromium(VI) formation from chromium(III)-bearing minerals in soils and sediments. *Soil Systems*, *3*(4), 1–14. https://doi.org/10.3390/soilsystems3040074

Hausladen, D. M., & Fendorf, S. (2017). Hexavalent chromium generation within naturally structured soils and sediments. *Environmental Science and Technology*, *51*(4), 2058–2067.

https://doi.org/10.1021/acs.est.6b04039

Hori, M., Shozugawa, K., & Matsuo, M. (2015). Reduction process of Cr(VI) by Fe(II) and humic acid analyzed using high time resolution XAFS analysis. *Journal of Hazardous Materials*, *285*, 140–147. https://doi.org/10.1016/j.jhazmat.2014.11.047

Hussain, S., Rahim, A., & Farooqui, M. (2012). Potentiometric studies of binary complexes of bivalent metal ions with 3, 5 dinitrosalicylic acid. *Journal of Chemical and Pharmaceutical Research*, *4*(8), 4012–4013.

Jardine, P. M., Fendorf, S. E., Mayes, M. A., Larsen, I. L., Brooks, S. C., & Bailey, W. B. (1999). Fate and transport of hexavalent chromium in undisturbed heterogeneous soil. *Environmental Science and Technology*, *33*(17), 2939–2944. https://doi.org/10.1021/es981211v

Jean-Soro, L., Bordas, F., & Bollinger, J. C. (2012). Column leaching of chromium and nickel from a contaminated soil using EDTA and citric acid. *Environmental Pollution*, *164*, 175–181. https://doi.org/10.1016/j.envpol.2012.01.022

Jiang, B., Gong, Y., Gao, J., Sun, T., Liu, Y., Oturan, N., & Oturan, M. A. (2019). The reduction of Cr(VI) to Cr(III) mediated by environmentally relevant carboxylic acids: State-of-the-art and perspectives. *Journal of Hazardous Materials*, *365*(Vi), 205–226. https://doi.org/10.1016/j.jhazmat.2018.10.070

Kabir-ud-Din, Hartani, K., & Khan, Z. (2000). Unusual rate inhibition of manganese(II) assisted oxidation of citric acid by chromium(VI) in the presence of ionic micelles. *Transition Metal Chemistry*, *25*(4), 478–484. https://doi.org/10.1023/A:1007010306107

Kelly, S. D., Hesterberg, D., & Ravel, B. (2015). Analysis of soils and minerals using x-ray absorption spectroscopy. *Methods of Soil Analysis, Part 5: Mineralogical Methods*, *5*(5), 387–463. https://doi.org/10.2136/sssabookser5.5.c14

Kotasâ, J., & Stasicka, Z. (2000). Chromium occurrence in the environment and methods of its speciation. *Environmental Pollution* , *107*, 263–283. https://doi.org/https://doi.org/10.1016/S0269-7491(99)00168-2

Kwak, S., Yoo, J. C., & Baek, K. (2018). Synergistic and inhibitory reduction of Cr(VI) by montmorillonite, citric acid, and Mn(II). *Journal of Soils and Sediments*, *18*(1), 205–210. https://doi.org/10.1007/s11368-017-1748-7

Landrot, G., Ginder-Vogel, M., Livi, K., Fitts, J. P., & Sparks, D. L. (2012). Chromium(III) oxidation by three poorly-crystalline manganese(IV) oxides. 1. chromium(III)-oxidizing capacity. *Environmental Science and Technology*, *46*(21), 11594–11600. https://doi.org/10.1021/es302383y

Lee, S. M., Cho, I. H., Chang, Y. Y., & Yang, J. K. (2007). Effects of the density of carboxyl groups in organic compounds on the photocatalytic reduction of Cr(VI) in a TiO2 suspension. *Journal of Environmental Science and Health - Part A Toxic/Hazardous Substances and Environmental Engineering*, *42*(4), 543–548. https://doi.org/10.1080/10934520701189836

LI, C., LAN, Y.-Q., & DENG, B.-L. (2007). Catalysis of Manganese(II) on Chromium(VI) Reduction by Citrate. *Pedosphere*, *17*(3), 318–323. https://doi.org/10.1016/s1002-0160(07)60038-1

Liu, X., Dong, H., Yang, X., Kovarik, L., Chen, Y., & Zeng, Q. (2018). Effects of citrate on hexavalent chromium reduction by structural Fe(II) in nontronite. *Journal of Hazardous Materials*, *343*(Ii), 245–254. https://doi.org/10.1016/j.jhazmat.2017.09.038

McClain, C. N., Fendorf, S., Webb, S. M., & Maher, K. (2017). Quantifying Cr(VI) Production and Export from Serpentine Soil of the California Coast Range. *Environmental Science and Technology*, *51*(1), 141–149. https://doi.org/10.1021/acs.est.6b03484

Nakayasu, K., Fukushima, M., Sasaki, K., Tanaka, S., & Nakamura, H. (1999). Comparative studies of the reduction behavior of chromium(VI) by humic substances and their precursors. *Environmental Toxicology and Chemistry*, *18*(6), 1085–1090. https://doi.org/10.1897/1551-5028(1999)018<1085:CSOTRB>2.3.CO;2

Oze, C., Bird, D. K., & Fendorf, S. (2007). Genesis of hexavalent chromium from natural sources in soil and groundwater. *Proceedings of the National Academy of Sciences of the United States of America*, *104*(16), 6544–6549. https://doi.org/10.1073/pnas.0701085104

Palmer, C. D., & Wittbrodt, P. R. (1991). Processes affecting the remediation of chromium-contaminated sites. *Environmental Health Perspectives*, *92*(6), 25–40. https://doi.org/10.1289/ehp.919225

Pan, C., Liu, H., Catalano, J. G., Wang, Z., Qian, A., & Giammar, D. E. (2019). Understanding the Roles of Dissolution and Diffusion in Cr(OH) 3 Oxidation by Î-MnO 2. *ACS Earth and Space Chemistry*, *3*(3), 357–365. https://doi.org/10.1021/acsearthspacechem.8b00129

Ravel, B., & Newville, M. (2005). ATHENA, ARTEMIS, HEPHAESTUS: Data analysis for X-ray absorption spectroscopy using IFEFFIT. *Journal of Synchrotron Radiation*, *12*(4), 537–541. https://doi.org/10.1107/S0909049505012719

Saad, E. M., Sun, J., Chen, S., Borkiewicz, O. J., Zhu, M., Duckworth, O. W., & Tang, Y. (2017). Siderophore and Organic Acid Promoted Dissolution and Transformation of Cr(III)-Fe(III)-(oxy)hydroxides. *Environmental Science and Technology*, *51*(6), 3223–3232. https://doi.org/10.1021/acs.est.6b05408

Saad, E. M., Wang, X., Planavsky, N. J., Reinhard, C. T., & Tang, Y. (2017). Redox-independent chromium isotope fractionation induced by ligand-promoted dissolution. *Nature Communications*, *8*(1). https://doi.org/10.1038/s41467-017-01694-y

Sarkar, B., Naidu, R., Krishnamurti, G. S. R., & Megharaj, M. (2013). Manganese(II)-catalyzed and clay-minerals-mediated reduction of chromium(VI) by citrate. *Environmental Science and Technology*, *47*(23), 13629–13636. https://doi.org/10.1021/es401568k

Schenkeveld, W. D. C., & Kraemer, S. M. (2018). Constraints to synergistic fe mobilization from calcareous soil by a phytosiderophore and a reductant. *Soil Systems*, *2*(4), 1–22. https://doi.org/10.3390/soilsystems2040067

Smith, R. M., & Martell, A. E. (1987). Critical stability constants, enthalpies and entropies for the formation of metal complexes of aminopolycarboxylic acids and carboxylic acids. *Science of The Total Environment*, *64*(1–2), 125–147. https://doi.org/10.1016/0048-9697(87)90127-6

Sun, Y., Guan, F., Yang, W., & Wang, F. (2019). Removal of chromium from a contaminated soil using oxalic acid, citric acid, and hydrochloric acid: Dynamics, mechanisms, and

concomitant removal of non-targeted metals. *International Journal of Environmental Research and Public Health*, *16*(15). https://doi.org/10.3390/ijerph16152771

Sutton, R. (2010). Chromium-6 in U.S. Tap Water. *Enviroenmental Working Group*, *4*, 68–70.

Tang, Y., Webb, S. M., Estes, E. R., & Hansel, C. M. (2014). Chromium(iii) oxidation by biogenic manganese oxides with varying structural ripening. *Environmental Sciences: Processes and Impacts*, *16*(9), 2127–2136. https://doi.org/10.1039/c4em00077c

Varadharajan, C., Beller, H. R., Bill, M., Brodie, E. L., Conrad, M. E., Han, R., Irwin, C., Larsen, J. T., Lim, H. C., Molins, S., Steefel, C. I., Van Hise, A., Yang, L., & Nico, P. S. (2017). Reoxidation of Chromium(III) Products Formed under Different Biogeochemical Regimes. *Environmental Science and Technology*, *51*(9), 4918–4927. https://doi.org/10.1021/acs.est.6b06044

Whitaker, A. H., Peña, J., Amor, M., & Duckworth, O. W. (2018). Cr(VI) uptake and reduction by biogenic iron (oxyhydr)oxides. *Environmental Science: Processes and Impacts*, *20*(7), 1056–1068. https://doi.org/10.1039/c8em00149a

Yang, F., Guo, J., Dai, R., & Lan, Y. (2014). Oxidation of Cr(III)-citrate/tartrate complexes by δ-MnO2: Production of Cr(VI) and its impact factors. *Geoderma*, *213*, 10–14. https://doi.org/10.1016/j.geoderma.2013.07.022

Zaffiro, a, Zimmerman, M., Wendelken, G., & Munch, D. (2011). *Method 218.7: Determination of Hexavalent Chromium in Drinking Water*. *November*, 1–30.

CHAPTER III.

MINERALOGICAL CONTROLS ON CHROMATE AND VANADATE MOBILITY IN THE NORTH CAROLINA PIEDMONT: IMPLICATIONS FOR GROUNDWATER CONTAMINATION.

Reproduced with permission from Balogun, F.O., Peel, H.R., Alvarado, T., Vinson, D.S., Duckworth O.W. and Polizzotto, M.L. (in preparation for submission) Mineralogical controls on chromate and vanadate mobility in the North Carolina Piedmont: Implications for groundwater contamination.

1 INTRODUCTION

Contamination of ground water by the redox-active, oxyanion forming elements chromium (Cr) and vanadium (V) is of environmental and health significance due to their carcinogenic properties and ability to disrupt insulin signaling in humans (Jardine et al., 1999; Wang et al., 2014). Under a wide pH range and oxidizing conditions, chromate exists as highly mobile and toxic $HCrO_4^-$ and CrO_4^{2-}, while vanadate exists as $H_2VO_4^-$ and HVO_4^{2-}. Chromium and V contamination have been widely linked to anthropogenic activities such as leather tanning, electroplating and crude oil refinery(B. Jiang et al., 2019; Larsson et al., 2017; Schlesinger et al., 2017; Shaheen et al., 2019). However, evidence in the last couple of decades has shown that rock-water interaction in areas underlain by mafic, ultramafic, andesitic and felsic rocks is an important geogenic source of these redox-active contaminants to groundwater (Coyte et al., 2020; Vengosh et al., 2016).

Of particular note, over three million people may be consuming groundwater sourced from regolith and aquifer materials rich in geogenic Cr and V across the Piedmont physiographic region of the southeastern United States. (Coyte et al., 2020; Coyte & Vengosh, 2020; Gillispie et al., 2016; Vengosh et al., 2016) Understanding rock-contaminant interactions will provide necessary insights needed to ameliorate this growing environmental concern. In North Carolina, the Piedmont is geologically diverse and comprises seven geologic terranes, which are mostly made up of metasedimentary and igneous rocks that host Cr and V-bearing primary minerals (Fig. 1). In the subsurface, where elemental abundances are spatially heterogenous, Cr and V mostly share similar geologic sources. Therefore, similar

biogeochemical processes may control Cr and V distribution, toxicity, and phase partitioning in groundwater and subsurface environments.(Gillispie et al., 2016; Vengosh et al., 2016; Wright & Belitz, 2010).

In the subsurface, heterogeneities in abundances of natural oxidants and sinks of Cr and V, such as ubiquitous reactive Mn, Fe and Al (oxyhydr)oxides (S. Jiang et al., 2020) and clay minerals, create complexities in determining the fate of these redox-sensitive contaminants. Manganese-oxide minerals are the most prolific oxidizers of Cr from Cr(III) to Cr(VI) and may oxidize V(IV) to V(V), thereby enhancing the mobility of Cr and V in subsurface (J. Abernathy et al., 2021; Landrot, Ginder-Vogel, et al., 2012; Liang et al., 2021; Oze et al., 2007; Pan et al., 2019). The fate of these species is further influenced by chemical interactions on mineral surfaces, which ultimately determine their mobility and species transformation (P. Johnston & Chrysochoou, 2012). The importance of crystalline and poorly ordered Fe and Al oxyhydroxides on the sorption of Cr and V in model synthetic systems has been extensively studied (Abernathy et al., 2022; Ding et al., 2022; Gustafsson, 2019; J. Abernathy et al., 2021; Liang et al., 2021; P. Johnston & Chrysochoou, 2012), however, limited information exists on the retention, release, and speciation of these contaminants in natural geologic materials with varying abundances of Fe and Mn-bearing secondary minerals. In recent times, the relationship between speciation of redox-sensitive metals and their host phases in naturals materials have been successfully deconvolved using spectroscopic and sequential extraction techniques (C. Scheinost et al., 2002; Oze et al., 2002; Wisawapipat & Kretzschmar, 2017).

The overall goal of this study was to quantify controls on Cr and V mobility in subsurface aquifers. Using saprolites weathered from metasedimentary and felsic metavolcanic rocks of the NC Piedmont, we specifically aimed to (i) evaluate the speciation, host phases, and extractability of Cr and V, (ii) characterize material binding capacities for chromate and vanadate, and (iii) quantify rate constants of Cr and V sorption by the geologic materials. Findings from this study will improve our understanding of the behavior of Cr and V in the natural environment and help parametrize mechanistic models to predict contaminant fate and transport.

2   MATERIAL AND METHODS

2.1 Site geology description.

Two chemically contrasting saprolite samples used in this study were collected from a Union County (UC) park (34°58'22.6" N 80°28'37.3" W) and the Redlair observatory (RL) (35°18'00.0" N 81°05'24.0" W) in Gaston County, North Carolina (Fig. 1). The Union County saprolite was obtained from a creek wall containing the mudstone member of the Cid formation, which consists primarily of stratified siltstone, an upper, laminated siltstone-mudstone unit, and minor tuff bed. The saprolite is of metasedimentary origin. The Redlair Observatory samples are associated with the Battleground formation derived from felsic metavolcanic rocks.
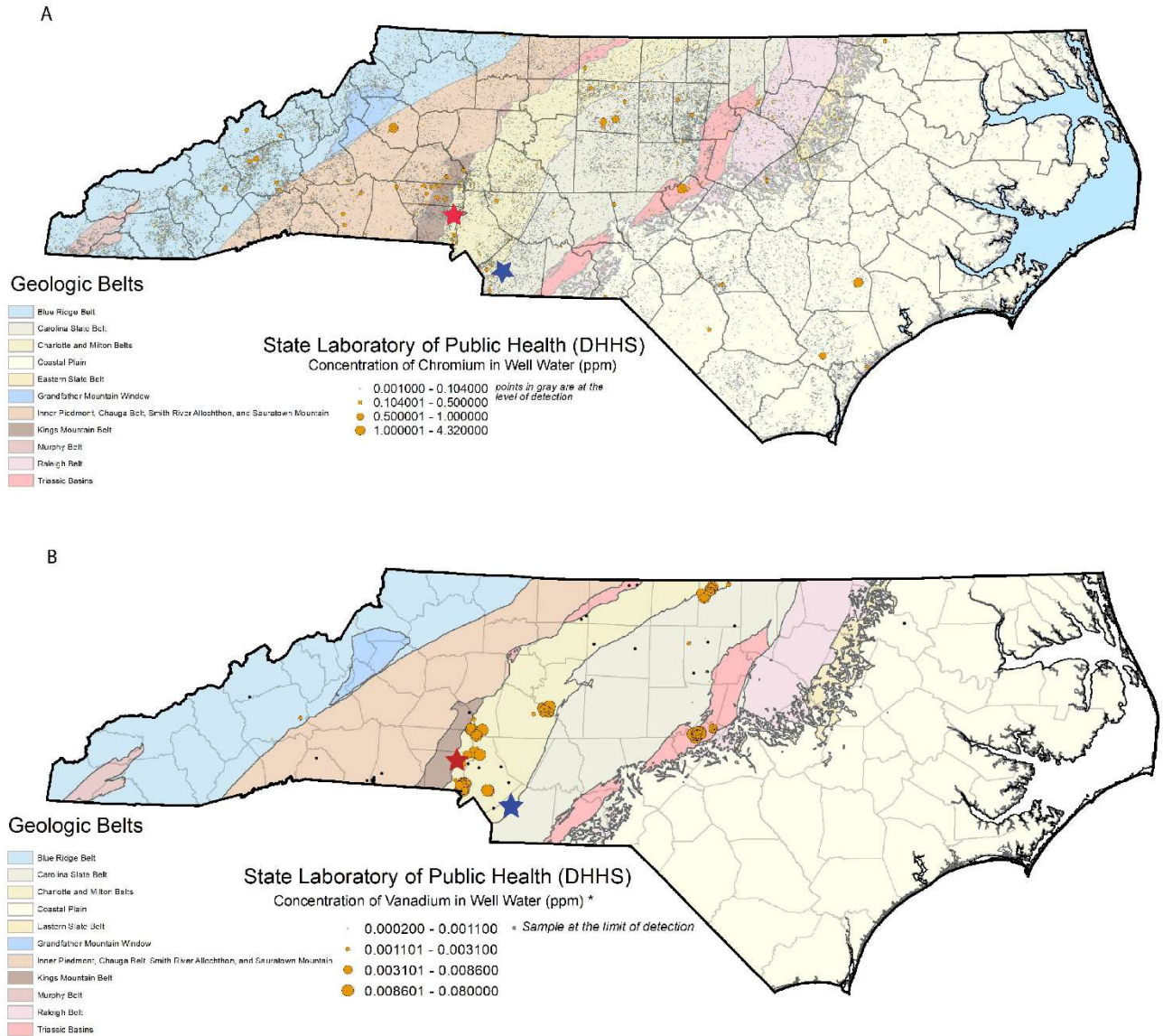
Fig 1: Well water chromium (A) and vanadium (B) concentrations across the NC. Blue and red stars indicate the Union County and Redlair observatory field sites, respectively. The Piedmont physiographic region sits in the center of the state, with the Coastal Plain to the east and the Blue Ridge Belt to the west.

2.2 Materials, sample collection and characterization.

All chemicals were reagent grade or higher and provided by Fisher Scientific unless otherwise noted. For Union County saprolite sample collection, a hammer and shovel were used to obtain samples from the surface of the creek wall. Samples were placed in ziplock bags before being moved into oxygen barrier sleeves with anaerobic packs. Redlair saprolite was collected from the bed of a 2–3 m incised streambed. Saprolite was collected using two adjacent auger holes. Each auger hole was ~2 inches in diameter and augured diagonally downward into the bank. Before use, saprolite samples were air-dried, passed through a 2 mm sieve, and stored in 50 mL centrifuge tubes. The pH of the saprolites was measured in 0.01 $CaCl_2$ with a soil solution ratio of 1:2 (w/w) using an Orion Star A111 pH meter.

The bulk mineralogy of the saprolites was characterized by X-ray diffraction (XRD), using a Rigaku benchtop X-ray diffractometer equipped with a Cu Kα X-ray radiation source. The saprolite materials were disaggregated using a mortar and pestle, sieved through 500 μm mesh sieve and mounted on an aluminum sample holder. Data were collected between 3˚ to 90˚ 2θ with a scan rate of 0.02° 2θ/min. The XRD pattern processing and phase identification for both saprolites were done using the JADE software (Fig. S1 and S2). The specific surface areas of each saprolite were analyzed from an 8-point N_2-BET isotherm (p/p0 = 0.01 – 0.23; Autosorb Quantachrome) after degassing the samples at 150 °C. Total concentrations of Cr, V, Fe, and Mn were determined by X-ray fluorescence (XRF). Samples were prepared by using a ball mill to grind saprolite materials into a fine powder, adding a binder, and pressing into a pellet with a smooth flat surface. The handheld XRF was moved over the flat surface of the samples multiple times and the data were average to obtain elemental compositions.

2.3 Chemical extractions.

Parallel chemical extractions were performed on untreated and Cr- and V-loaded samples to quantify the solid-phase fractions of Cr, V, Fe, and Mn. Extractions targeted ionically bound species [1 M magnesium chloride ($MgCl_2$)], amorphous-oxide-bound phases [0.2 M ammonium oxalate], crystalline-oxide-bound phases [citrate-bicarbonate-dithionite (CBD)] and "environmentally available" phases (strong-acid digestible), utilizing standard protocols (Keon et al., 2001; LaFayette et al., 2020). Specific procedures are outlined in Table S1. Concentrations of Cr, V, Fe and Mn in extracts were determined by inductively coupled plasma-mass spectrometry (ICP-MS), as described below.

2.4 Kinetic and sorption experiments.

Kinetic experiments were conducted to establish rates of Cr and V sorption to the saprolite samples. To establish kinetics, 3.06 mg/L of chromate (~29 µM) and vanadate (60 µM) were prepared in 0.02 M NaCl. In duplicate, solutions were introduced to the saprolites and monitored over time, with 1 mL of sample taken at 0.25, 0.5, 0.75, 1, 2, 4, 6, 8, 12, 24, 48 and 72 hours for analysis. Samples were passed through a 0.22 µm filter, filtrates were acidified with 1 drop of 15.8 M HNO_3, and the resulting samples were refrigerated at 4°C prior analysis via ICP-MS. At every sampling interval, pH was adjusted to 6.5 ± 0.1; Kinetic data were fitted with pseudo first- and second-order kinetic models, and data were fitted using SigmaPlot. The equations for these models can be found in the supplementary material.

For sorption isotherm experiments, solutions containing seven concentrations of Cr (5 to 100 µM Cr(VI)) and nine concentrations of V (20 to 450 µM V(V)) were prepared by using $K_2Cr_2O_7$ and Na_3VO_4 in 0.02 M NaCl. Sorbate controls (i.e., no Cr and V) and soil blanks (no soil) were also included. The sorption experiments were carried out in a batch experiment using 50 mL test tubes with 2 g of saprolite and 40 mL of chromate or vanadate solution.

All sorption and control experiments were conducted in triplicate. Slurry pH was adjusted to 6.5 ± 0.2 by the addition of HCl or NaOH before the start of the experiment and every 24 hours thereafter. Vials were covered with aluminum foil and allowed to equilibrate at while shaking at 175 rpm on an orbital shaker for 48 hours. After 48 hours, vials were centrifuged at 4200 rpm for 10 minutes, pH was adjusted, and solutions were passed through 0.22 µm

polyethersulfone (PES) syringe filters. Samples were acidified with 15.8 M HNO_3 and stored at 4°C before analysis by ICP-MS.

The maximum adsorption capacity (q max), Langmuir constant, K_L, the Freundlich constants K_F and n were calculated using Langmuir and Freundlich adsorption models. A chi-square test was coupled with the coefficient of determination, R^2, to determine the best isotherm model for the resulting data (Table S2). A follow up experiment to test the impact of ionic strength of Cr and V adsorption was also done using 0.002 and 0.2 M NaCl.

To examine phase associations of sorbed Cr and V, adsorption experiments were performed with 10 mL of 40 µM Cr(VI) or 300 µM V(V), 0.02 M NaCl, and 0.5 g of saprolite. Samples were equilibrated and collected as described above. Resulting solids were characterized by chemical extractions, as described in section 2.3, and µ-XRF, as describe below.

2.5 Aqueous analysis

Dissolved concentrations of Cr, V, Fe, and Mn from experimental products were measured using a Thermoscientific iCAP-RQ single quadrupole ICP-MS at the Oregon State University Keck Center for Plasma Spectrometry. The instrument detection limits for Cr, V, Fe, and Mn were 1.2, 2.7, 1600, and 10 ng/L respectively. For follow-up ionic strength experiments, dissolved Cr(VI) was determined via the colorimetric diphenyl carbazide (DPC) method using a Shimadzu 1280 UV-VIS spectrophotometer. The detection limit for this technique was 5 µg/L.

2.6 Bulk and micro-focused X-ray absorption spectroscopy.

X-ray absorption spectroscopy (XAS) was conducted at the Stanford Synchrotron Radiation Lightsource (SSRL). Bulk Cr and V X-ray absorption near edge structure (XANES) spectroscopy data for native saprolite materials, Cr- and V-loaded samples, and standards were collected at beamline 4-3. Solid-phase samples from the second highest and highest loading experiments (60 µM Cr and 450 µM V) were prepared for XAS, and Na_3VO_4 and $K_2Cr_2O_7$ reference materials, diluted in BN_3 at 1:10, were also analyzed. The samples were loaded onto acrylic sample holders and sealed with Kapton tape (non-adhesive part of Kapton in contact with sample), mounted on the digivert motor and placed at 45° to the incident X-ray beam. Absorption spectra were collected in fluorescence mode using a vortex detector positioned 90° to

I_0, equipped with V and Ti filters for Cr and V data acquisition, respectively. A double-crystal Si (111) LN-cooled monochromator was used for energy selection.

Data processing for Cr and V speciation and estimates of relative percentages of Cr and V in the samples were made using the linear combination fitting (LCF) function in Athena. For Cr-loaded samples, this procedure was done using two model compounds, $Cr(OH)_3$, and $K_2Cr_2O_7$, and spectra from the native saprolite materials (UC sap and RL sap). For Cr analysis, data were plotted in derivative space and compared with reference materials of known oxidation states, allowing for the determination of proportions of Cr(III) and Cr(VI) in the samples. Vanadium speciation was done using reference spectra from Wisawapipat and Kretzschmar, 2017 (Tables S3, S4, and S5).(Wisawapipat & Kretzschmar, 2017) Fits were based on a minimum of three standards, and the summed contribution was between 97-117% for all fits. Fitting ranges were from -20 to 30 eV about the edge energy (E_0) of Cr and -20 to 40 eV about the edge energy of V.

Bulk Fe and Mn XANES and extended X-ray absorption fine structure (EXAFS) spectroscopy data for native saprolite materials were collected at SSRL beamline 11-2. Native saprolite materials were loaded on sample slides and mounted on the digivert motor at 45° to the incident beam. The incident beam energy was selected using a Si (220) double crystal monochromator. For each sample, six spectra were collected for Fe in fluorescence mode, using a PIPS detector from -200 to 680 eV about the Fe edge. For Mn XANES, six spectra were collected in fluorescence mode using a 100 element Ge detector from -40 to 90 eV about the Mn edge. Data processing for the determination of Fe (Tables S6 and S7) and Mn speciation was done in Athena. Spectra were energy-calibrated by adjusting the maxima of the first derivative of the Fe and Mn foils to 7112 eV and 6539 eV, respectively, and then averaged, deglitched, baseline corrected and normalized. Fe EXAFS were fitted from -30 to 600 eV. For Mn analysis, data were plotted in derivative space and compared with reference materials of known oxidation states, allowing for the determination of proportions of Mn(II), Mn(III) and Mn(IV) in the samples.

Finally, Cr- and V-loaded saprolite samples for Union County and Redlair Observatory were air-dried and shipped to Spectrum Petrographics Inc for thin section preparation. Samples were mounted on quartz 4.5 x 2.8 cm quartz glass slides using Epotex-301 resin, cut, and polished before analysis. Spatial distributions of Cr, V, Fe and Mn in Cr- and V-loaded saprolite

samples were determined by μ–X-ray fluorescence (μ-XRF) at SSRL Beamline 2-3. Data were collected in fluorescence mode, using harmonic rejection mirrors, a channel-cut Si (111) monochromator, and a 1-channel vortex detector. Beam size was ~ 5 μm x 5 μm, and μ-XRF images were obtained with incident X-ray energies set to 7200 eV by rastering sample slides in step sizes of 7 μm with 15 ms of dwell time. The areas mapped areas for UC-1 (60 μM Cr-loaded Union County saprolite), UC-2, (450 μM V-loaded Union County saprolite) and RL-1 (60 μM Cr-loaded Redlair saprolite) were 2 mm × 1.3 mm, 1.9 mm × 1.6 mm, and 2.7 mm × 2.1 mm, respectively.

3 RESULTS

3.1 Saprolite characterization.

Results from XRF analysis revealed that total Cr, V and Mn were higher in the UC saprolite than in the RL sample (Table 1). However, total Fe in the RL saprolite was ~ 2.4 times greater than in the UC saprolite. Chromium was undetectable by XRF in the RL saprolite, but follow-up strong-acid digestion showed that the "environmentally available" Cr was ~16 mg/kg, a value that does not include Cr bound with all silicate minerals.

Chemical extractions indicated that native Cr and V in both saprolites were associated with crystalline oxides over amorphous oxides and ionically bounded species (Table 1). Amorphous and crystalline Fe in the UC saprolite were 1140 and 10700 mg/kg, respectively, and 530 and ~15000 mg/kg in the RL saprolite. Amorphous and crystalline Mn-oxide in the UC saprolite were ~4 times greater than in the RL saprolite.

Table 1: Physicochemical properties of the saprolites

Saprolite property	Union County	Redlair
pH	7.7	5.9
*Total Cr (mg/kg)	54 ± 14	< LOD
*Total V (mg/kg)	330 ± 55	217 ± 31
*Total Fe (mg/kg)	31000 ± 577	74210 ± 1856
*Total Mn (mg/kg)	1100 ± 39	924 ± 36
Amorphous Fe (mg/kg)	1140 ± 30	530 ± 20
Crystalline Fe (mg/kg)	10700 ± 900	15000 ± 300
Amorphous Mn (mg/kg)	100 ± 10	25 ± 1
Crystalline Mn (mg/kg)	130 ± 12	32 ± 1

*Determined through XRF analysis

X-ray absorption spectroscopy showed that the speciation of Fe, V and Mn in both the UC and RL saprolites was diverse. In the UC and RL saprolites, the average oxidation states of Fe, V, Mn and Cr were +3, +4, +2/3, and +3 respectively, (Figs. S3, Fig. S4, Fig. S5, Fig. S6). On the other hand, the dominant oxidation state of Cr in both saprolites was +3.

3.2 Cr and V kinetic experiments.

Chromium and V sorption kinetic data are shown in Figure 2. Fitting our empirical data with pseudo-first order and pseudo-second order kinetic models (Fig. 2A-D) shows that the rate of V sorption on both saprolites was 5-6 times faster than for Cr. For both Cr and V sorption on UC and RL, the pseudo-second order kinetic model was a better-fitting model than the pseudo-first order model, with R^2 values of 0.969 and 0.972 for Cr sorption on UC and RL saprolites, respectively, and >0.999 for V sorption on both saprolites. The sorption rate k_2 of Cr on UC was ~2 times more than that for Cr sorption to RL (Fig. 2A and B), and the rate of V sorption on UC was similarly ~2.4 times greater than that for V sorption to the RL saprolite (Fig. 2C and D). For both elements and both saprolites, >90% of the observed and modeled maximum sorption occurred by 48 h of reaction.
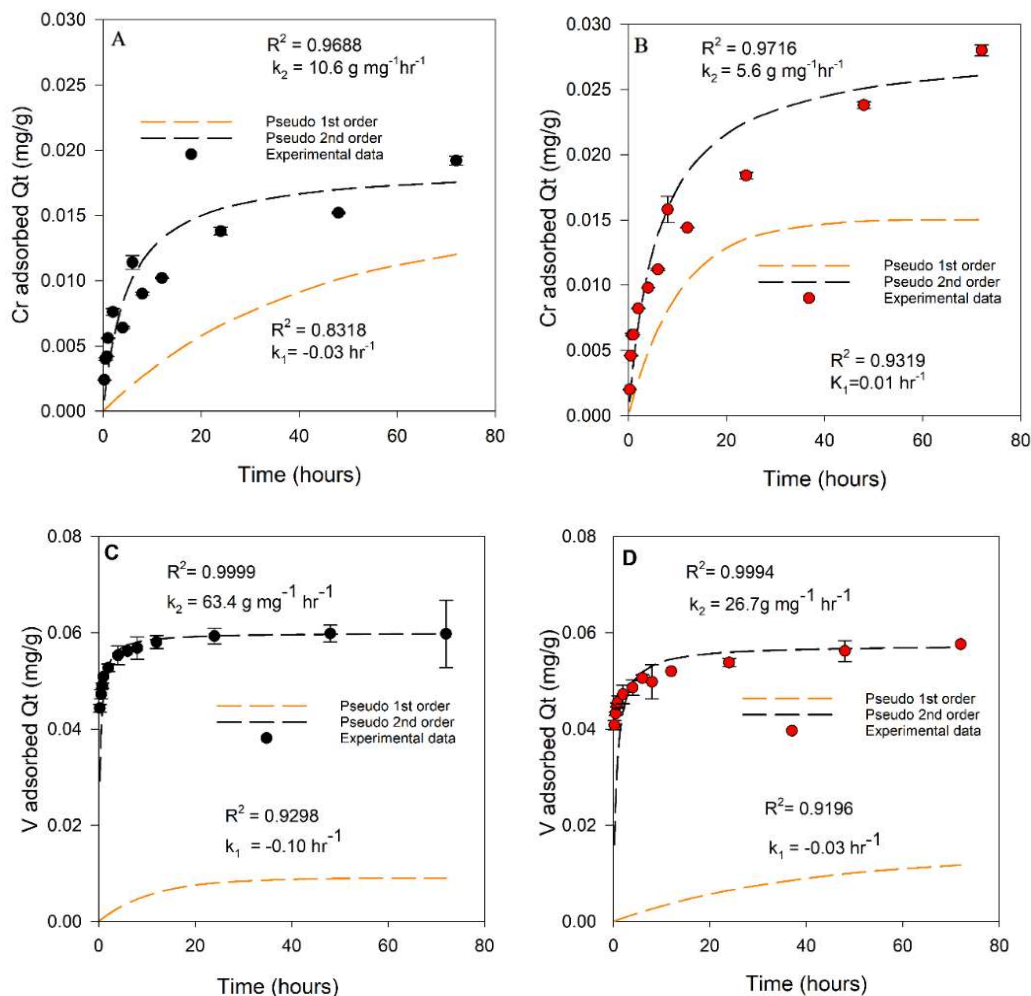
Fig 2: Sorption kinetics of A) Cr on Union County saprolite (black data points), B) Cr on Redlair saprolite (red data points), C) V on Union County saprolite, and D) V on Redlair saprolite. For each plot, yellow dashed lines represent pseudo first order kinetic models and black dashed lines represent pseudo second order kinetic models of the experimental data. Error bars on data points indicate standard error of experimental replicates. Reaction conditions: Ionic strength (I) = 0.02 M NaCl; pH = 6.5; initial [Cr] = 29 μM; initial [V] = 60 μM; solid solution ratio = 2g/40mL.

3.3 Sorption of Cr

Chromium sorption isotherm data for both saprolites are shown in Fig. 3A. The sorption of Cr on the UC and RL saprolites was best described by Langmuir models (R^2 = 0.977 and

0.994, respectively), over Freundlich models (Fig. S7A), and each isotherm is characterized by a relatively steep initial slope at low Cr(VI) concentrations and plateaus at higher adsorbate concentrations, characteristic of L-type isotherms (Fig. 3A). The maximum sorption capacities of Cr on both saprolites predicted by the Langmuir models were similar, with values of 36.4 mg Cr/kg UC saprolite and 31.2 mg Cr/kg RL saprolite.
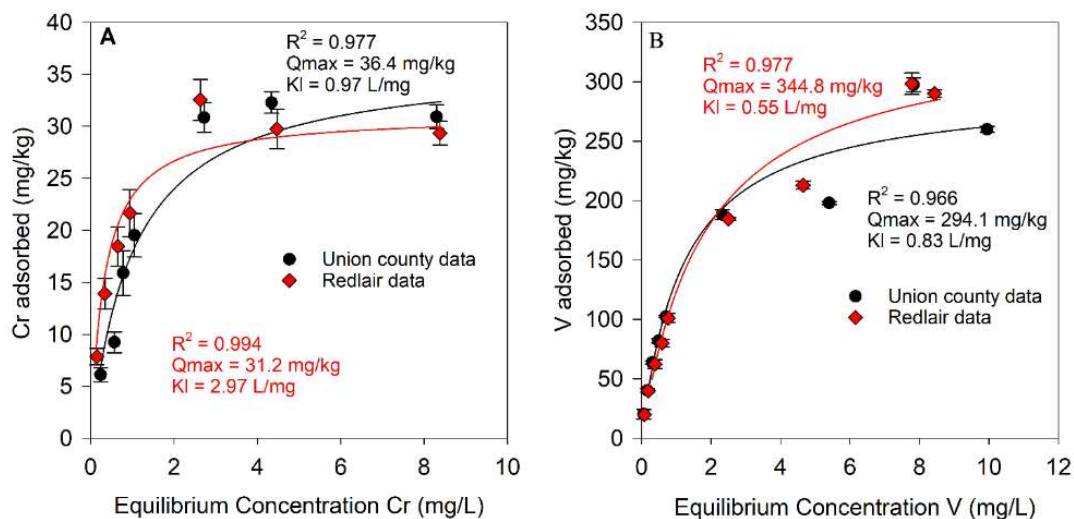
Fig 3: Sorption of A) Cr on Union County and Redlair saprolites, and B) V on Union County and Redlair observatory saprolites. For each plot, black and red lines represent Langmuir isotherm models for Union County and Redlair data, respectively. Error bars indicate standard error of experimental replicates. Reaction conditions: Ionic strength (I) = 0.02 M NaCl; pH = 6.5; initial [Cr] = 5 - 100 μ;, Initial [V] = 20 - 450 μM; solid solution ratio was 2g/40mL.

3.4 Sorption of V

Vanadium sorption isotherm data for both saprolites are presented in Fig. 3B. Compared to Cr sorption isotherms, the sorption of V was higher in both saprolite samples. In comparison, UC and RL saprolites preferentially sorbed 8-11 times more V than Cr (on a molar basis). The V sorption data were well explained by both Langmuir (Fig. 3B) and Freundlich models (Fig. S7B), but a chi-square test found that the Langmuir isotherm model yielded the lower χ^2 value for V sorption onto both saprolites (Table S2). The maximum sorption capacities predicted by the Langmuir model were 294.1 and 344.8 mg V/kg saprolite for the UC and RL samples, respectively (Fig. 3B).

3.5 Chemical extractions of Cr- and V-loaded saprolites

Solid-phase Cr and V concentrations from chemical extractions of Cr and V-loaded samples and native saprolites are shown in Fig. 4. The CBD extraction targeting Cr and V bound to crystalline oxides released the most Cr and V from both the native UC (3.7 mg/kg Cr and 16.5 mg/kg V) and RL (6.4 mg/kg Cr and 80 mg/kg V) saprolites. In the UC saprolite, CBD-extractable Cr and V were ~7 and 5% of the total Cr and V, whereas in the RL saprolites, CBD-extractable V was 37% of the total V. Ammonium oxalate targeting ions coprecipitated with amorphous oxyhydroxides released the second highest amount of Cr and V from both UC (0.9 mg/kg Cr and 3.2 mg/kg V) and RL native saprolites (0.9 mg/kg Cr and 15.7 mg/kg V). $MgCl_2$ extraction targeting ionically bound Cr and V released no detectable Cr from the native UC and RL saprolites, while 0.25 and 1.4 mg/kg V was released from the native UC and RL saprolites, respectively.

In the Cr-loaded saprolites, CBD extraction released the most amount of Cr (14 and 21 mg/kg for UC and RL), followed by the oxalate (9.6 and 10.5 mg/kg) and $MgCl_2$ (5.2 and 3.9 mg/kg) extractions. CBD-extracted Cr from the Cr-loaded samples was ~3.8 and 3.4 times greater than it was from the native saprolites, while oxalate extractions mobilized ~10.5 and 12 times more Cr in the UC and RL Cr-loaded saprolites than for the native saprolites.

In V-loaded saprolites, the greatest amount of V was released by $MgCl_2$ (111.1 mg/kg) and oxalate extractions (169.5 mg/kg) in the UC and RL saprolites, respectively. The second greatest amount of V was released by the CBD (108.3 mg/kg) and $MgCl_2$ (126.9 mg/kg) extractions from the UC and RL saprolites, respectively, while the least amount of V was released by the oxalate (103.1 mg/kg) and CBD extractions (119.8 mg/kg) from the UC and RL saprolites, respectively.
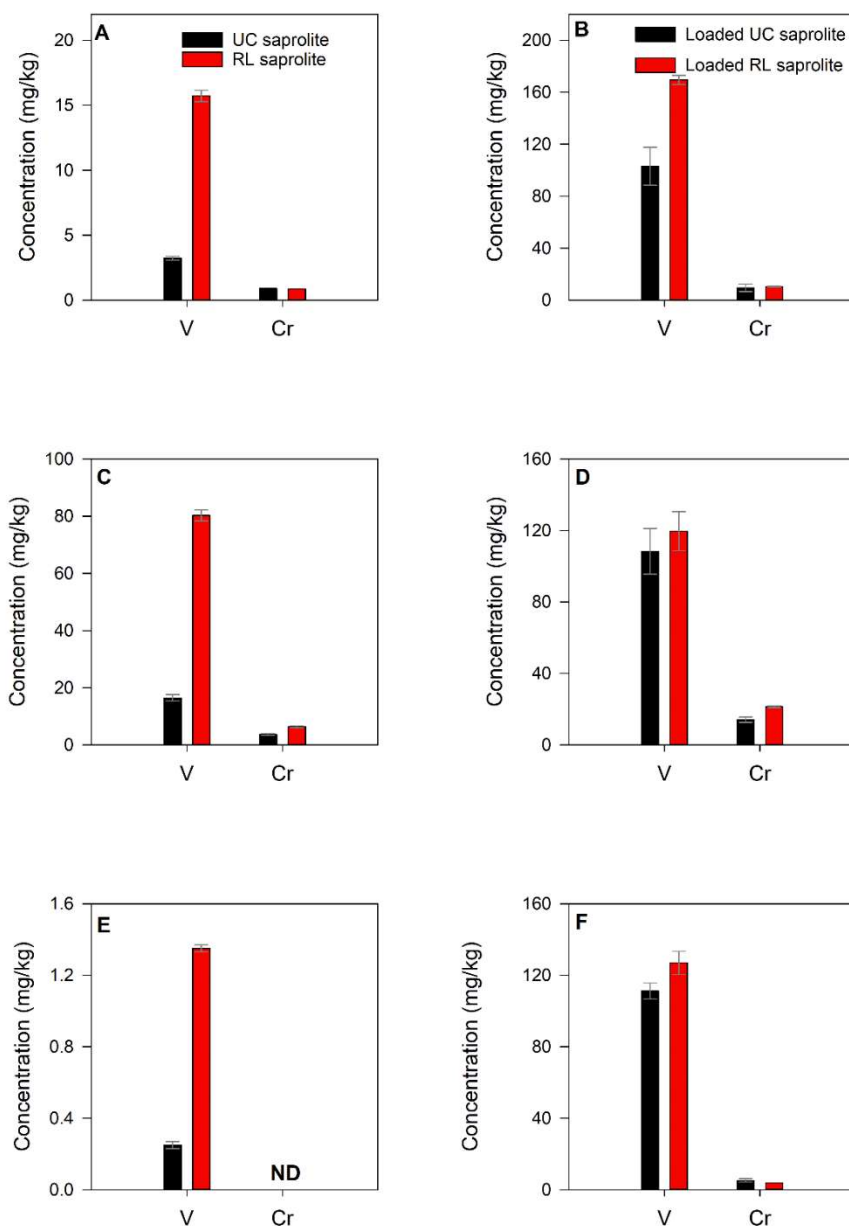
Fig 4: A) Concentrations of Cr and V desorbed from native saprolites via oxalate extractions. B) Concentrations of Cr and V desorbed from Cr- and V-loaded saprolites via oxalate extractions. C) Concentrations of Cr and V desorbed from native saprolites via CBD extractions. D) Concentrations of Cr and V desorbed from Cr- and V-loaded saprolites via CBD extractions. E) Concentrations of Cr and V desorbed from native saprolites via MgCl$_2$ extractions. F) Concentrations of Cr and V desorbed from Cr- and V-loaded saprolites via MgCl$_2$ extractions. Elemental release from Cr- and V- loaded saprolites was corrected for the measured oxalate-, CBD- and MgCl$_2$-extracted Cr and V from the native saprolites. Error bars represent standard error of replicates.

3.6 Bulk XANES and μ-XRF analysis

XANES analysis of our Cr- and V-loaded samples showed Cr and V in reduced phases (Figs. 5 and 6). Linear-combination fits (LCF) of the Cr XANES spectra indicate that the predominant oxidation state of Cr in Cr-loaded UC and RL saprolite was Cr(III), with fits comprised of native saprolite and Cr(OH)$_3$ standard spectra but only negligible Cr(VI) (Fig. 5). The average oxidation state of V was 4.17 ± 0.31 and 4.17 ± 1.37 in the UC and RL V-loaded saprolites, respectively (Fig. 6). Vanadium XANES spectra LCF showed that V^{4+}-substituted kaolinite and V^{5+}-sorbed kaolinite were important components of our UC saprolite spectra fit. On the other hand, in addition to V^{4+} substituted in or V^{5+} sorbed on well-ordered kaolinite, RL V-loaded XANES fits were improved by ~10% with a standard of V^{5+} sorbed on a ferrihydrite-humic substance complex.

μ-XRF results show that Cr and V were associated with Fe-bearing phases, however, the distribution of Cr and V across the UC sample was diffuse (Figs. 7 and 8). Due to this, three hotspots were selected for microscale elemental spatial correlation analysis in some samples. Correlation analysis in Cr-loaded Union County (UC-1) sample showed that Cr was positively correlated with Fe and Mn at the different spots ($R^2 = 0.84$ and 0.73 for Cr-Fe and Cr-Mn, respectively in spot A; 0.72 and 0.75, respectively, in spot B; and 0.93 and 0.89, respectively, in spot C) (Fig. 7). Cr was highly positively correlated with Fe and Mn-bearing in Cr-loaded RL saprolites (Fig. S8). Vanadium was also correlated with Fe and Mn at spots A, B and C in V-loaded Union County saprolite (UC-2) ($R^2 = 0.94$ and 0.97 respectively; 0.71 and 0.56 respectively and, 0.61 and 0.48 respectively) (Fig. 8).
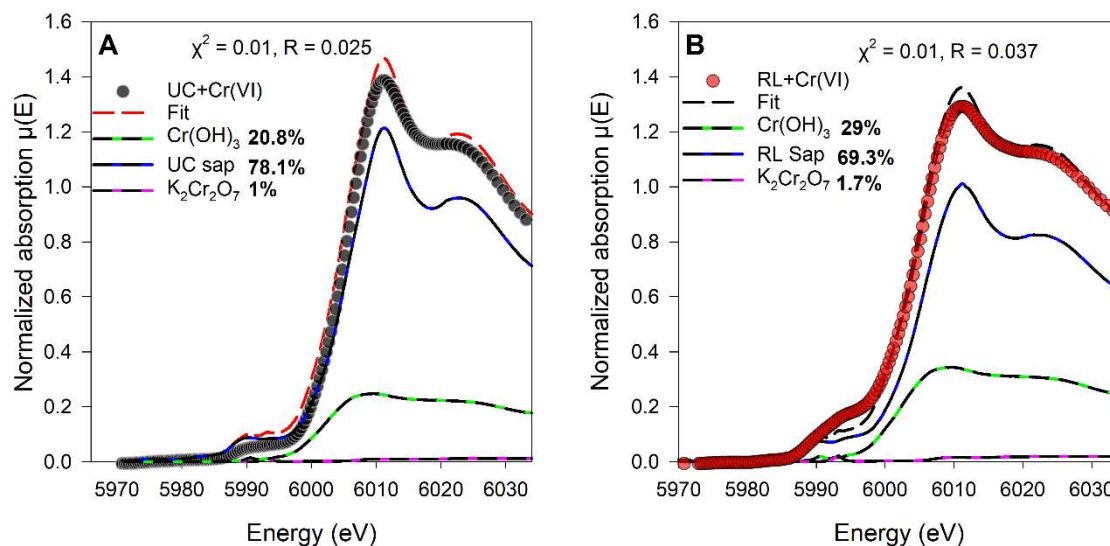
Fig 5: Linear combination fits of Cr K-edge XANES normalized spectra of A) Cr-loaded (60 μM) Union County saprolite and B) Cr-loaded (60μM) Redlair saprolite. Native saprolite, $K_2Cr_2O_7$ and $Cr(OH)_3$ standard spectra are shown as references. Black and red dots show experimental data and red and black dashed lines represent the LCF fits for Cr-loaded UC and RL saprolites, respectively.
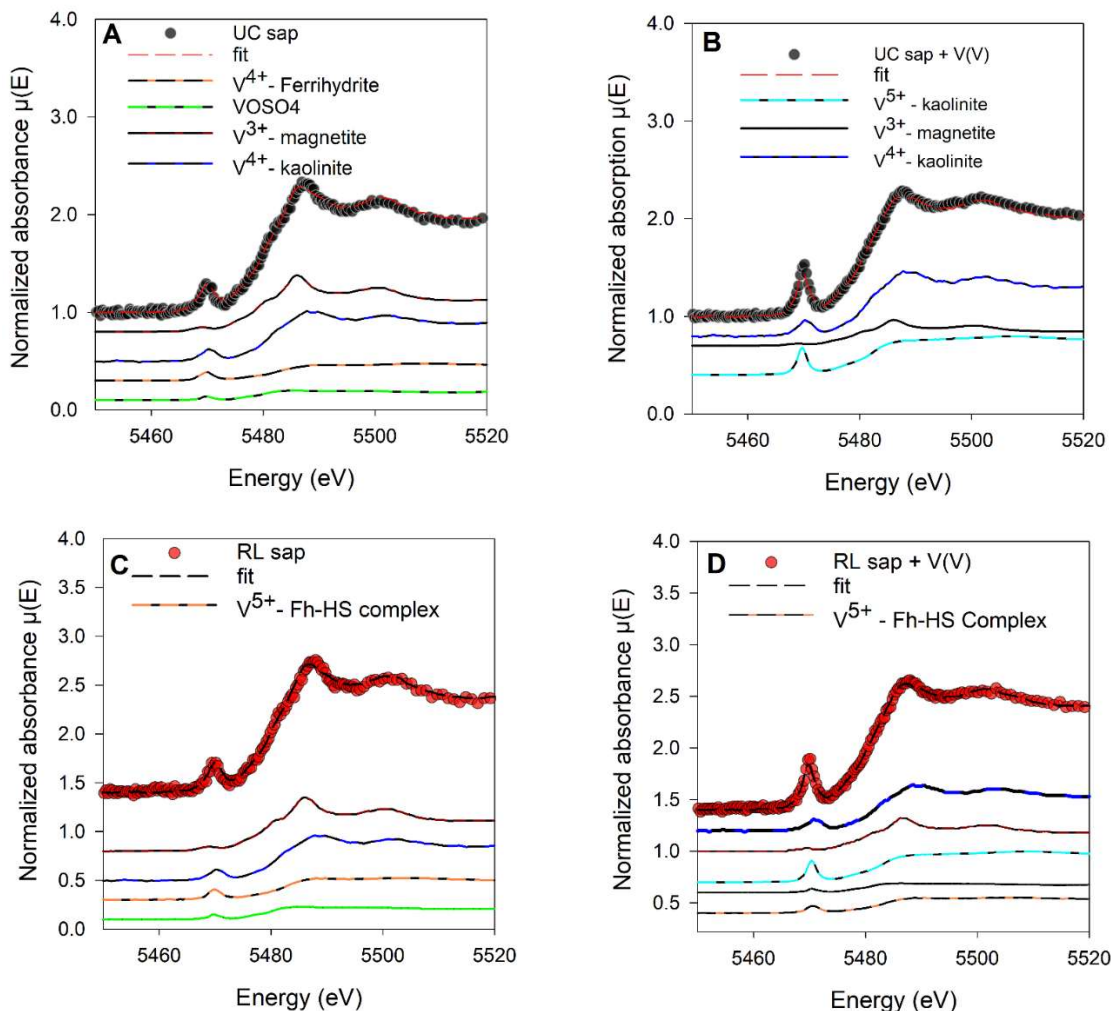
Fig 6: Linear combination fits of V K-edge XANES normalized spectra of A) native Union County saprolite materials, B) V-loaded (450 μM) Union County, C) native Redlair saprolite, and D) V-loaded (450 μM), Redlair saprolite. Black and red dots show experimental data and red and black dashed lines represent the LCF fits for native and V-loaded UC and RL saprolites, respectively.
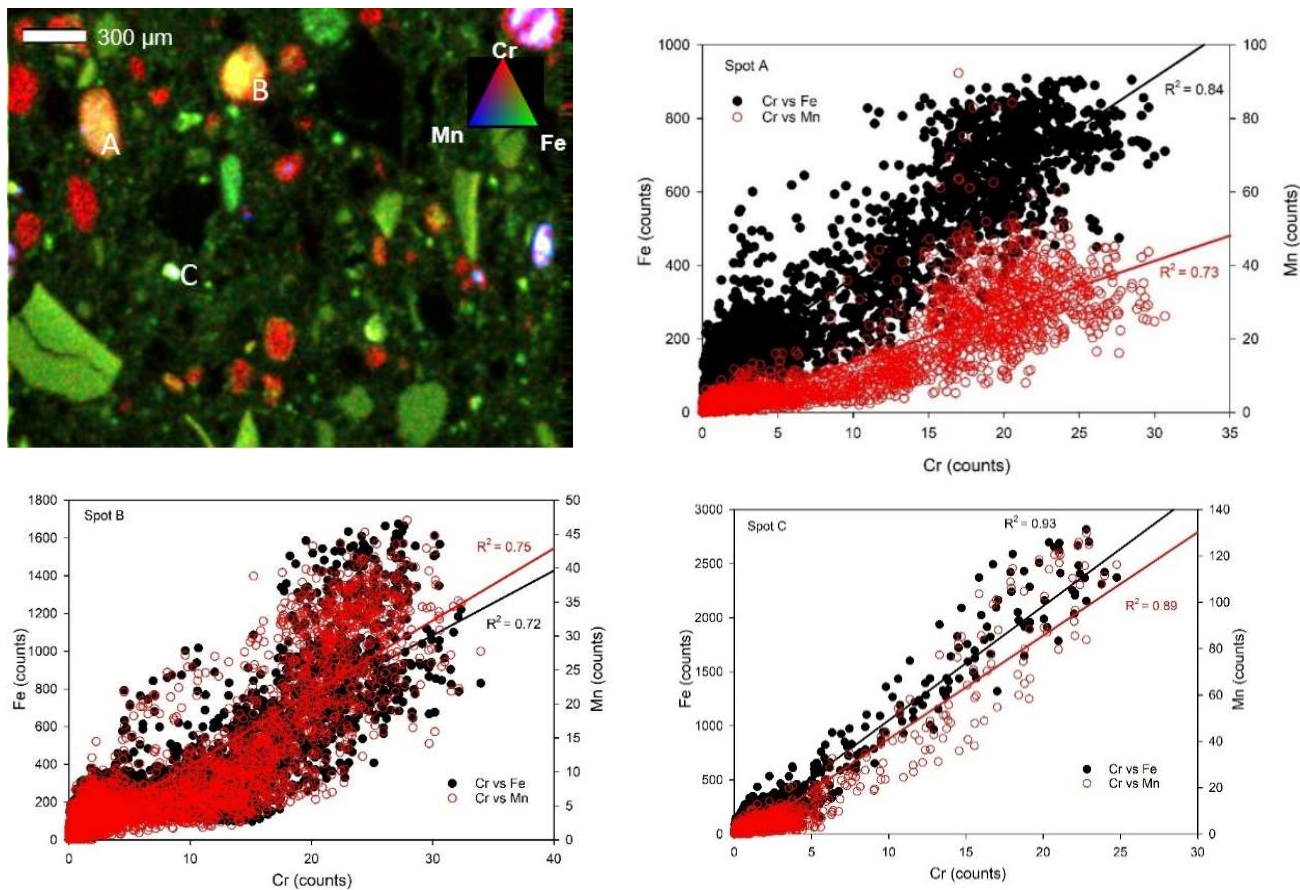
Fig 7: Solid-phase Cr, Fe and Mn spatial associations. (A) Tricolor μ-XRF maps of Cr-loaded (60 μM) Union County saprolite (UC-1). Alphabetical labels represent areas chosen for elemental correlation analysis. Red, green, and blue colors represent Cr, Fe and Mn counts, respectively. (B-D) Correlation plots of Cr, Fe and Mn at spots A, B and C, respectively.
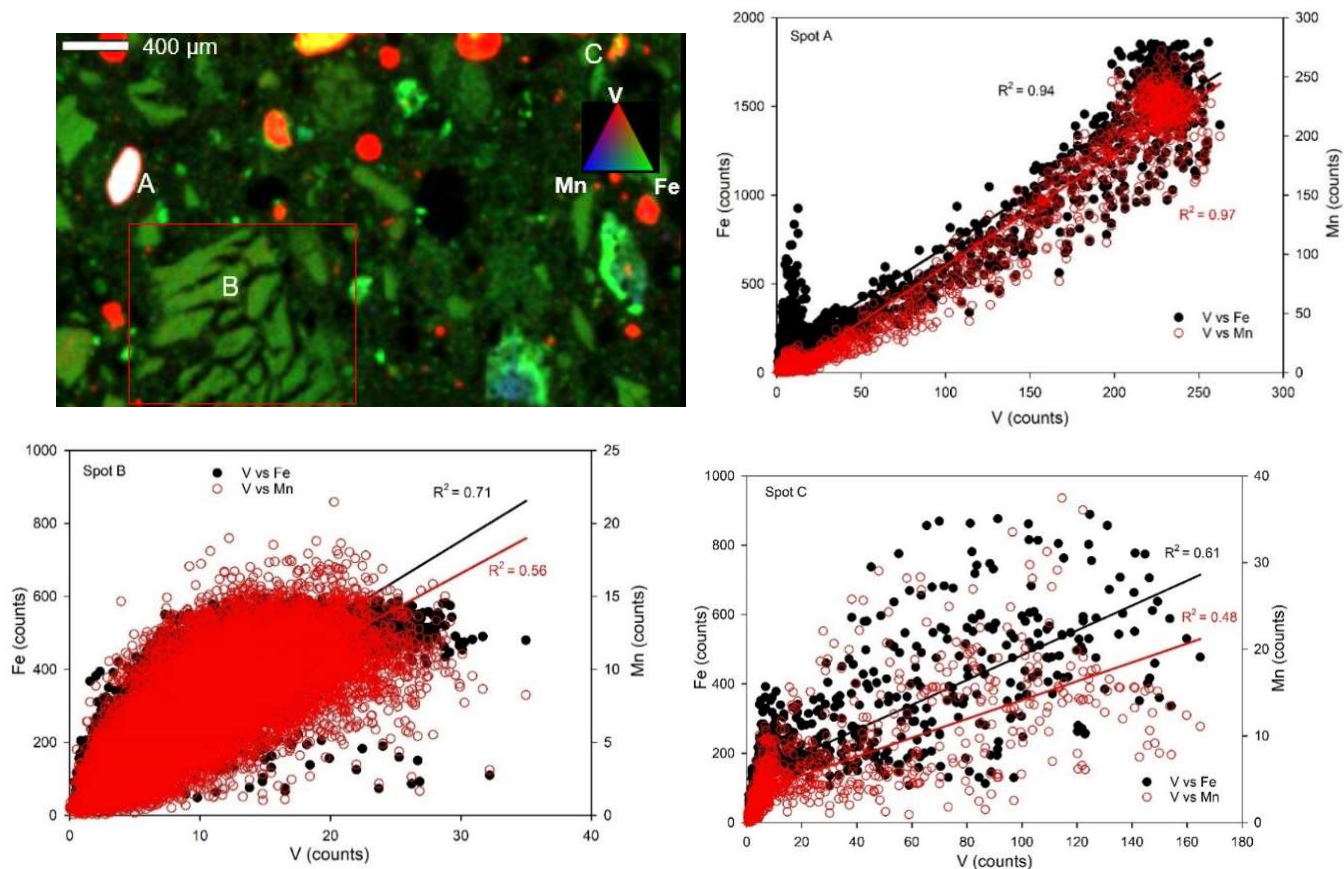
Figure 8: Solid-phase V, Fe and Mn spatial associations. (A) Tricolor μ-XRF maps of V-loaded (450 μM) Union County saprolite (UC-2). Alphabetical labels represent areas chosen for elemental correlation analysis. Red, green, and blue colors represent V, Fe and Mn counts, respectively. (B-D) Correlation plots of V, Fe and Mn at spots A, B and C, respectively.

4 DISCUSSION

4.1 Controls on Cr biding to saprolites

Prior studies have shown the sorption of Cr(VI) on the surface of soils and synthetic Fe and Mn(oxyhydr)oxide surfaces.(Gonzalez-Rodriguez & Fernandez-Marcos, 2021; Landrot, Ginder-vogel, et al., 2012; Whitaker et al., 2018) Here, the results of our sorption experiments showed extensive Cr sorption on UC and RL saprolites, with both saprolites sorbing similar amounts of Cr. The maximum sorption capacities (36.4 mg Cr/kg and 31.2 mg Cr/kg) calculated from Langmuir isotherm models for both UC and RL saprolites were in close agreement with the experimental equilibrium capacities (32.3 ± 1.0 mg Cr/kg and 32.6 ± 1.9 mg Cr/kg). While both

saprolites sorbed similar amounts of Cr, additional kinetic studies showed that the rates of sorption of Cr onto UC (10.6 mg g hr^{-1}) and RL (5.6 mg g hr^{-1}) predicted by pseudo second order reaction differed considerably. We hypothesize that this may be due to the greater proportions of amorphous Fe and Mn(oxyhydroxide) surfaces present in the UC saprolite, (Choppala et al., 2018; Lilli et al., 2019) a supposition that is in concert with other authors who have found that natural and synthetic Fe oxyhydroxides could increase Cr sorption. (S. E. Fendorf, 1995; Johnston & Chrysochoou, 2014; P. Johnston & Chrysochoou, 2012; Whitaker et al., 2018) In addition, our XANES results show the presence of mixed-valence Fe-bearing phases, which can reduce added Cr(VI) and sorb the resulting Cr(III), and the lack of defined Cr(VI) peak in our Cr K-edge XANES spectra and LCF fits indicate the reduction of Cr on both Cr-loaded saprolites (Fig. 5). This is in agreement with other researchers who have reported extensive evidence of Fe(II) minerals participating in the abiotic reduction of Cr(VI) to Cr(III).(Agrawal et al., 2009; S. Fendorf et al., 2000; Joe-Wong et al., 2017; Liao et al., 2019; Whitaker et al., 2018).

Although we could not distinguish primary and secondary Fe-phases with our spectroscopic imaging technique, µ-XRF analysis showed that Fe-bearing minerals are important host phases for added Cr. This was highlighted by the positive correlation between Cr, Fe and Mn in our Cr-loaded (UC-1 and RL-1) samples (Figs. 7 and S8). Although Mn is < 0.15 wt.% in our saprolites, the correlation between Cr and Mn may be because the surface function group on the mixed-valence variably charged Mn-bearing phase was slightly deprotonated at the pH of our experiment the electrostatic attraction could have resulted in the sorption of Cr(III) on Mn-bearing phases, and/or Mn was simply associated with the same Fe phases that retained Cr.(Zhang et al., 2020) Nevertheless, spectroscopic imaging confirms that Fe and Mn-bearing minerals are important sorbents for Cr in both the UC and RL saprolites, findings also supported by the chemical extractions of Cr-loaded saprolites. Overall, our analytical data supports structural incorporation and sorption on amorphous variably charged Fe-oxides and crystalline Fe phases as the main mechanisms for Cr retention.

4.2 Controls on V biding to saprolites

Vanadium has been shown to strongly adsorb on the surface of Fe, Mn, Al-bearing, and clays minerals (Gäbler et al., 2009; Gonzalez-Rodriguez & Fernandez-Marcos, 2021; Larsson et al., 2015, 2017; Shaheen et al., 2019). Here, maximum sorption capacities from our Langmuir

adsorption isotherm model show that the UC (294.1 mg/kg) and RL saprolites (344.8 mg/kg) could sorb similar amounts of V. Interestingly, both saprolites' affinity for V was about an order of magnitude greater than for Cr. This could be as result of the binding mechanism of Cr and V on Fe-oxide oxide phases. Cr is known to form both inner- and outer-sphere complexes with Fe-oxides, however, V has been shown to exclusively form strong covalent, inner-sphere polymeric complexes with Fe oxides, especially at higher concentrations such those used in our study (Abernathy et al., 2022; Vessey & Lindsay, 2020) In our studies, although speciation of V in native saprolites was V(IV), XANES analyses of V-loaded samples suggested the mixed-species of V(IV&V) may coexist (Fig 6B and D). The presence of small amounts of Fe(II)-bearing minerals in UC and RL saprolites could have reduced V(V), producing mixed-valence V species and modulating the retention and reduction of V. (Wisawapipat & Kretzschmar, 2017) (O'Loughlin et al., 2021).

Kinetic studies showed that the rate of sorption for V species onto UC saprolite (63.4 g mg hr^{-1}) was higher than onto the RL saprolite (26.7 g mg hr^{-1}). These rates are higher than for V sorption onto soil materials such as yellow cinnamon, manual loessal and aeolian soil (11.4, 9.6 and 4.2 g mg^{-1} hr^{-1}).(Y. Jiang et al., 2019) The reason for slightly higher maximum sorption capacity of V on RL remains unclear, though the greater amount of Fe (oxyhydr)oxides in RL, sorption of V on organic matter or Fe mineral phases with higher surface areas could be factors. Previous studies have shown that due to high surface area, site density and abundant singly and doubly coordinated -OH groups, Fe (oxyhydr)oxides can display high adsorption capacities for V and the adsorption capacity of these Fe-bearing phases may be further increased with the addition of organic matter.(Abernathy et al., 2022).

Chemical extractions revealed that for any of our extractants, CBD released the most amounts of total V from the native UC (5% of total V released) and RL (37% of total V released) saprolites, highlighting the occurrence of V in crystalline mineral phases. This is comparable with the work of Wisawapipat and Kretzschmar (Wisawapipat & Kretzschmar, 2017) which showed that ~38% of V was extracted from crystalline Fe-oxides in well weathered soils. Contrastingly, CBD extractions released the least V in the V-loaded RL saprolite, while the highest V was released by amorphous phases in UC saprolite. Our collective data suggest V was preferentially substituted into vacant sites in crystalline Fe phases in the native RL saprolites, but when these sites became saturated due to increased V sorption in V-loaded RL saprolites, V was

either sorbed onto amorphous surfaces or ionically bound on surfaces of other minerals in the saprolite.(Baldermann & Stamm, 2022; Kajjumba et al., 2018) $MgCl_2$ extractions which targeted ionically sorbed metals showed that ~250 and 100 times the initial native V concentration was released in the V-loaded UC and RL saprolites indicating a dominant electrostatic interaction mechanism for V(V) retention. To further highlight this, our follow-up experiment showed that increasing ionic strength increased V adsorption in UC saprolite (Fig. S9). Results from XANES analysis suggest that V in native and V-loaded UC and RL saprolites may be associated with Fe oxide phases. In addition, XANES LCF also indicated that up to 34 – 83% V in both native and loaded saprolite samples were associated kaolinite phases. This is unsurprising because XRD showed the presence of 1:1 crystalline clay minerals (nacrite and kaolinite) in our saprolites. Lastly, μ-XRF results also corroborated the association of V with Fe and Mn phases in UC V-loaded saprolites, with strongly positive correlations of up to 0.94 and 0.97 recorded for V-Fe and V-Mn, respectively.

Our data indicate that the proposed possible mechanism of retention in both Cr and V-loaded saprolites is a combination of sorption by surface complexation, electrostatic interactions, and ion exchange, while structurally incorporation is the dominant process in native saprolites. The presence of exchangeable Cr and V in Cr- and V-loaded saprolites indicates a potential for easy release. In our native saprolites, minimal amounts of Cr and V were associated with ionically active species. However, in Cr- and V-loaded saprolites, a small fraction of Cr was found to be environmentally labile (4 E and F). This finding holds significant environmental implications, especially in the presence of chloride and phosphate introduced into the environment. Under conditions explored in this study, phosphates and chlorides can outcompete weakly sorbed Cr and V for adsorption sites, potentially facilitating their release into the environment.

4.3. Significance for groundwater quality

The release of Cr and V into groundwater poses significant health and environmental risks. Our study demonstrates the potential for elemental release from various host phases in these chemically diverse piedmont saprolites. Although these native saprolites contain relatively less toxic and mobile Cr(III) and V(IV), moderate fractions of these species could still be released into the environment. Particularly in settings with complex and evolving groundwater

chemistry, and in the presence of abundant reactive Mn-oxides, interactions with saprolites may oxidize Cr and V. These contaminants, once mobilized, could easily be transported by advection currents, posing a threat to groundwater quality. However, in the absence of anthropogenic influences, amorphous and crystalline phases like Fe and Mn(oxyhydr)oxides, as well as aluminosilicate clays, might temporarily serve as crucial host phases in sorbing and immobilizing a significant proportion of mobile Cr and V.

The influx of anthropogenic chemicals like dissolved organic carbon and fertilizers from surface sources significantly impacts the fate and transport of Cr and V. Activities such as fertilizer application and concentrated animal feeding operations (CAFOs) can lead to the release of nitrate and phosphate into the environment. Nitrate, as a strong oxidant, influences soil and groundwater redox chemistry, while phosphates can substitute for adsorbed Cr or V, facilitating their release from amorphous and crystalline host phases. This effect is particularly pronounced for weakly sorbed and exchangeable Cr and V. In addition, shifts in land use can introduce dissolved organic carbon, modulating the release of Cr and V from amorphous Fe and clay mineral phases into groundwater. Our findings underscore the significant influence of Cr and V bound to amorphous and ionically exchangeable host phases on contaminant release and retention dynamics in chemically diverse saprolites. Future research could therefore examine the role of common organic carbon proxies in facilitating the transport of Cr and V from near surface sediments and aquifer materials.

5. CONCLUSION

Analytical techniques such as XAS and μ-XRF revealed that Cr and V in both native and loaded saprolite samples were associated with iron oxides and Mn-bearing minerals. Across all samples and treatments, Cr primarily existed as Cr(III), likely precipitated as Cr(OH)$_3$ even after being introduced as Cr(VI) in solution. Vanadium, on the other hand, existed as a combination of V(IV) and V(V) species, and introduced V was associated with Fe-oxides, kaolinite, and other clay minerals. Overall, this study has shown that the mechanisms controlling Cr and V retention include sorption on clay minerals, Fe and Mn-oxides by surface complexation and electrostatic interactions.

Although both Cr and V were strongly retained onto NC Piedmont saprolites, higher sorption capacities were observed for V over Cr, but sorption of each species was rapid and

conformed to pseudo-second order kinetic models, indicating binding by chemisorption. Finally, although Cr and V were primarily strongly sorbed to mineral phases, the presence of exchangeable forms of V in native and loaded saprolites was also observed, indicating a repository of easily mobilizable forms of this emerging contaminant. More studies are needed to determine how land use and management strategies may impact the release of both Cr and V from their host phases to compromise groundwater quality.

REFRENCES

Abernathy, M. J., Schaefer, M. V., Ramirez, R., Garniwan, A., Lee, I., Zaera, F., Polizzotto, M. L., & Ying, S. C. (2022). Vanadate Retention by Iron and Manganese Oxides. *ACS Earth and Space Chemistry*, *6*(8), 2041–2052. https://doi.org/10.1021/acsearthspacechem.2c00116

Agrawal, S. G., Fimmen, R. L., & Chin, Y. P. (2009). Reduction of Cr(VI) to Cr(III) by Fe(II) in the presence of fulvic acids and in lacustrine pore water. *Chemical Geology*, *262*(3–4), 328–335. https://doi.org/10.1016/j.chemgeo.2009.02.001

Baldermann, A., & Stamm, F. M. (2022). Effect of kinetics, pH, aqueous speciation and presence of ferrihydrite on vanadium (V) uptake by allophanic and smectitic clays. *Chemical Geology*, *607*(July). https://doi.org/10.1016/j.chemgeo.2022.121022

C. Scheinost, A., Kretzschmar, R., Pfister, S., & R. Roberts, D. (2002). Combining Selective Sequential Extractions, X-ray Absorption Spectroscopy, and Principal Component Analysis for Quantitative Zinc Speciation in Soil. *Environmental Science & Technology*, *36*(23), 5021–5028. https://doi.org/10.1021/es025669f

Choppala, G., Kunhikrishnan, A., Seshadri, B., Park, J. H., Bush, R., & Bolan, N. (2018). Comparative sorption of chromium species as influenced by pH, surface charge and organic matter content in contaminated soils. *Journal of Geochemical Exploration*, *184*, 255–260. https://doi.org/10.1016/j.gexplo.2016.07.012

Coyte, R. M., McKinley, K. L., Jiang, S., Karr, J., Dwyer, G. S., Keyworth, A. J., Davis, C. C., Kondash, A. J., & Vengosh, A. (2020). Occurrence and distribution of hexavalent chromium in groundwater from North Carolina, USA. *Science of the Total Environment*, *711*. https://doi.org/10.1016/j.scitotenv.2019.135135

Coyte, R. M., & Vengosh, A. (2020). Factors Controlling the Risks of Co-occurrence of the Redox-Sensitive Elements of Arsenic, Chromium, Vanadium, and Uranium in Groundwater from the Eastern United States. *Environmental Science and Technology*, *54*(7), 4367–4375. https://doi.org/10.1021/acs.est.9b06471

Ding, Z., Sun, G., Fu, F., & Ye, C. (2022). Phase transformation of Cr(VI)-adsorbed ferrihydrite in the presence of Mn(II): Fate of Mn(II) and Cr(VI). *Journal of Environmental Sciences*

(China), *113*, 251–259. https://doi.org/10.1016/j.jes.2021.06.012

Fendorf, S. E. (1995). Surface reactions of chromium in soils and waters. *Geoderma*, *67*(1–2),
55–71. https://doi.org/10.1016/0016-7061(94)00062-F

Fendorf, S., Wielinga, B. W., & Hansel, C. M. (2000). Chromium transformations in natural
environments: The role of biological and abiological processes in chromium(vi) reduction.
International Geology Review, *42*(8), 691–701.
https://doi.org/10.1080/00206810009465107

Gäbler, H. E., Glüh, K., Bahr, A., & Utermann, J. (2009). Quantification of vanadium adsorption
by German soils. *Journal of Geochemical Exploration*, *103*(1), 37–44.
https://doi.org/10.1016/j.gexplo.2009.05.002

Gillispie, E. C., Austin, R. E., Rivera, N. A., Bolich, R., Duckworth, O. W., Bradley, P.,
Amoozegar, A., Hesterberg, D., & Polizzotto, M. L. (2016). Soil Weathering as an Engine
for Manganese Contamination of Well Water. *Environmental Science and Technology*,
50(18), 9963–9971. https://doi.org/10.1021/acs.est.6b01686

Gonzalez-Rodriguez, S., & Fernandez-Marcos, M. L. (2021). Sorption and desorption of
vanadate, arsenate and chromate by two volcanic soils of equatorial africa. *Soil Systems*,
5(2). https://doi.org/10.3390/soilsystems5020022

Gustafsson, J. P. (2019). Vanadium geochemistry in the biogeosphere –speciation, solid-solution
interactions, and ecotoxicity. *Applied Geochemistry*, *102*(October 2018), 1–25.
https://doi.org/10.1016/j.apgeochem.2018.12.027

J. Abernathy, M., V. Schaefer, M., J. Vessey, C., Liu, H., & C. Ying, S. (2021). Oxidation of
V(IV) by Birnessite: Kinetics and Surface Complexation. *Environmental Science &
Technology*, *55*(17), 11703–11712. https://doi.org/10.1021/acs.est.1c02464

Jardine, P. M., Fendorf, S. E., Mayes, M. A., Larsen, I. L., Brooks, S. C., & Bailey, W. B.
(1999). Fate and transport of hexavalent chromium in undisturbed heterogeneous soil.
Environmental Science and Technology, *33*(17), 2939–2944.
https://doi.org/10.1021/es981211v

Jiang, B., Gong, Y., Gao, J., Sun, T., Liu, Y., Oturan, N., & Oturan, M. A. (2019). The reduction

of Cr(VI) to Cr(III) mediated by environmentally relevant carboxylic acids: State-of-the-art and perspectives. In *Journal of Hazardous Materials* (Vol. 365, pp. 205–226). Elsevier B.V. https://doi.org/10.1016/j.jhazmat.2018.10.070

Jiang, S., Yan, X., Peacock, C. L., Zhang, S., Li, W., Zhang, J., Feng, X., Liu, F., & Yin, H. (2020). Adsorption of Cr(VI) on Al-substituted hematites and its reduction and retention in the presence of Fe2+ under conditions similar to subsurface soil environments. *Journal of Hazardous Materials*, *390*, 122014. https://doi.org/10.1016/J.JHAZMAT.2019.122014

Jiang, Y., Yin, X., Luo, X., Yu, L., Sun, H., Wang, N., & Mathews, S. (2019). Sorption of vanadium (V) on three typical agricultural soil of the Loess Plateau, China. *Environmental Pollutants and Bioavailability*, *31*(1), 120–130. https://doi.org/10.1080/26395940.2019.1590162

Joe-Wong, C., Brown, G. E. J., & Maher, K. (2017). Kinetics and Products of Chromium(VI) Reduction by Iron(II/III)-Bearing Clay Minerals. *Environmental Science & Technology*, *51*(17), 9817–9825. https://doi.org/10.1021/acs.est.7b02934

Johnston, C. P., & Chrysochoou, M. (2014). Mechanisms of chromate adsorption on hematite. *Geochimica et Cosmochimica Acta*, *138*, 146–157. https://doi.org/10.1016/j.gca.2014.04.030

Kajjumba, G. W., Aydın, S., & Güneysu, S. (2018). Adsorption isotherms and kinetics of vanadium by shale and coal waste. *Adsorption Science and Technology*, *36*(3–4), 936–952. https://doi.org/10.1177/0263617417733586

Keon, N. E., Swartz, C. H., Brabander, D. J., Harvey, C., & Hemond, H. F. (2001). Validation of an arsenic sequential extraction method for evaluating mobility in sediments. *Environmental Science and Technology*, *35*(13), 2778–2784. https://doi.org/10.1021/es001511o

LaFayette, G. N., Knappett, P. S. K., Li, Y., Loza-Aguirre, I., & Polizzotto, M. L. (2020). Geogenic sources and chemical controls on fluoride release to groundwater in the Independence Basin, Mexico. *Applied Geochemistry*, *123*(December 2019), 104787. https://doi.org/10.1016/j.apgeochem.2020.104787

Landrot, G., Ginder-Vogel, M., Livi, K., Fitts, J. P., & Sparks, D. L. (2012). Chromium(III) oxidation by three poorly-crystalline manganese(IV) oxides. 1. chromium(III)-oxidizing capacity. *Environmental Science and Technology*, *46*(21), 11594–11600. https://doi.org/10.1021/es302383y

Landrot, G., Ginder-vogel, M., Livi, K., Fitts, P., & Sparks, D. L. (2012). *Chromium (III) Oxidation by Three Poorly-Crystalline Manganese (IV) Oxides . 1 . Chromium (III) - Oxidizing Capacity*. *Iii*.

Larsson, M. A., D'Amato, M., Cubadda, F., Raggi, A., Öborn, I., Kleja, D. B., & Gustafsson, J. P. (2015). Long-term fate and transformations of vanadium in a pine forest soil with added converter lime. *Geoderma*, *259–260*, 271–278. https://doi.org/10.1016/j.geoderma.2015.06.012

Larsson, M. A., Hadialhejazi, G., & Gustafsson, J. P. (2017). Vanadium sorption by mineral soils: Development of a predictive model. *Chemosphere*, *168*, 925–932. https://doi.org/10.1016/j.chemosphere.2016.10.117

Liang, J., Huang, X., Yan, J., Li, Y., Zhao, Z., Liu, Y., Ye, J., & Wei, Y. (2021). A review of the formation of Cr(VI) via Cr(III) oxidation in soils and groundwater. *Science of The Total Environment*, *774*, 145762. https://doi.org/10.1016/J.SCITOTENV.2021.145762

Liao, W., Ye, Z., Yuan, S., Cai, Q., Tong, M., Qian, A., & Cheng, D. (2019). Effect of Coexisting Fe(III) (oxyhydr)oxides on Cr(VI) Reduction by Fe(II)-Bearing Clay Minerals. *Environmental Science and Technology*, *53*(23), 13767–13775. https://doi.org/10.1021/acs.est.9b05208

Lilli, M. A., Nikolaidis, N. P., Karatzas, G. P., & Kalogerakis, N. (2019). Identifying the controlling mechanism of geogenic origin chromium release in soils. *Journal of Hazardous Materials*, *366*, 169–176. https://doi.org/10.1016/j.jhazmat.2018.11.090

O'Loughlin, E., Boyanov, M., & Kemner, K. (2021). *Reduction of Vanadium (V) by Iron (II)-Bearing Minerals. Minerals 2021, 11, 316*. 1–21. https://doi.org/https://doi.org/10.3390/

Oze, C., Bird, D. K., & Fendorf, S. (2007). Genesis of hexavalent chromium from natural sources in soil and groundwater. *Proceedings of the National Academy of Sciences of the*

United States of America, *104*(16), 6544–6549. https://doi.org/10.1073/pnas.0701085104

Oze, C., Fendorf, S., & Coleman, R. G. (2002). *Chromium Geochemistry in Serpentinized Ultramafic Rocks and Serpentine Soils From the Franciscan Formation of California Organic Matter Mineralization and Metal Cycling During Flood Plain Evolution View project Uranium sequestration View project*. https://www.researchgate.net/publication/252099396

P. Johnston, C., & Chrysochoou, M. (2012). Investigation of Chromate Coordination on Ferrihydrite by in Situ ATR-FTIR Spectroscopy and Theoretical Frequency Calculations. *Environmental Science & Technology*, *46*(11), 5851–5858. https://doi.org/10.1021/es300660r

Pan, C., Liu, H., Catalano, J. G., Wang, Z., Qian, A., & Giammar, D. E. (2019). Understanding the Roles of Dissolution and Diffusion in Cr(OH) 3 Oxidation by Î-MnO 2. *ACS Earth and Space Chemistry*, *3*(3), 357–365. https://doi.org/10.1021/acsearthspacechem.8b00129

Schlesinger, W. H., Klein, E. M., & Vengosh, A. (2017). Global biogeochemical cycle of vanadium. *Proceedings of the National Academy of Sciences of the United States of America*, *114*(52), E11092–E11100. https://doi.org/10.1073/pnas.1715500114

Shaheen, S. M., Alessi, D. S., Tack, F. M. G., Ok, Y. S., Kim, K. H., Gustafsson, J. P., Sparks, D. L., & Rinklebe, J. (2019). Redox chemistry of vanadium in soils and sediments: Interactions with colloidal materials, mobilization, speciation, and relevant environmental implications - A review. *Advances in Colloid and Interface Science*, *265*, 1–13. https://doi.org/10.1016/j.cis.2019.01.002

Vengosh, A., Coyte, R., Karr, J., Harkness, J. S., Kondash, A. J., Ruhl, L. S., Merola, R. B., & Dywer, G. S. (2016). Origin of Hexavalent Chromium in Drinking Water Wells from the Piedmont Aquifers of North Carolina. *Environmental Science and Technology Letters*, *3*(12), 409–414. https://doi.org/10.1021/acs.estlett.6b00342

Vessey, C. J., & Lindsay, M. B. J. (2020). Aqueous Vanadate Removal by Iron(II)-Bearing Phases under Anoxic Conditions. *Environmental Science and Technology*, *54*(7), 4006–4015. https://doi.org/10.1021/acs.est.9b06250

Wang, Z. Q., Yu, Y., Zhang, X. H., & Komorowski, J. (2014). Chromium-insulin reduces insulin clearance and enhances insulin signaling by suppressing hepatic insulin-degrading enzyme and proteasome protein expression in KKAy mice. *Frontiers in Endocrinology*, *5*(JUL), 1–6. https://doi.org/10.3389/fendo.2014.00099

Whitaker, A. H., Peña, J., Amor, M., & Duckworth, O. W. (2018). Cr(VI) uptake and reduction by biogenic iron (oxyhydr)oxides. *Environmental Science: Processes and Impacts*, *20*(7), 1056–1068. https://doi.org/10.1039/c8em00149a

Wisawapipat, W., & Kretzschmar, R. (2017). Solid Phase Speciation and Solubility of Vanadium in Highly Weathered Soils. *Environmental Science and Technology*, *51*(15), 8254–8262. https://doi.org/10.1021/acs.est.7b01005

Wright, M. T., & Belitz, K. (2010). Factors controlling the regional distribution of vanadium in groundwater. *Ground Water*, *48*(4), 515–525. https://doi.org/10.1111/j.1745-6584.2009.00666.x

Zhang, H., Xu, F., Xue, J., Chen, S., Wang, J., & Yang, Y. (2020). Enhanced removal of heavy metal ions from aqueous solution using manganese dioxide-loaded biochar: Behavior and mechanism. *Scientific Reports*, *10*(1), 1–13. https://doi.org/10.1038/s41598-020-63000-z

IMPACT OF LABILE ORGANIC CARBON AND MANGANESE OXIDE ON CHROMIUM AND VANADIUM TRANSPORT: IMPLICATIONS FOR GROUNDWATER CONTAMINATION

Reproduced with permission from Balogun, F.O., Koeneke M.W., Peel, H.R., Vinson, D.S., Duckworth O.W. and Polizzotto, M.L. (in preparation for submission) Mineralogical controls on chromate and vanadate mobility in the North Carolina Piedmont: Implications for groundwater contamination.

INTRODUCTION

Geogenic contaminants represent substantial threats to human health through natural contamination of well water, yet great variability remains in how these threats are understood and managed. For instance, chromium (Cr) is on the list of the top 25 hazardous substances known to pose significant health and safety risks at superfund sites.[1] Numerous studies have documented cases of groundwater exceeding the 100 µg/L maximum contaminant level (MCL) set by both the United States Environmental Protection Agency (USEPA) and the World Health organization (WHO) for total Cr in drinking water, and millions of people in the United States consume Cr-contaminated drinking water. On the other hand, vanadium (V) is an emerging unregulated contaminant of equal public health concern in drinking water.[2] But while pentavalent V has been listed by the International Agency for Research on Cancer (IARC) as a possible carcinogen [3,4], very limited data exist on V in drinking water.[5] Occasionally, contamination of well and groundwater by Cr and V results from point sources such agricultural and industrial applications. However, due to the failure of the USEPA to regulate the carcinogenic forms of Cr and V in drinking water, the release of these elements from chemically variable geogenic sources has gained attention over the last few decades.

Although Cr and V are recognized and regulated differently, these two contaminants frequently co-occur in groundwater because they share similar geologic provenances and redox profiles that govern their distributions and solubilities. The predominant factors that control Cr and V mobility and solubility in these settings are pH and oxidation state. Weathering of primary host phases in geologic materials often results in the association of Cr and V with reactive secondary alteration products, such as Fe and Mn(oxyhydr)oxides. Depending on the prevalent

groundwater chemistry and mineralogy, Fe and Mn-bearing minerals are involved in the biotic and abiotic retention, release, or transformation of Cr and V via pH-dependent biogeochemical processes such as desorption and dissolution.[6–8] Iron and Mn (oxyhydr)oxides are particularly important because apart from sorbing contaminants, they can thermodynamically poise redox reactions responsible for Cr and V mobility, depending on the availability of organic carbon and other critical reductants.

In the natural environment, Mn oxides (MnO_2) are widespread and play important roles in controlling Cr and V release into groundwater through sorption and redox transformation [9,10]. With the exception of hausmanite, a strong correlation between Mn oxide surface area and oxidative capacity has been observed, with birnessite being the most reactive Mn oxide commonly found in the environment.[11–14] Research has also shown that the amount of Mn-oxides may be a good predictor of the release to groundwater of certain redox-active trace elements, such as Cr and As [5,15,16], though notably not V.[17,18] [14,19] Numerous studies have investigated the oxidative release of Cr and V from pure mineral phases, but the our understanding of their release profiles by Mn oxides in heterogenous geologic phases is poorly understood.

In addition to Mn-oxides, natural organic matter (NOM) has been observed to impact cycling of Cr, V and other redox-active elements.[20] Soil organic matter is comprised of different types of organic fragments and microbial products at varying stages of decomposition, which can stimulate metal dissolutions and release. [20,21] These organic products are made up of aliphatic and aromatic compounds which differ in reactivity towards redox-active elements depending on prevailing redox conditions.[17,22–25] For instance, organic acids such as citric acid (CA) and oxalate have been reported to release Cr from soil by complexation reactions and competition for adsorption sites.[24,26] However, the combined interactions of these low-molecular weight organic acids (LMWOA) and minerals on contaminants in natural systems remain unclear.

Changes to redox conditions, mineralogical properties, biological activity and sorption parameters can all influence contaminant cycles in the environment.[8,27–29] We hypothesized that introduction of LMWOA or Mn oxides to aquifer materials would enhance Cr and V release from natural aquifer materials by enhancing microbial stimulation, promoting abiotic dissolution of Cr and V host phases, or poising redox conditions at states conducive to Cr and V mobilization. By using chemically and geologically variable saprolite materials from two field sites in the North Carolina Piedmont, we aimed to 1) quantify the biotic and abiotic release of Cr

and V due to OA and birnessite inputs, and 2) determine how changes in elemental speciation and mineralogy may impact the release of Cr and V from the solid to solution phase. Results from this study may provide insights into how natural chemical inputs to aquifers, such as those stemming from changes in land management patterns, may impact contaminant mobility and threaten environmental quality.

MATERIALS AND METHODS

Saprolite characterization

Our saprolite samples were collected from a park in Union County (UC; metasedimentary terrain) and Redlair Observatory, Gaston County (RL; felsic metavolcanic terrain), North Carolina, in a method described in the previous chapter (Fig. S1). Several bags of saprolite were collected from these sites based on their colors, which gave insights into the relative abundance of secondary Fe minerals. Native saprolite materials were characterized with X-ray diffraction (XRD), X-ray absorption spectroscopy (XAS), Brunauer-Emmett-Teller (BET) surface-area analysis, and chemical extraction. For mineral phase identification, XRD patterns of native saprolite samples were obtained using a Rigaku benchtop X-ray diffractometer with a diffracted beam monochromator for Cu Kα radiation with a scan range of $3 - 90°$ 2θ and a scan rate of $0.02°$ 2θ/min. The XRD pattern processing and phase identification were done using the JADE software. The specific surface areas of each saprolite were calculated using the multipoint BET method and the total pore volume from the nitrogen adsorbed at relative pressures ranging from $0.01 - 0.23$.

Chemicals and birnessite synthesis

All chemicals, including citric acid, used in this study were purchased from Fischer scientific. Manganese oxide in the form of acid birnessite (AB) was synthesized by using the method described by Ying et al.[30,31] The Mn-oxide was synthesized by dissolving 31.5 g of $KMnO_4$ in 1 L of double deionized (DDI) water in a 2L flask. The solution was heated on a hot plate while continuously stirred until a steady temperature of 90 °C was attained. After this, 32 mL of 12 M hydrochloric acid (HCl) was introduced into the solution while the reaction continued for another ten minutes at 90 °C. The solution was allowed to cool for 30 minutes before vacuum filtration. The precipitate oxide retained by the filter paper was resuspended in

250 mL DDI water and the suspension was again vacuum filtered. This process was repeated five times to remove the purple colored $KMnO_4$ before the oxide was collected in a weighing boat. The resulting birnessite was dried for 2 days and crushed using a porcelain mortar and pestle. The overall yield of Mn-oxide was ~6.3 g.

Anaerobic batch incubation experiment

A 40-day incubation experiment was conducted to determine the impact of chemical inputs – citric acid and birnessite Mn-oxide – on the biotic and abiotic release of Cr and V. The method used in this experiment was modified from Gillispie et al.[16] Two and a half grams of the two different saprolite materials were added to 30 mL glass vials. The first, second and third treatments were 0.05 g of MnO_2, 3 mM (low carbon), and 8 mM (high carbon) citric acid. The treatments, blank and control samples were set up for 5 sample dates. Sampling was done destructively, hence each treatment, blank, and control had its own unique sampling date.

To prepare the treatments, 6 L of 18 mΩ DDI water was purged of oxygen by boiling the water and bubbling nitrogen gas through it. Solutions, with or without citric acid, were made with 25 mM HEPES buffer and 10 mM KCl as background electrolyte; 10 mM bronopol was added to half of the total number of samples to establish abiotic controls. Vials containing 2.5 g of saprolite material were brought into the anaerobic glovebox and purged with 92% nitrogen and 8% hydrogen to remove O_2; 25 mL solution was added to each vial. Soil-free controls and blank samples were established in triplicate. The soil-free controls had 8 mM CA and/or 0.05 g of Mn-oxide, along with background solutions as described above. 420 vials containing UC and RL saprolites with various treatment solutions were crimp-sealed in the anaerobic glovebox, removed from the glovebox, covered in foil, and shaken at 165 rpm on a rotary shaker.

Samples were collected after 3, 7, 14, 28, and 40 days of incubation. At each respective sampling day, unique vials (42 per day) were taken off the shaker and brought back to the anaerobic chamber for processing. Samples were decrimped and measured for pH and Eh. The samples were then decanted into separate 15 mL test tubes, centrifuged at 4200 rpm for 10 minutes, decanted into a 15 mL syringe, and passed through a 0.2 μm nylon syringe filter. Five drops 15.8 M HNO_3 were added to each filtrate. The saprolite residue at the bottom of the decanted glass vials was resealed and stored in the anaerobic chamber. The acidified filtrates were stored at 4 °C prior to aqueous phase metal analysis.

Aqueous-phase analysis

Aqueous phase analysis for Cr, V, Mn, and Fe was conducted at the Keck Lab at the Oregon State University campus. One-hundred µL of sample was diluted at 1:50 in 4.7 mL of 2% nitric acid (HNO_3), and indium was used as an internal standard. The analysis was done using a Thermoscientific Icap-RQ single quadrupole inductively coupled plasma-mass spectrometer (ICP-MS). The instrument detection limits for Cr, V, Fe, and Mn were 1.2, 2.7, 1600, and 10 ng/L, respectively.

Bulk iron X-ray absorption spectroscopy

Native saprolite and experimentally treated material (biotic and abiotic incubations with 0-, 3- and 8-mM CA from 14, 28 and, 40 days incubation) were analyzed by extended X-ray absorption fine structure (EXAFS) spectroscopy to obtain information about Fe-mineral transformations among treatments in both saprolites. During preparation, replicate samples from each treatment were consolidated into one single composite sample, stored, and prepared for analysis under anaerobic conditions.

X-ray analysis was conducted at Beamline 11-2 at the Stanford Synchrotron Radiation Lightsource (SSRL). The samples were loaded onto acrylic sample holders and sealed with Kapton tape (non-adhesive part of Kapton in contact with sample), mounted on a digivert motor and placed at 45° to the incident X-ray beam I_0. The incident beam energy was selected using a Si(220) double crystal monochromator. Spectra were collected in fluorescence mode using a Lytle detector equipped with Soller slits positioned 90° to the incident beam. Spectra were energy calibrated by adjusting the maxima of the first derivative of a reference Fe foil to 7112 eV, background-subtracted, averaged and normalized. Iron EXAFS spectra were fitted in k-space of 3-10 with a set of mineral standards listed in Table S3. Normalized Fe EXAFS linear combination fitting (LCF) was conducted in Athena[32] for all treatments using a range Fe-bearing mineral standards to gain insights on Fe mineral phase transformations. From the combinatorial fits, the six best standards were chosen and standards that contributed less than 9% to the spectra fit were removed, then the combinatorial fits were recalculated using the remaining standards. The reported fits were normalized to 100%, but the raw summations ranged from 95-107 ± 3-8%.

Strong acid digestion

The native saprolite materials used for the anaerobic incubation experiment were analyzed for V, Cr, Fe, and Mn after an acid digestion protocol modified from EPA method 3050B.[33] This method provides "environmentally available" elemental concentrations and are referred to as "total" in this study. For acid digestion, 0.5 g of wet UC and RL saprolite material was weighed and put in a 50 mL digestion tube. 2.5 mL of 18.2 MΩ DDI water and 2.5 mL of 15.8 M HNO3 were added to each tube and vortexed. Samples were prepared in triplicates. The slurries were covered with a watch glass and allowed to sit for 16 hours. After 16 hours, the samples were heated to 95 °C on a digestion block for 15 minutes, then removed to cool for 10 minutes. After this step, 2.5 mL of 15.8 M of HNO_3 was added to each sample, vortexed, covered with watch glasses, and heated again for 30 minutes. This step was repeated once. After this, the watch glasses were removed, and digestion tubes were heated again to 95 °C for 2 hours. Following this step, the samples were again removed from the digestion block and allowed to cool for 10 minutes. After 10 minutes, 1.5 mL of 18.2 MΩ DDI water and 1 mL of 30% hydrogen peroxide (H_2O_2) were added to the samples. The tubes were returned on the digestion block, capped with watch glasses, and heated to 95 °C. An additional 1 mL of 30% hydrogen peroxide was added after the effervescence from the previous addition subsided. This step was repeated until a total of 5 mL of H_2O_2 had been added to the samples. After the effervescence from the 5th addition had stopped, all the samples were vortexed, watch glasses were removed, and the tubes were heated to 95 °C for another 2 hours. After this 2-hour heating period, the samples were removed from the digestion block and allowed to cool for 10 minutes. Upon cooling, 2.5 mL of 12 M HCl was added to samples; samples were again put on the digestion block and heated to 95 °C for 45 minutes. The samples were removed from the digestion block, allowed to cool, and filtered with #41 Whatman paper. The concentrated filtrates were collected in 50 mL centrifuge tubes, filled with 18.2 MΩ DDI water to 50 mL volume mark and stored at 4 °C prior to analysis by ICP-MS.

RESULTS

Characterization of saprolite materials

Data in Table S1 and S2 summarize the total concentrations of Cr, V, Fe, and Mn in both saprolites obtained from strong-acid digestions. The native Union County saprolite had 25 mg/kg Cr, 31 mg/kg V, 24000 mg/kg Fe, and 426 mg/kg Mn. The Redlair observatory saprolite had 16 mg/kg Cr, 191 mg/kg V, 47200 mg/kg Fe, and 280 mg/kg Mn. The UC and RL saprolites had pH values of 7.7 and 5.9, respectively. Surface area analysis revealed that the surface areas of the UC and RL saprolites were ~10 m^2/g and 25 m^2/g, respectively.

Results from our XRD analysis indicated the presence of both primary and secondary Fe-bearing mineral phases and aluminosilicate clay minerals in the UC and RL saprolites. X-ray diffraction patterns of the 500 μm fraction of the UC saprolite confirmed the presence of 1:1 clay mineral kaolinite and likely in primary mineral e.g., hornblende (Fig. S2). In the RL saprolite, the dominant clay minerals were kaolinite and nacrite (Fig. S3), the primary Fe-bearing phase was biotite, and. there was also the presence of goethite.

Quantitative Fe XNAES and EXAFS data of Union County and Redlair saprolites are presented in (Table S4, S5 and 6). The presence of hornblende in both native saprolites was corroborated in our Fe EXAFS data fit, where ~24% and 16% of the Fe in our samples could be attributed to hornblende. A secondary Fe oxide, hydrous ferric oxide with silica (HFO_Si), contributed the highest proportions of Fe to the UC (32%) and RL (59%) Fe EXAFS fits, while goethite had the second highest Fe contribution with ~24-25% in both saprolites. A chlorite standard (composition: 26.8% Fe^{3+} and 20.8% Fe^{2+}) contributed significantly (20%) to the fit of our UC Fe EXAFS data, indicating the presence of mixed-valence Fe species in that sample. Our chemical extraction data (oxalate and CBD) for UC saprolite indicated that at least ~5% of total Fe was from amorphous secondary minerals, whereas at least 45% was associated with crystalline Fe phases. From CBD extractions of RL saprolites it can be inferred that crystalline Fe minerals contributed at least ~32% to total Fe, while amorphous Fe was ~1% of total Fe in the RL saprolite. Strong-acid digestion revealed that 46%, 10%, and ~77% of Cr, V and, Fe respectively in UC saprolite is present as "environmentally available" fraction.. In RL saprolites ~88% and 64% of all V and Fe is environmentally available.

Chromium, V, Fe and Mn release from Union County saprolite, with and without chemical inputs.

Incubation without amendment (no carbon or Mn-oxide) released the least amounts of Cr, V, Fe, and Mn in Union County saprolite for any set of treatments (Fig.1). In both biotic and abiotic treatments, the amounts of Cr, V, Fe, and Mn released from the UC saprolite were negligible (< 0.5 % of total found in the original solids). In our abiotic treatments, a small increase was observed in all metals at day 40. Overall, background chemical constituents for pH stabilization and biotic control had minimal-to-no effects on native Cr, V, Fe, and Mn release in both our biotic and abiotic UC Saprolites, based on controls and blanks.

Carbon incubations yielded the highest Cr, V, and Fe release in our UC saprolite experiments, but released modest amounts of Mn (Fig. 1). In our biotic incubations, the highest released concentrations were recorded after 7 days when CA amendments stimulated release of ~1 mg Cr per kg saprolite, ~3 mg V/kg, and ~2000 mg Fe/kg (Fig. 1A, C, and E), corresponding to ~4%, 10%, and 8% of total Cr, V and Fe originally in the saprolite. However, after 14 days of incubation with CA, aqueous Cr and V concentrations decreased by ~96% while dissolved Fe concentrations decreased by ~85% from their highest levels respectively. Biotic Mn release from CA amendments was stable over the course of the experiment, with release of ~100 mg Mn per kg saprolite (~24% of the total Mn) (Fig. 1G). Contrarily, in our abiotic CA incubations, there was steady release of Cr, V, Fe and to a lesser extent, Mn with time, and there was a clear trend of CA-concentration-induced metal release (Fig 1. B, D, F and H). At the early stages of incubation, both low and high CA treatments released ~2.4%, 5% and 4% of total Cr, V, and Fe, respectively. However, at the end of the experiment, release of total Cr, V and Fe was 1.5-2 times greater in that high CA treatments than in the low CA treatments. Mn data showed no CA concentration-dependent release, as ~23% of total Mn was released in both low and high CA treatments (Fig. 1H). This is comparable to the Mn released in the biotic CA amendments.

Lastly, Mn-oxide inhibited Cr, V and Fe release in our incubations, but resulted in the greatest amounts of Mn in solution. The amounts of Mn solubilized in the biotic treatments appeared to reach equilibrium at 28 days. On the other hand, aqueous Mn continued to increase in the abiotic treatments until the end of the experiment. In comparison, Mn solubilized in the abiotic Mn-oxide amendment was 4 times greater than the level observed in the corresponding biotic amendments. In our soil-free (Mn-oxide+ additives; Fig. S4A), we observed that some

chemical additives for pH stabilization and or biotic control had an effect on dissolution of added Mn-oxide; approximately 25 mg/L and 200 mg/L of Mn was solubilized in biotic and abiotic soil-free (Mn-oxide+ additives) controls, respectively.
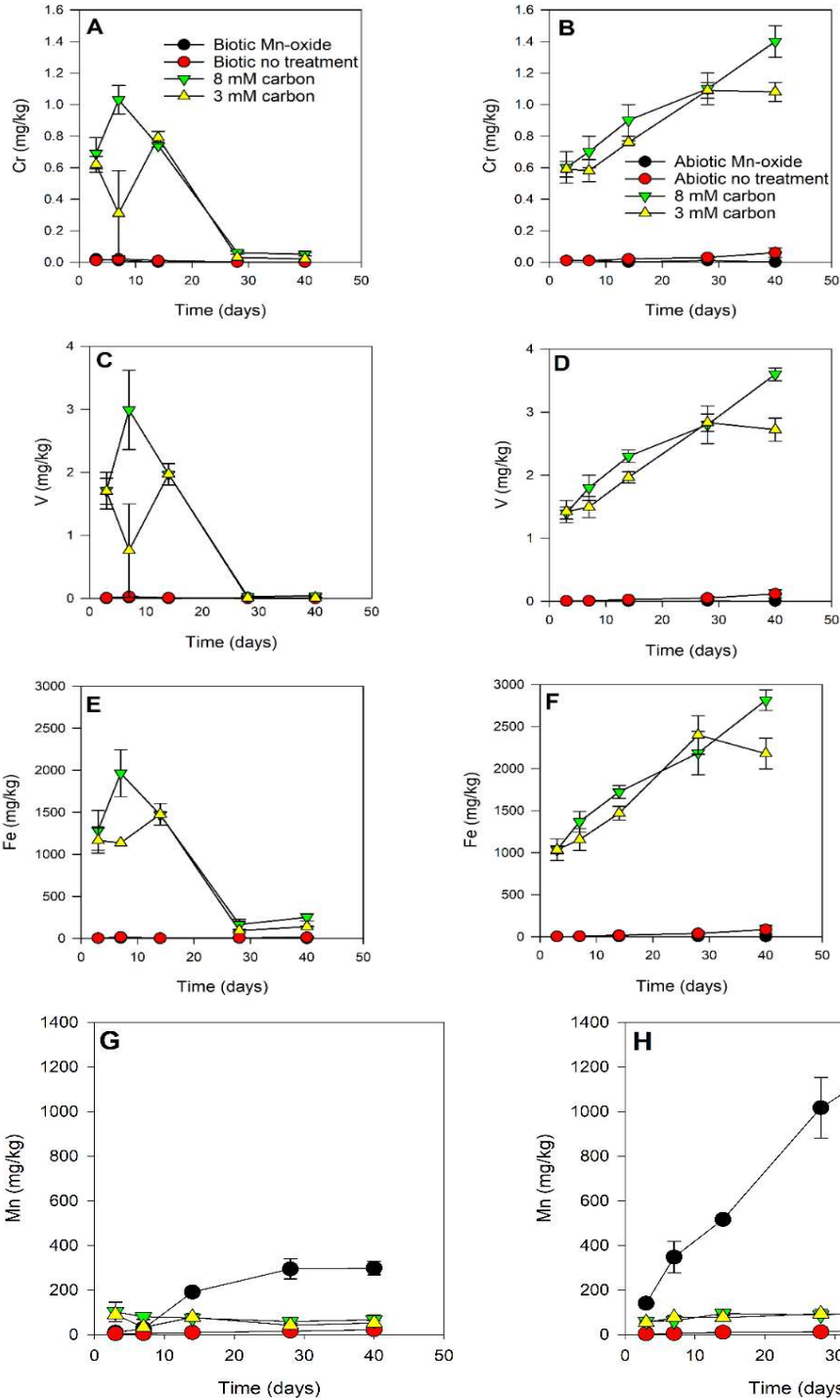
Figure 1: Biotic and abiotic elemental release (mg element released/kg saprolite) from Union County saprolite. Black, red, green, and yellow represent treatment with MnO_2, no treatment (no CA or MnO_2 addition), 8 mM citric acid, and 3 mM citric acid, respectively. Treatments without bronopol (biotic) are on the left column and treatments with bronopol (abiotic) are in the right column. Error bars represent standard error of experimental triplicates. Experimental conditions: Ionic strength (I) = 10 mM; KCl = 10 mM, HEPES = 25 mM, Bronopol = 10 mM (right column), pH = 6.6 ± 0.1.

Spectroscopy, pH and Eh measurements of Union County reaction products

EXAFS spectra from reaction products of our biotic CA-amended samples after days 14 and 40 of incubation show transformation in Fe mineral phases during the experiment. Quantitative combinatorial fitting of EXAFS spectra revealed that chlorite (42%) and hydrous ferric oxide with silica (29%) were the dominant Fe-bearing phases in solids after 14 days. However, on day 40, hornblende (38%), goethite (28%), and hydrous ferric oxide with silica (24%) were the dominant phases (Table S5). A shift in the peak around 6 Å^{-1} in reaction products indicates a phase transformation in Fe-bearing minerals between 14 - 40 days (Fig. 2A). Our abiotic incubation spectra showed no discernable differences in Fe speciation between native saprolite materials or day 14 and 28 samples. (Fig. 2B).

Redox potential data widely varied in biotic incubations compared to abiotic samples (Fig S5). The largest decrease in Eh was measured at 7 days in our CA-amended and no-treatment biotic incubations, where values dropped below ~ -400 mV before stabilizing around -200 mV after 2 weeks (Fig. S5A). In our biotic system, the highest Eh measurement was recorded in our Mn-oxide amendment (~50 mV). Little variations were recorded in our abiotic system, with Eh values ranging from 230-290 mV (Fig. S5B). In our biotic and abiotic incubations, variations in pH of amended and unamended samples were minimal at each timepoint, varying by ~0.05-0.3 pH units across all the samples (Fig. S5C and 5D).
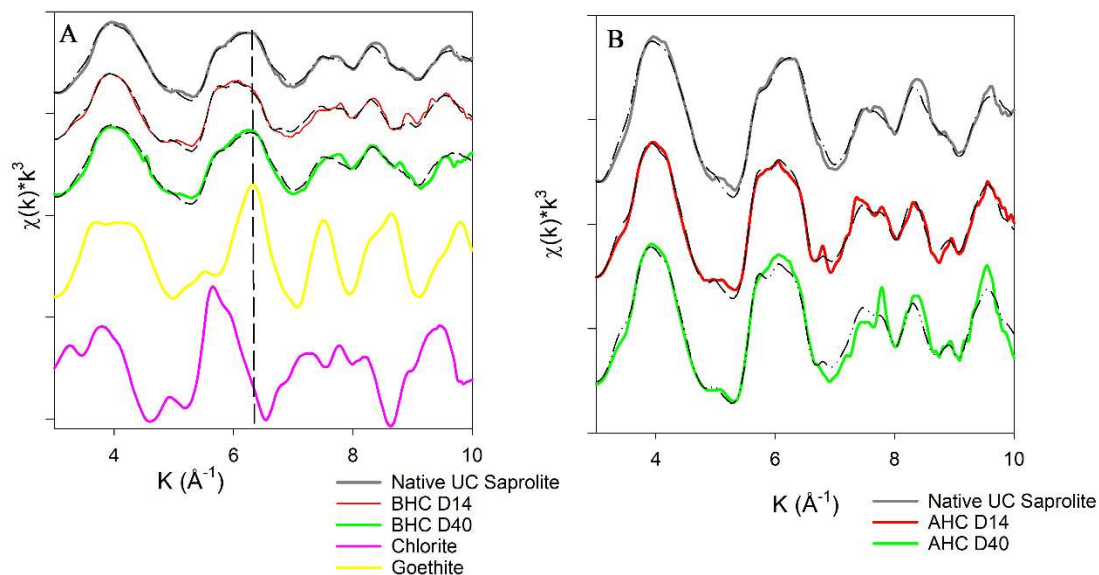
Figure 2: Iron K-edge EXAFS spectra for Union County saprolite and reaction products at days 14 and 40 for CA-amended A) biotic B) abiotic incubations. Dashed lines represent LCF fits. Fit parameters are shown in Table S5. Initial experimental conditions: Ionic strength (I) = 10 mM KCl, CA = 8 mM, pH = 6.6 ± 0.1.

Chromium, V, Fe and Mn release in Redlair saprolites with and without chemical input and biotic controls.

As observed with the UC saprolite, incubations with no amendments released the least amounts of metals from the RL saprolite (Fig. 3A-H). Here, concentrations of metals released from solid phase materials were highest 3 days after the start of the experiment but then decreased until the end of the experiment. After 3 days, incubations with no amendments released ~1.3% and 0.4 % of total Cr and V, respectively, while Fe and Mn release was minimal throughout the experiment. Without other amendments, abiotic release of all elements was comparable to biotic release of those elements.

Our carbon amendments stimulated the greatest Cr, V, and Fe release from RL saprolite (Fig. 3). Metal release proceeded rapidly within the first 7 days, before sharply decreasing in our biotic CA treatments (Fig. 3A, C, and E). At the highest point of release, CA treatments solubilized ~ 2.6, 1.6, and 1.5% of total Cr, V, and Fe from the original saprolite. This is lower

than the amounts released in our UC CA biotic incubations. Across all CA amendments, by day 28, Cr, V, and Fe released dropped by ~75 – 85%, 87 – 96% and 90 – 94%, respectively. These are comparable to levels measured in UC incubations. Abiotic CA amendments initially showed a fast release of Cr, V and Fe, but aqueous concentrations decreased over time and stabilized after two weeks (Fig. 3B, D, and F), with maxima of ~2.5, 1.4 and 1.1 % of the total Cr, V and Fe being abiotically solubilized. These values are comparable to biotic incubations, but lower than levels recorded in similar UC incubations. Contrary to our UC CA amendments, CA had little effect on Mn release from RL saprolite in either biotic or abiotic incubations.

Manganese oxide amendments stimulated a small fraction of total Cr to be released but had minimal impact on V release (Fig. 3 A-D). The highest release was observed in the early stages of the experiment, but release decreased as the experiment progressed. Mn dissolution in the biotic treatment was appreciable, with ~600 mg Mn released per kg of RL saprolite at 28 days (Fig. 3G). In our soil-free biotic controls (Mn-oxide+ additives), moderate amounts of Mn (~30 mg/L) were solubilized in solution (Fig. S4B). On the other hand, abiotic dissolution accounted for ~2000 mg/kg of Mn release in RL saprolites (Fig. 3H). Also, soil-free abiotic controls (Mn-oxide+ additives) solubilized ~240 mg/L Mn (Fig. S4B).
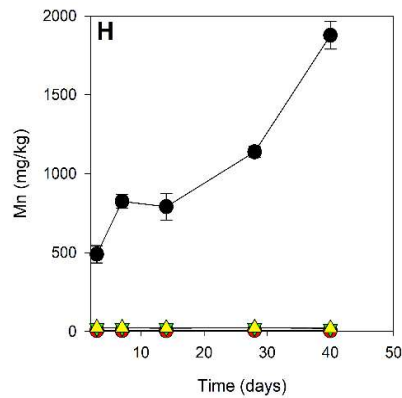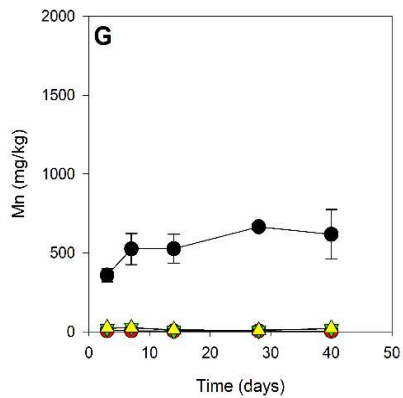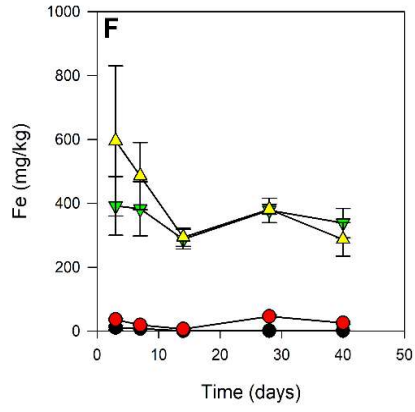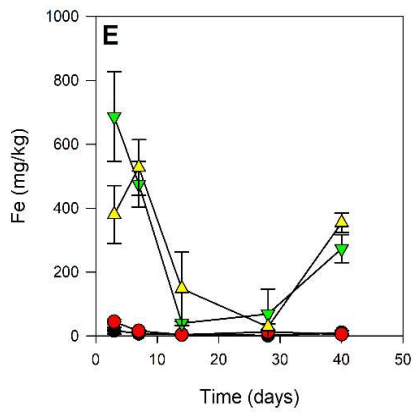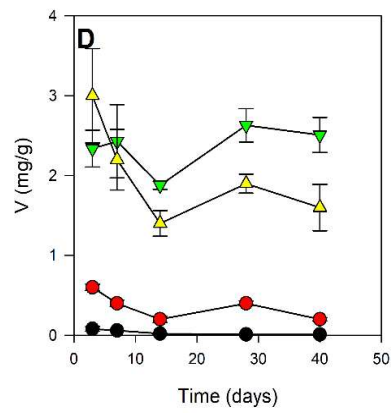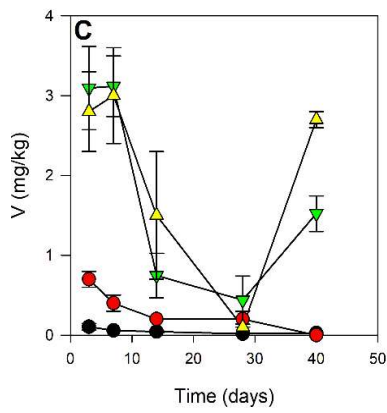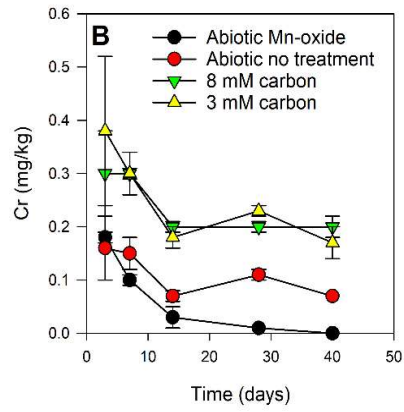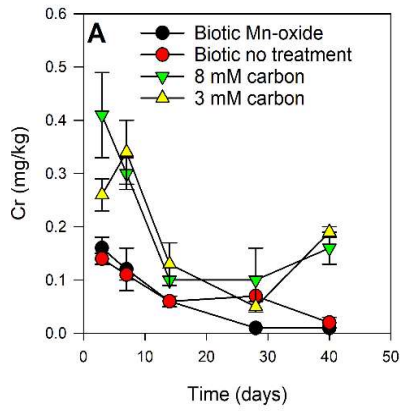
Figure 3: Biotic and abiotic elemental release (mg/kg) from Redlair saprolite. Black, red, green, and yellow represent treatment with MnO_2, no treatment (no CA or MnO_2 amendment), 8 mM CA, and 3 mM CA, respectively. Treatments without bronopol (biotic, left) and with bronopol (abiotic, right). Error bars represent standard error of experimental triplicates. Experimental conditions: Ionic strength (I) = 10 mM KCl, HEPES = 25 mM, Bronopol = 10 mM, pH = 6.6 ± 0.1.

Spectroscopy, pH and Eh measurements of Redlair saprolite reaction products

EXAFS spectra of composite samples from 8mM CA biotic and abiotic incubations collected at timepoints 14 and 28 days showed little to no transformation in Fe phases for the RL saprolite (Figs. S6 and 7). Quantitative combinatorial fitting of EXAFS spectra revealed ferrihydrite (33%) and hydrous ferric oxide with silica (18%) were the dominant phases after 14 days. On day 28, ferrihydrite (39%) and hydrous ferric oxide with silica (23%) were the dominant phases (Table S6). Our EXAFS spectra from abiotic incubations show no significant transformations in Fe speciation in both 14- and 28-days samples with ferrihydrite (42-13%) and hydrous ferric oxide with silica (20-37%) being the dominant Fe-bearing phases across the samples.

Redox potential data in RL biotic incubations were comparable to trends observed in UC incubations. Samples from incubations without amendment showed a transition from oxic to anoxic conditions within 2 weeks, however, a drastic reduction in Eh (~ -400 mV) was recorded in just 7 days in our carbon amendments. Mn-oxide amendments showed ~100 mV reduction in redox potential, but the system remained oxic throughout the 40-day period (Fig. S8A). Solutions for all amendments in our abiotic incubations remained oxic through the experiments, but a sudden sharp decrease in Eh of ~100 mV was recorded in carbon amendment samples after 14 days (Fig. S8B). After this timepoint, the Eh levels rose by ~120 mV for all amendments and remained stable. The pH variations recorded in the RL samples showed more variations than UC incubations, but still only varied between 0.05 – 0.3 pH units across all samples (Figs. S8C and 8D).

DISCUSSION

Dynamics of Cr and V release in Union County and Redlair saprolites

Our results suggest observed metal release from UC saprolite was mainly abiotically mediated. However, biotic sequestration of Cr, V and Fe was observed after 14 days in our experiments. Prior studies have shown that Cr, V, Fe and Mn cycling is often biotically driven. However, alignment of Cr and V release data from biotic and abiotic incubations in our experiments (Fig. 1A-D) shows minimal impact of biologic processes on Cr and V concentration profiles. Mass-balance calculations between our different controls and amendments revealed that during the first two weeks of UC saprolite incubations, approximately 0-4% of Cr release may have been due to biologically driven processes, and this was observed only in our 3 mM CA incubations (Fig. 1). Vanadium was likely not solubilized due to microbial activity in any of our incubations. Similarly, in our RL CA incubations, a very significant proportion of Cr and V release was likely due to abiotic processes (Fig. 3). These results are in concert with reports from other researchers who found that CA can abiotically mobilize Cr and other metals from solids via complexation reactions involving its three carboxyl functional groups.[34–36]

Metal release under different environmental conditions has been largely considered to be biotically mediated. Coupled biotic and abiotic mechanisms have previously proven to be viable pathways for the release of Cr and V, and microbial production of Mn-oxide and enzymatic reduction of Fe(III)-bearing minerals have been identified as processes that release Cr and V from sediments.[37,38] Gillispie et al. also reported the release of As, Fe, and Mn from Cambodian aquifer sediments in the presence of labile organic carbon, with the dominant mechanism of As release involving microbial utilization of organic carbon, the reductive dissolution of Fe, and release of associated As into solution.[16] In our experiments, the highest metal release from our samples was also observed with organic carbon amendment, but the release mechanism was predominantly abiotic. These findings highlight the importance of considering both biotic and abiotic processes in modeling the cycling of Cr and V. Although, our experiments did not for account initial determination of the microbial assemblage in these saprolites, this may be a limitation to our results.

Carbon amendments mostly influenced abiotic release of metals in our saprolites. This corroborated our hypothesis and validates our earlier studies[25] that organic carbon can facilitate Cr and V release from solids. Low amounts of metals were released (<< 0.5% of the native

amounts in the saprolites) in our biotic and abiotic incubations without C amendment, but at least 12 – 22 times more Cr, V and Fe were released with carbon amendments. Although our experiments did not account for the attenuation and consumption of CA in concert with the release of Cr, V and Fe, our data strongly suggest that organic carbon plays a fundamental role in either the abiotic or coupled biotic-abiotic release of Cr and V. Dissolved Fe in both biotic and abiotic CA amendments in our saprolites show similar concentration profile as Cr and V for the entire duration of the experiment (Figs. 1 and 3), with Fe release strongly correlated ($r^2 = 0.81 – 0.99$) to Cr and V release for CA treatments of both saprolites (Figs. 4 and 5).

Ligand promoted dissolution facilitated by surface complexation and reductive dissolution have been reported to enhance metal release. Previous studies have highlighted the importance of organic carbon in trace element cycling by facilitating reductive dissolution of Fe-bearing minerals and concomitant release of associated metals in sediments. In a study by Saad et al. (2017), siderophores and oxalate have been shown to influence the solubilization and release of Cr(III) from Cr(III)Fe(III)hydroxides.[39] The main mechanism of release proposed by these studies was ligand-promoted dissolution and resulting to increases in mineral solubility. Organic acids such as citric, fulvic and humic acid have also been revealed to release Cr from Cr-bearing phases via surface complexation by their -COOH group, initiating formation of Cr-organic ligand in solution.[40] In a study by Pan et al. (2017), natural organic matter such as humic acid was observed to complex with Cr(III), forming stable complexes which could be transported via advective currents.[41] These studies, in conjunction with our results, underscore the importance of ligand-promoted dissolution through surface complexation in metal release from model and natural solids.

Microbial activities may be responsible for the difference in biotic and abiotic release profiles. Although, it is expected that aqueous elemental concentrations increase with time due to microbial respiration of Fe(III) and other electron acceptors in the presence of organic carbon, the mechanism responsible for the drastic decrease in Cr, V and Fe in our biotic carbon amendments is still unclear. The emergence of reaction pathways involving certain Fe(II) oxidizing bacteria and organic carbon in anerobic sediments may provide a new route for Fe(III) precipitation.[42,43] After 14 days, Cr and V decreased sharply in our abiotic CA amendments in UC, saprolites, and after 3 days for the RL saprolites. Based on differences between treatments with and without bronopol, we suspect that a biotically controlled mechanism which scavenges

Fe from solution could be responsible for concomitant Cr and V sequestration, a hypothesis supported by increases in amorphous Fe(oxyhydr)oxide and goethite in biotic, UC CA-treated samples observed in our EXAFS data (Fig. 2A; Table S5).

The release profiles of Cr, V and, Fe for the two saprolites did show differences, especially for the abiotic incubations. The steady increase in Fe concentration in our abiotic CA amendments for UC sediments was not observed in our RL abiotic incubations. With the RL saprolite, Cr, V and Fe release was initially rapid over 3 days before plateauing after 14 days. We hypothesize that this could be because of disparities in the mineralogy of the Fe(oxyhydr)oxide and other silicate phases hosting Fe, Cr and V for the different saprolites. Results of Fe EXAFS analysis showed the presence of ferrihydrite in native RL saprolite, and day 14 and 28 samples (Fig. S7), and ferrihydrite could have resorbed released Cr and V explaining the reason for the decreases in metal concentration for the RL saprolite.
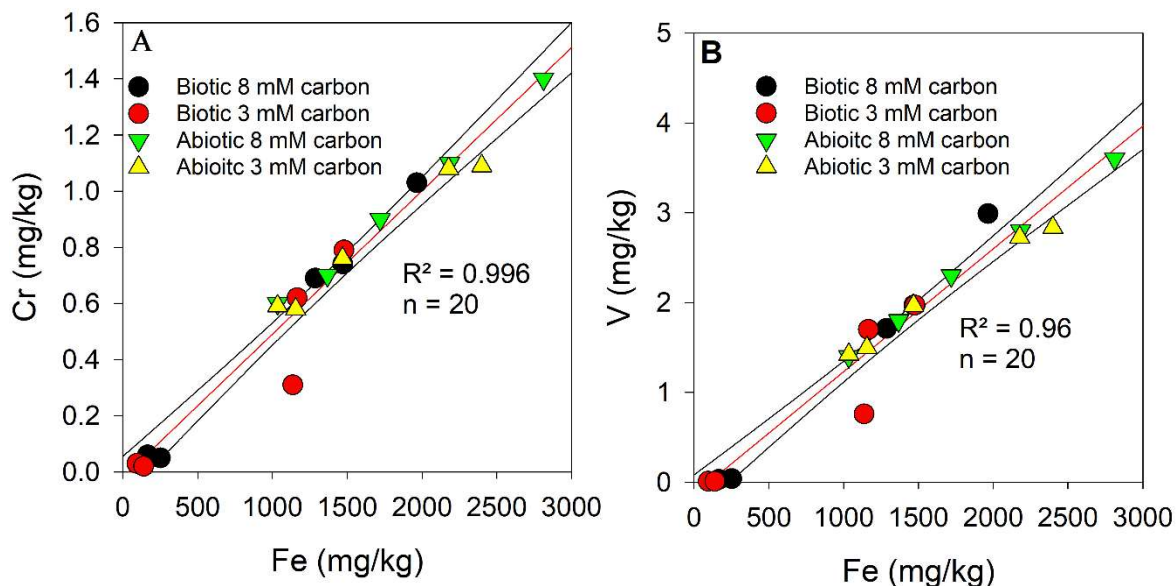
Figure 5: Relationship between (A) chromium, (B) vanadium and Fe concentrations released in Union County saprolite biotic and abiotic citric acid incubations (n =20, P < 0.05). Grey lines represent 95% confidence interval of the observations.
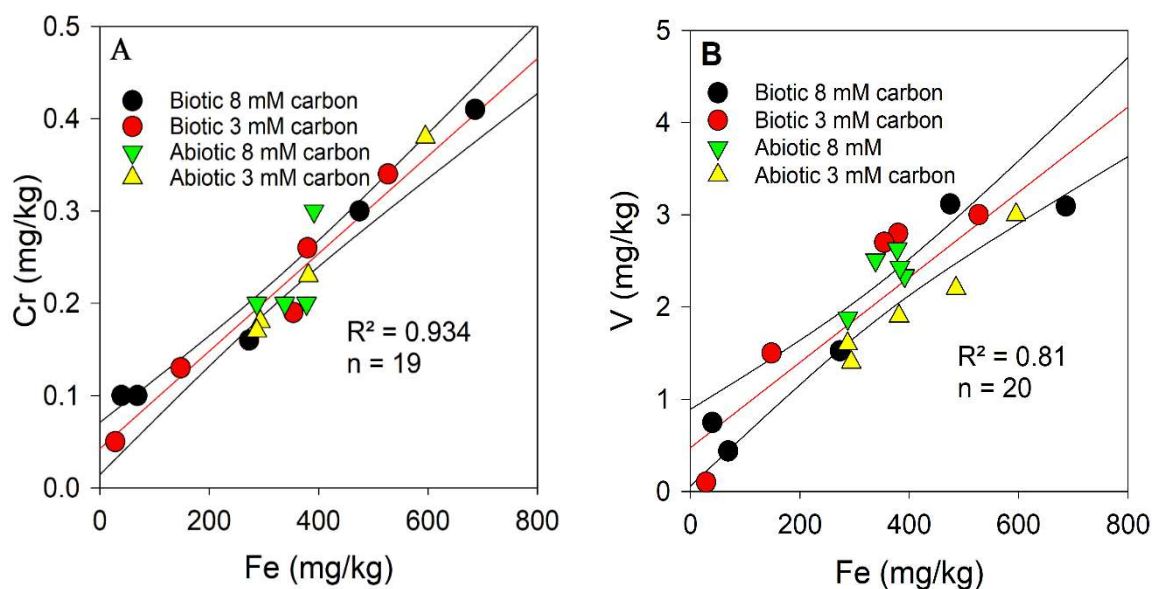
Figure 6: Relationship between (A) chromium, (B) vanadium and Fe concentrations released in Redlair Observatory saprolite biotic and abiotic citric acid incubations (n =20, P < 0.05; except for Fe Vs Cr, n =19). Grey lines represent 95% confidence interval of the observations.

Interactions of Mn-oxide in abiotic and biotic incubations

We had hypothesized that Mn-oxide could release Cr and V from solids via redox reactions. However, Mn-oxide amendment inhibited Cr and V release from UC saprolite but influenced Cr release from RL saprolite. This observation is confounding, and it could be that abundant Fe-bearing minerals limited Cr and V release via Mn-oxide driven oxidation in our system. Several research works have found that Mn-oxide could participate in oxidative release of Cr and V from host mineral phases.[44–46] However, little evidence for this was found in our study, especially in both biotic and abiotic UC saprolite Mn-oxide amendments. On the other hand, Cr and V were rapidly released from RL saprolite upon Mn-oxide amendment, confirming the potential effect of Mn-oxide on metal release. It is possible that the mechanism responsible for this release was oxidation, however bronopol and/or HEPES could have interfered in the redox process by disproportioning of added Mn-oxide.[47]

Numerous studies have investigated Cr and V mobility in the presence of Mn-oxide and highlighted oxidation and sorption as dominant mechanisms controlling metal solubility.[5,45] These studies have shown that the amounts of Mn-oxide, microbial interactions and pH influence the oxidative release of Cr from natural and model system.[5,14,37] The dynamics of V release were interesting in our research as oxidative release by Mn-oxide appears not to be the dominant mechanism for V release. Under reducing conditions, sorbed V may be released.[18] A study by Abernathy et al. 2022, also indicated that V may form strong inner-sphere complexes with Mn-oxide, highlighting sorption as an important mechanism for V release and retention. Overall, under environmental conditions where Mn-oxides are in proximity to Cr(III) bearing minerals, oxidative Cr release could produce Cr(VI). Also, Mn-oxide may sorb V which may be released and transported into ground water.

BROADER ENVIRONMENTAL IMPLICATIONS

The North Carolina (NC) Piedmont region is a rapidly developing area with millions dependent on well water for drinking water. Our study has shown that chemical inputs, such as organic carbon generated from developmental and other land use activities can stimulate abiotic release of Cr and V from saprolites. Anthropogenic activities such as tree logging, concentrated animal feeding operations, septic tank usage etc. may increase the quantity and species of organic carbon introduced into the environment. Organic carbon from these sources can alter water-rock reactions via biogeochemical and hydrological pathways resulting in the release and transport of Cr and V from solids. Aside from the influx of organics, superfund sites with history of battery recycling may introduce Mn-oxide into the environment. In the presence of organic carbon, this may facilitate the oxidative release of Cr and V from solid host phases, and eventually into groundwater as shown in our earlier study.

The results of this study indicate that LMWOAs play important roles in the biogeochemical cycling of Cr and V in chemically variable saprolites. Although small amounts of Cr were released by Mn-oxide in some of our saprolites, we postulate that Cr(VI), and V(V) are most likely to be formed and released in the presence of increased concentrations of Mn-oxide with small amounts of organic carbon. Additionally, this process could be more prolific in Fe-poor environments where there is little Fe to poise redox reactions or reduce oxidized Cr and V species. Although our study revealed minimal involvements of microbially driven metal

release, sequencing analyses need to be done to ascertain the presence of microbial communities in future experiments. This will help in unraveling biotic or coupled biotic-abiotic pathways for metals release in environmental samples. Our finding highlights that abiotic chemically-induced processes driving the release of elevated levels of geogenic Cr and V, compromising groundwater quality should be taken into consideration when making groundwater vulnerability assessments plans. Furthermore, this may improve our current understanding of the environmental behaviors of these contaminants in such complex multicomponent systems, thus guiding predictive, preventive, and remediation strategies in superfund sites.

REFERENCES

1. Sueker, J. K. Chromium. *Environ. Forensics Contam. Specif. Guid.* 81–95 (2005) doi:10.1016/B978-012507751-4/50027-6.

2. Coyte, R. M. & Vengosh, A. Factors Controlling the Risks of Co-occurrence of the Redox-Sensitive Elements of Arsenic, Chromium, Vanadium, and Uranium in Groundwater from the Eastern United States. *Environ. Sci. Technol.* **54**, 4367–4375 (2020).

3. Rousseau, M. C., Straif, K. & Siemiatycki, J. IARC carcinogen update [1]. *Environ. Health Perspect.* **113**, 580–583 (2005).

4. Lagerkvist, B. J. & Oskarsson, A. Vanadium. *Handb. Toxicol. Met. Third Ed.* 905–923 (2007) doi:10.1016/B978-012369413-3/50101-4.

5. Pan, C. *et al.* Understanding the Roles of Dissolution and Diffusion in Cr(OH) 3 Oxidation by Î-MnO 2. *ACS Earth Sp. Chem.* **3**, 357–365 (2019).

6. Borch, T. *et al.* Biogeochemical redox processes and their impact on contaminant dynamics. *Environ. Sci. Technol.* **44**, 15–23 (2010).

7. Gillispie, E. C. *et al.* Chemical variability of sediment and groundwater in a Pleistocene aquifer of Cambodia: Implications for arsenic pollution potential. *Geochim. Cosmochim. Acta* **245**, 441–458 (2019).

8. Gillispie, E. C., Taylor, S. E., Qafoku, N. P. & Hochella, M. F. Impact of iron and manganese nano-metal-oxides on contaminant interaction and fortification potential in agricultural systems-a review. *Environ. Chem.* **16**, 377–390 (2019).

9. Fendorf, S. E. Surface reactions of chromium in soils and waters. *Geoderma* **67**, 55–71 (1995).

10. McClain, C. N., Fendorf, S., Webb, S. M. & Maher, K. Quantifying Cr(VI) Production and Export from Serpentine Soil of the California Coast Range. *Environ. Sci. Technol.* **51**, 141–149 (2017).

11. Fischel, J. S., Fischel, M. H. & Sparks, D. L. *Advances in Understanding Reactivity of Manganese Oxides with Arsenic and Chromium in Environmental Systems Manganese Oxide Reactivity with Arsenic*. vol. 7 https://pubs.acs.org/sharingguidelines (2019).

12. Kim, J. G., Dixon, J. B., Chusuei, C. C. & Deng, Y. Oxidation of Chromium(III) to (VI) by Manganese Oxides. *Soil Sci. Soc. Am. J.* **66**, 306–315 (2002).

13. Landrot, G., Ginder-vogel, M., Livi, K., Fitts, P. & Sparks, D. L. Chromium (III) Oxidation by Three Poorly-Crystalline Manganese (IV) Oxides . 1 . Chromium (III) - Oxidizing Capacity. (2012).

14. Butler, E. C. *et al.* Biological versus mineralogical chromium reduction: Potential for reoxidation by manganese oxide. *Environ. Sci. Process. Impacts* **17**, 1930–1940 (2015).

15. Gonzalez, A. R., Ndung'u, K. & Flegal, A. R. Natural occurrence of hexavalent chromium in the Aromas Red Sands aquifer, California. *Environ. Sci. Technol.* **39**, 5505–5511 (2005).

16. Gillispie, E. C., Andujar, E. & Polizzotto, M. L. Chemical controls on abiotic and biotic release of geogenic arsenic from Pleistocene aquifer sediments to groundwater. *Environ. Sci. Process. Impacts* **18**, 1090–1103 (2016).

17. Frohne, T., Diaz-Bone, R. A., Du Laing, G. & Rinklebe, J. Impact of systematic change of redox potential on the leaching of Ba, Cr, Sr, and V from a riverine soil into water. *J. Soils Sediments* **15**, 623–633 (2015).

18. Shaheen, S. M. *et al.* Redox chemistry of vanadium in soils and sediments: Interactions with colloidal materials, mobilization, speciation, and relevant environmental implications - A review. *Adv. Colloid Interface Sci.* **265**, 1–13 (2019).

19. Pan, C. *et al.* Rates of Cr(VI) Generation from CrxFe1–x(OH)3 Solids upon Reaction with Manganese Oxide. *Environ. Sci. Technol.* **51**, 12416–12423 (2017).

20. Lehmann, J. & Kleber, M. The contentious nature of soil organic matter. *Nature* **528**, 60–68 (2015).

21. Cotrufo, M. F., Wallenstein, M. D., Boot, C. M., Denef, K. & Paul, E. The Microbial Efficiency-Matrix Stabilization (MEMS) framework integrates plant litter decomposition with soil organic matter stabilization: Do labile plant inputs form stable soil organic matter? *Glob. Chang. Biol.* **19**, 988–995 (2013).

22. Shaheen, S. M., Rinklebe, J., Frohne, T., White, J. R. & DeLaune, R. D. Biogeochemical Factors Governing Cobalt, Nickel, Selenium, and Vanadium Dynamics in Periodically Flooded Egyptian North Nile Delta Rice Soils. *Soil Sci. Soc. Am. J.* **78**, 1065–1078 (2014).

23. Yang, F., Guo, J., Dai, R. & Lan, Y. Oxidation of Cr(III)-citrate/tartrate complexes by δ-MnO2: Production of Cr(VI) and its impact factors. *Geoderma* **213**, 10–14 (2014).

24.   Sun, Y., Guan, F., Yang, W. & Wang, F. Removal of chromium from a contaminated soil using oxalic acid, citric acid, and hydrochloric acid: Dynamics, mechanisms, and concomitant removal of non-targeted metals. *Int. J. Environ. Res. Public Health* **16**, (2019).

25.   Balogun, F. O., Aiken, M. L., Namayandeh, A., Duckworth, O. W. & Polizzotto, M. L. Dissolved Organic Carbon Diminishes Manganese Oxide-Driven Oxidation of Chromium. *Chemosphere* **344**, 140424 (2023).

26.   Jean, L., Bordas, F. & Bollinger, J. C. Chromium and nickel mobilization from a contaminated soil using chelants. *Environ. Pollut.* **147**, 729–736 (2007).

27.   Liao, P. *et al.* Formation and Transport of Cr(III)-NOM-Fe Colloids upon Reaction of Cr(VI) with NOM-Fe(II) Colloids at Anoxic-Oxic Interfaces. *Environ. Sci. Technol.* **54**, 4256–4266 (2020).

28.   Rinklebe, J., Shaheen, S. M., Schröter, F. & Rennert, T. Exploiting biogeochemical and spectroscopic techniques to assess the geochemical distribution and release dynamics of chromium and lead in a contaminated floodplain soil. *Chemosphere* **150**, 390–397 (2016).

29.   Vessey, C. J. & Lindsay, M. B. J. Aqueous Vanadate Removal by Iron(II)-Bearing Phases under Anoxic Conditions. *Environ. Sci. Technol.* **54**, 4006–4015 (2020).

30.   Ying, S. C., Kocar, B. D. & Fendorf, S. Oxidation and competitive retention of arsenic between iron- and manganese oxides. *Geochim. Cosmochim. Acta* **96**, 294–303 (2012).

31.   Ying, S. C., Kocar, B. D., Griffis, S. D. & Fendorf, S. Competitive microbially and Mn oxide mediated redox processes controlling arsenic speciation and partitioning. *Environ. Sci. Technol.* **45**, 5572–5579 (2011).

32.   Ravel, B. & Newville, M. ATHENA, ARTEMIS, HEPHAESTUS: Data analysis for X-ray absorption spectroscopy using IFEFFIT. in *Journal of Synchrotron Radiation* vol. 12 537–541 (2005).

33.   EPA, Method 3050B: Acid Digestion of Sediments, Sludges, and Soils. 1–12 (1996).

34.   Lee, S. M., Cho, I. H., Chang, Y. Y. & Yang, J. K. Effects of the density of carboxyl groups in organic compounds on the photocatalytic reduction of Cr(VI) in a TiO2 suspension. *J. Environ. Sci. Heal. - Part A Toxic/Hazardous Subst. Environ. Eng.* **42**, 543–548 (2007).

35.   Jiang, B. *et al.* The reduction of Cr(VI) to Cr(III) mediated by environmentally relevant

carboxylic acids: State-of-the-art and perspectives. *Journal of Hazardous Materials* vol. 365 205–226 (2019).

36.   Taghipour, M. & Jalali, M. Influence of organic acids on kinetic release of chromium in soil contaminated with leather factory waste in the presence of some adsorbents. *Chemosphere* **155**, 395–404 (2016).

37.   Hausladen, D. M. & Fendorf, S. Hexavalent chromium generation within naturally structured soils and sediments. *Environ. Sci. Technol.* **51**, 2058–2067 (2017).

38.   O'Loughlin, E., Boyanov, M. & Kemner, K. Reduction of Vanadium (V) by Iron (II)-Bearing Minerals. Minerals 2021, 11, 316. 1–21 (2021) doi:https://doi.org/10.3390/.

39.   Saad, E. M. *et al.* Siderophore and Organic Acid Promoted Dissolution and Transformation of Cr(III)-Fe(III)-(oxy)hydroxides. *Environ. Sci. Technol.* **51**, 3223–3232 (2017).

40.   Gustafsson, J. P. *et al.* Chromium(III) complexation to natural organic matter: Mechanisms and modeling. *Environ. Sci. Technol.* **48**, 1753–1761 (2014).

41.   Pan, C. *et al.* Effect of Humic Acid on the Removal of Chromium(VI) and the Production of Solids in Iron Electrocoagulation. *Environ. Sci. Technol.* **51**, 6308–6318 (2017).

42.   Laufer, K. *et al.* Anaerobic microbial Fe(II) oxidation and Fe(III) reduction in coastal marine sediments controlled by organic carbon content. *Environ. Microbiol.* **18**, 3159–3174 (2016).

43.   Bryce, C. *et al.* Microbial anaerobic Fe(II) oxidation – Ecology, mechanisms and environmental implications. *Environ. Microbiol.* **20**, 3462–3483 (2018).

44.   Oze, C., Bird, D. K. & Fendorf, S. *Genesis of hexavalent chromium from natural sources in soil and groundwater*. www.pnas.orgcgidoi10.1073pnas.0701085104 (2007).

45.   J. Abernathy, M., V. Schaefer, M., J. Vessey, C., Liu, H. & C. Ying, S. Oxidation of V(IV) by Birnessite: Kinetics and Surface Complexation. *Environ. Sci. & Technol.* **55**, 11703–11712 (2021).

46.   Pan, C. *et al.* Understanding the Roles of Dissolution and Diffusion in Cr(OH)3 Oxidation by Î-MnO 2. *ACS Earth Sp. Chem.* **3**, 357–365 (2019).

47.   Hausladen, D. M. & Peña, J. Organic buffers act as reductants of abiotic and biogenic manganese oxides. *Sci. Rep.* **13**, 1–12 (2023).

CHAPTER V
DISSERTATION CONCLUSION

Our understanding of the fate and transport of Cr and V in multicomponent systems is limited by various confounding factors. One significant challenge stem from the presence of organic ligands in both model and natural environments, which can form complexes with these metals. This raises some fundamental questions: do these metal-ligand complexes possess the stability necessary to prevent Cr oxidation or V release? What is the sequence of processes facilitating Cr and Mn release? The intricacy amplifies in natural systems rich in Fe and Mn(oxyhydr)oxides, where biogeochemical processes govern the retention and release of Cr and V, especially in the presence of labile organic carbon. Several researchers have investigated the dynamic of Cr and V in the presence of Mn-oxide or organic carbon in model systems, but a few studies have explored this process in natural geologic materials – understanding biogeochemical processes facilitating the release of Cr and V in model and natural systems in the context of labile organic carbon could help improve our understanding of global Cr and V cycling as well as help make informed management and remediation strategies of contaminated sites. My dissertation aimed to deconvolve the mechanisms responsible for Cr and V retention and release in the presence of organic carbon using an array of wet chemistry, spectrometry, and spectroscopic approaches. The objectives of this dissertation were to 1) gain a more detailed mechanistic understanding of how ubiquitous inputs such organic carbon proxies, and Mn-oxide influence Cr oxidation and release; 2) determine the host phases for Cr and V in naturally distinct geologic materials weathered from different tectonic settings, and parameterize their adsorption capacities; 3) determine the impact of organic matter and Mn-oxide proxies on the biotic and abiotic release of Cr and V in near surface natural geologic materials; a process that has largely been reported to be biotically-mediated.

In Chapter II, we delved into the influence of diverse organic carbon types on limiting Mn-oxide driven oxidation of Cr. Our initial hypothesis was that aromatic organic carbon, especially those capable of electron shuttling, would effectively inhibit Mn-oxide-induced oxidation of Cr(III). Surprisingly, our experiments demonstrated that aliphatic organic carbon, specifically citric acid, was approximately eight times more efficient at inhibiting Mn-oxide driven oxidation of Cr compared to aromatic organic carbon like gallic acid. By combining

synchrotron-based X-ray absorption spectroscopy (XAS) with wet chemistry methods, we found that less than 4% of Cr(VI) was present in the solid phase reaction products across all treatments. Our reaction modeling efforts indicated a decrease in $CrOH^{2+}$ with increasing citric acid concentration, suggesting that this Cr(III) species might control Cr oxidation in our system. Overall, our experiments suggested a sequential mechanism for Cr oxidation: dissolution of Cr(OH)3, followed by metal-organic carbon complexation, transport of unchelated free Cr(III) to Mn-oxide surface, oxidation, desorption of Cr(VI) into solution, and passivation of the Mn-oxide surface. Future directions for this research encompass elucidating the reactivity of different environmentally relevant Mn-oxide in such multicomponent systems to quantify Cr(VI) production.

Chapter III centered on unraveling the fate and transport of Cr and V in chemically variable saprolites, aiming to quantify adsorption capacities, kinetics, and identify contaminant solid host phases. Notably, our Cr and V isotherm revealed that saprolite materials exhibited approximately ten times higher affinity for V than Cr, attributed to the formation of polyvanadate species binding strongly to Fe(oxyhydr)oxides through inner-sphere complexation. Despite Langmuir adsorption isotherms predicting equivalent adsorption of both elements by saprolites, chemical extractions indicated that proportions of amorphous and crystalline host phases may have a marked impact Cr and V retention. Kinetic experiments supported the influence of amorphous phases in Cr and V sorption, with saprolites rich in amorphous Fe sorbing approximately 2 and 2.4 times more Cr and V respectively. Additionally, added Cr(VI) and V(V) were reduced to Cr(III) in the form of Cr(OH)3, while V existed as mixed V(IV) and V(V) species. Synchrotron-based X-ray absorption spectroscopy highlighted the role of Fe(II)-bearing minerals and ferrihydrite-humic substance complexes in facilitating redox processes controlling V cycling in saprolites. Although μ-XRF indicated Cr and V were associated with Fe-bearing minerals, distinguishing between primary and secondary Fe mineral phases spectroscopically proved challenging. Overall, structural incorporation, sorption onto Fe- and Mn(oxyhydr)oxides, and kaolinite emerged as dominant mechanisms governing Cr and V release and retention in chemically variable piedmont saprolites. Further research is imperative to elucidate Cr and V retention and release mechanisms, especially in tropical soils abundant in clay minerals and Fe oxides, posing potential threats to surface waters in mining areas.

Chapter IV aimed at quantifying the release of geogenic Cr and V due to labile organic carbon and birnessite input to understand how changes in land management strategies could influence contaminant release from chemically variable saprolites. After a 40-day period of experiments, we were able to observe that organic carbon-induced abiotic release of Cr and V was overall higher than biotic release. The mechanisms responsible for the increase and sudden decrease in microbially released Cr and V were unclear, but XAS analysis suggested that this was due to Fe(III) precipitation – a phenomenon not observed in abiotic Union County saprolites. On the other hand, Mn-oxide (birnessite) additions did not influence Cr and Mn release in the Union County saprolites, however, fast initial release up to 0.2 mg Cr/kg and 0.8 mg V/kg was observed in the Redlair saprolite. Overall, consistent with previous studies, low molecular weight organic acid (LMWOA) could abiotically accelerate the release of Cr and V from sediments. Although Mn-oxide exerted minimal influence on Cr and V release, future work could explore the reactivities of different structural types of Mn-oxide and organic carbon on Cr and V release from natural sediments.

Previous works have examined the release of contaminants from near surface soils and aquifer materials, but little has been done in context of contaminant transport from partially weathered materials in the presence of anthropogenic or geogenic chemical inputs such as organic carbon and Mn-oxide. A major finding of this dissertation is that under environmentally relevant conditions, LMWOA, Mn-oxide, Fe and Mn(oxyhydr)oxides are capable of modulating biogeochemical processes that affect the fate and transport of Cr and V in model and natural systems. Therefore, such confounding processes must be taken into consideration when developing predictive mechanistic models for Cr and V mobility and environmental toxicity.

APPENDIX A

SUPPLEMENTAL MATERIAL FOR CHAPTER II

Table S1. Cr XANES linear combination fits (LCFs) for reaction products of 0-10 mM citric acid treatments were performed in ATHENA and normalized to 100%. Error is reported from the software output.

Citrate acid concentration	Component	% Contribution	R-value
0 mM	$Cr(OH)_3$	98.7 ± 1.5	0.012
	K_2CrO_4	1.3 ± 1.6	
0.5 mM	$Cr(OH)_3$	98.3 ± 0.9	0.055
	K_2CrO_4	1.7 ± 1.6	
1 mM	$Cr(OH)_3$	97.0 ± 1.1	0.0838
	K_2CrO_4	3.0 ± 1.7	
5 mM	$Cr(OH)_3$	97.8 ± 1.1	0.068
	K_2CrO_4	2.2 ± 1.7	
10 mM	$Cr(OH)_3$	97.7 ± 0.8	0.041
	K_2CrO_4	2.3 ± 1.6	

Table S2. Cr XANES linear combination fits (LCFs) for reaction products of 0 - 10 mM gallic acid treatments were performed in ATHENA and normalized to 100%. Error is reported from the software output.

Gallic acid concentration	Component	% Contribution	R-value
0 mM	$Cr(OH)_3$	98.8 ± 0.5	0.017
	K_2CrO_4	1.2 ± 0.5	
0.5 mM	$Cr(OH)_3$	98.8 ± 1.2	0.017
	K_2CrO_4	1.2 ± 0.5	
1 mM	$Cr(OH)_3$	100 ± 0	0.018
	K_2CrO_4	NA	
5 mM	$Cr(OH)_3$	98.8 ± 1.3	0.012
	K_2CrO_4	1.2 ± 1.3	
10 mM	$Cr(OH)_3$	98.9 ± 1.1	0.083
	K_2CrO_4	1.1 ± 1.1	
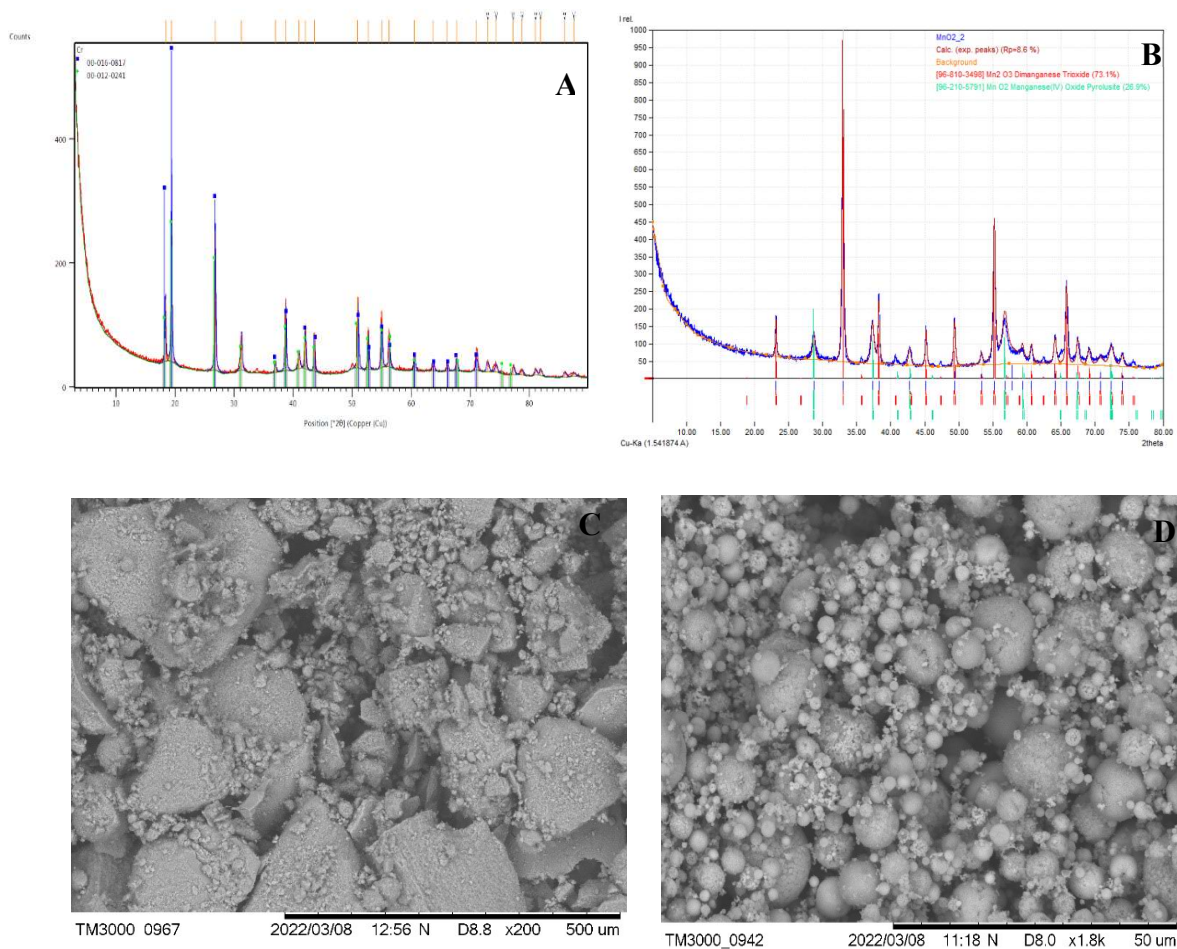
Figure S1. A) X-ray diffraction patterns showing Cr(OH)$_3$ starting material. B) X-ray diffraction patterns showing Mn-oxide starting material. C) SEM image of Cr(OH)$_3$ starting material. D) SEM image of Mn-oxide starting material.
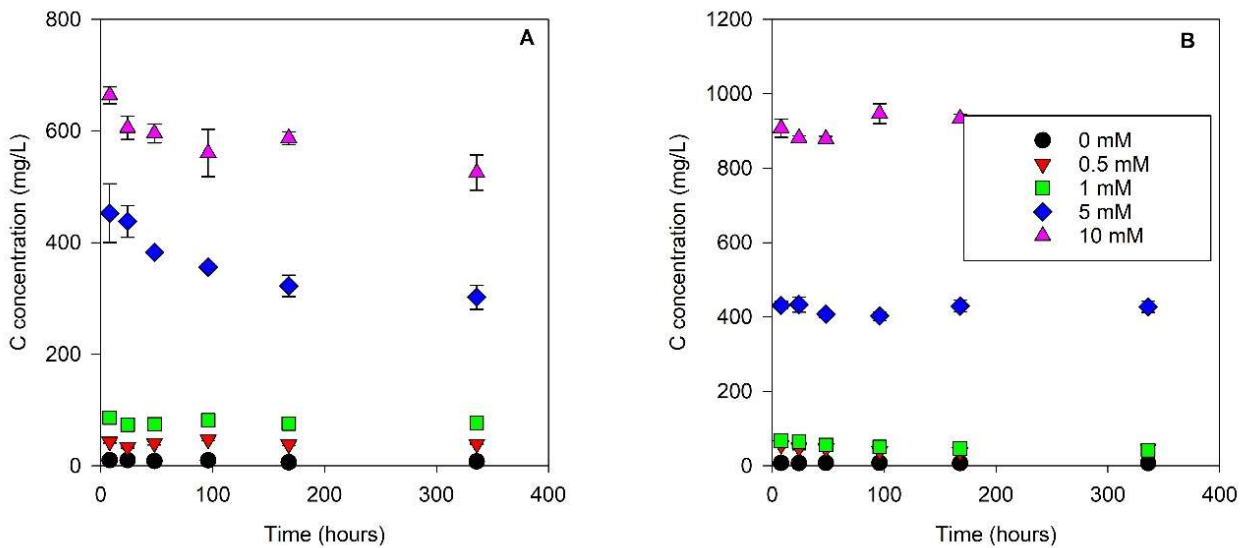
Figure S2. A) Dissolved organic carbon concentrations over time in citric acid experiments. B) Dissolved organic carbon concentrations over time in gallic acid experiments. Error bars represent standard error of replicates.
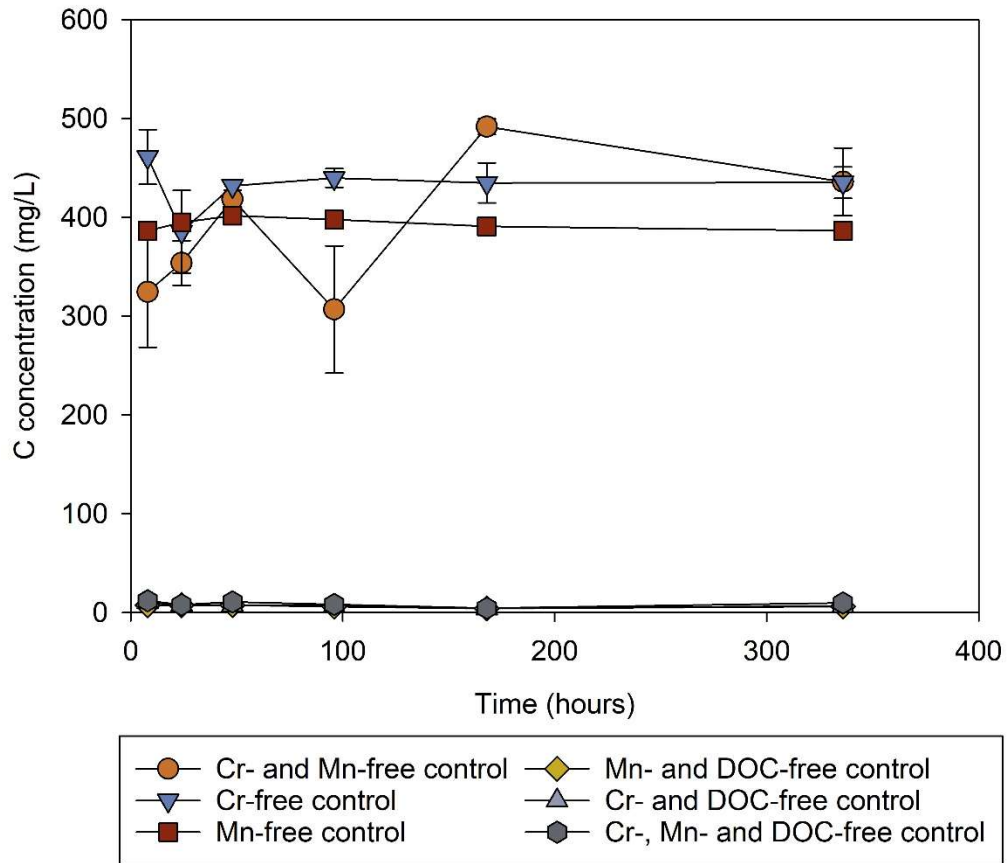
Figure S3. Dissolved organic carbon concentrations in citric acid experimental controls. Error bars represent standard error of replicates.
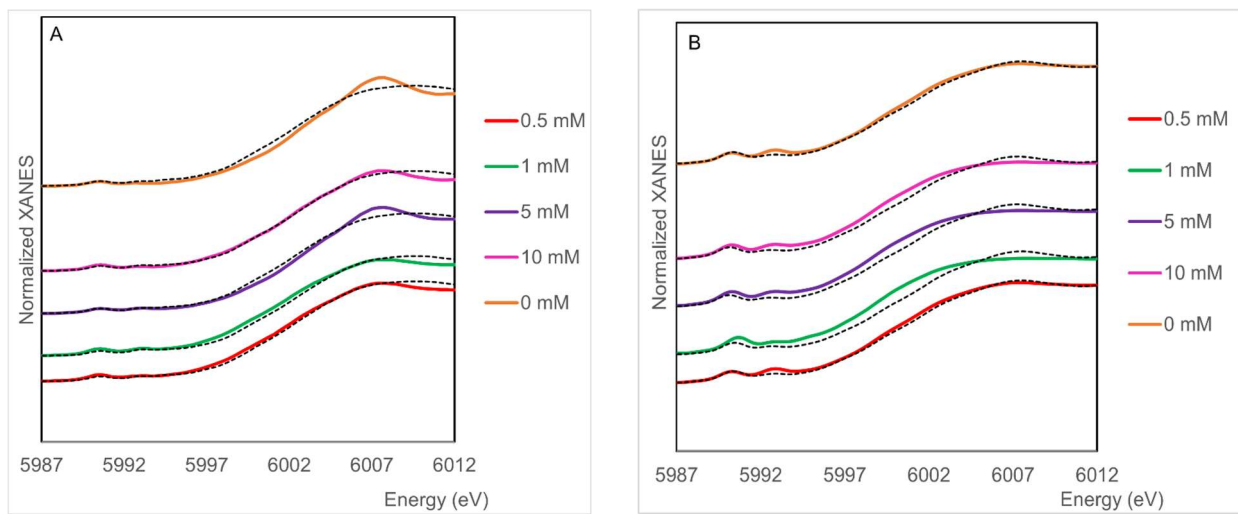
Figure S4. A) Linear combination fits of normalized Cr k-edge XANES spectra for citric acid experiment reaction products and treatment blank. B) Linear combination fits of normalized Cr k-edge XANES spectra for gallic acid experiment reaction products and treatment blank. Fit data are provided in Tables S1 (citric acid experiments) and S2 (gallic acid experiments).
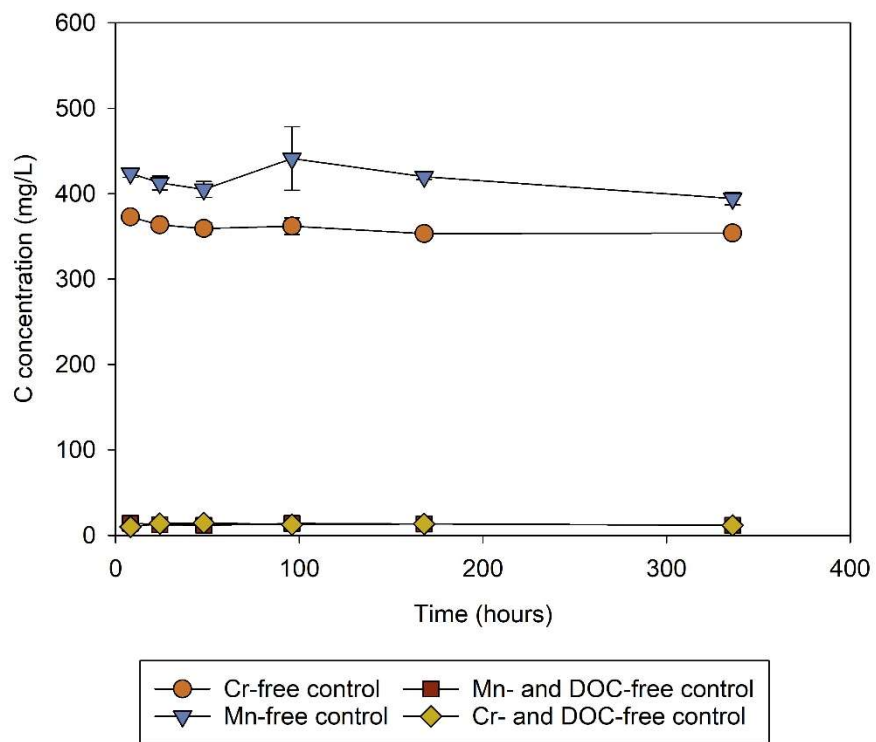
Figure S5. Dissolved organic carbon concentrations in gallic acid experimental controls. Error bars represent standard error of replicates.
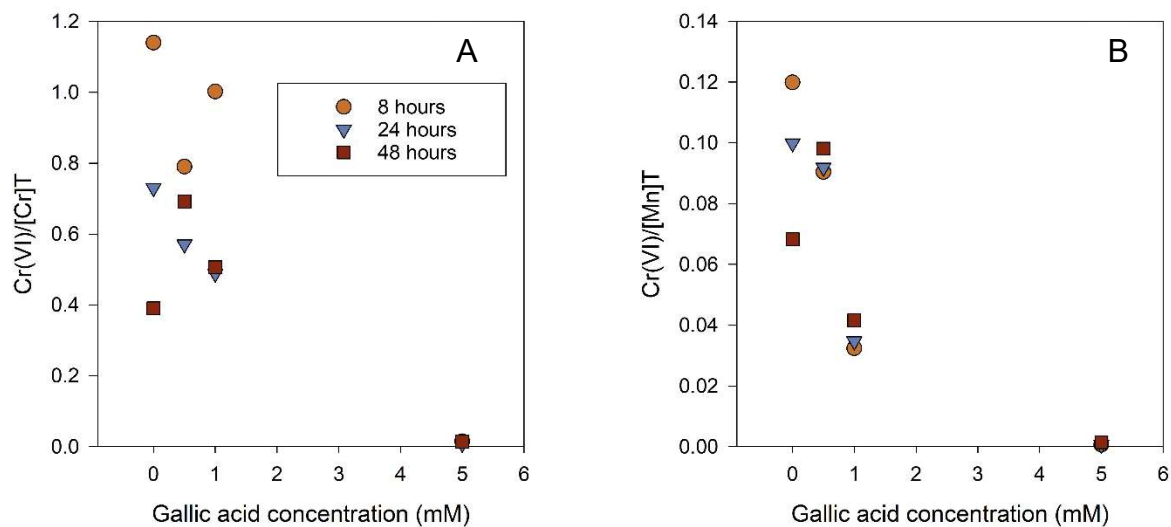
Figure S6. A) Molar ratio of dissolved Cr(VI) and total Cr produced from different initial gallic acid concentrations for 8-48 h time points in mixed batch experiments. B) Molar ratio of dissolved Cr(VI) and total Mn produced from different initial gallic acid concentrations for 8-48 h time points in mixed batch experiments.
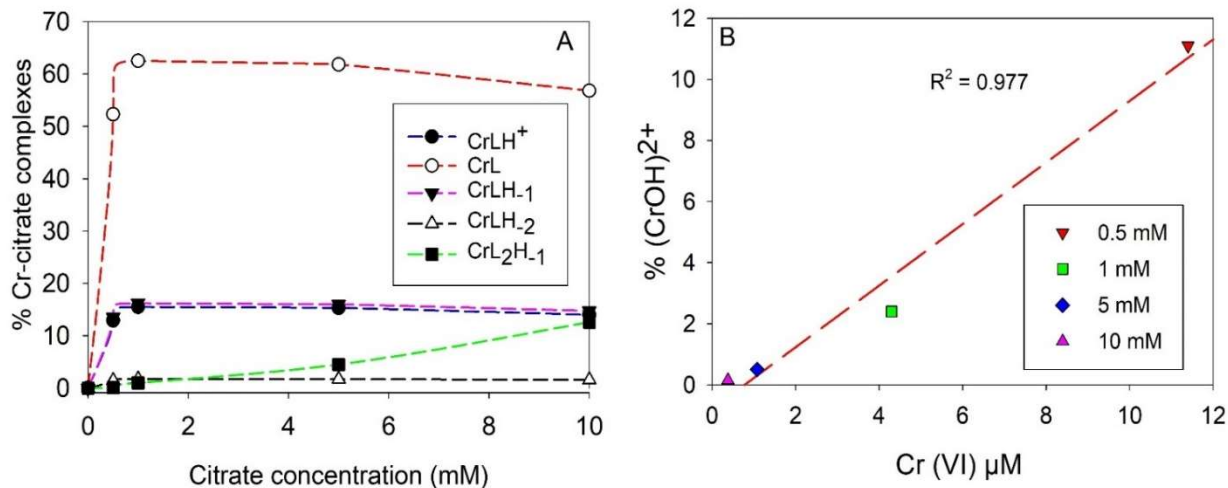
Figure 7. A) Proportions of protonated and unprotonated Cr(III)-citrate complexes, and B) CrOH^{2+} of total aqueous Cr produced across citric acid treatments (0.5 – 10 mM). Data were modeled with Visual MINTEQ using Cr(III), Mn(II) and citrate concentrations from 168 hours of incubation, pH 5 and ionic strength of 0.005 M.
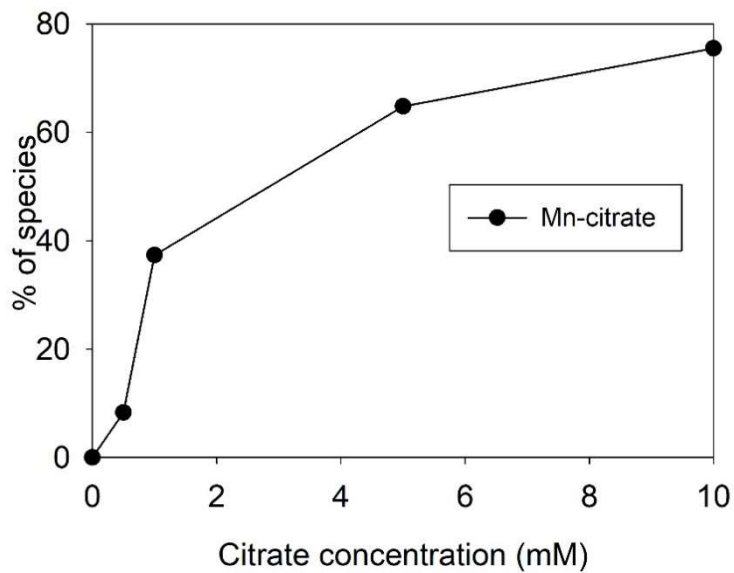
Figure S8. Proportions of Mn-citrate complexes out of total aqueous Mn produced across citric acid treatments (0 – 10 mM). Data were modeled with Visual MINTEQ using Cr(III), Mn(II) and citrate concentrations from 168 hours of incubation, pH 5 and ionic strength of 0.005 M.

1. Adsorption Isotherm experiment

Plots for Cr(VI) and V (V) adsorbed as a function of the solution concentration at equilibrium were fitted to both linear and nonlinear Langmuir and Freundlich mathematical isotherm models. The nonlinear Langmuir isotherm model is given by $Qe = \frac{K_L * Q_{max} * Ce}{(1 + K_L * Ce)}$ where Qe (mg/kg) is the concentration of sorbed anion at equilibrium, K_L (L/mg) is the Langmuir constant which is related to the adsorption energy of a given site, Qmax (mg/kg) is the maximum adsorption capacity, and C (mg/L) is the aqueous phase concentration of the anion at equilibrium. The nonlinear Freundlich isotherm model is described by the equation $Qe = K_F * C^n$. Qe and C are the same as in the Langmuir equation, however, K_F is the Freundlich constant describing the solid-aqueous phase partition coefficient, and n is a constant describing the intensity of adsorption on the adsorbent. Details on the linearized version can be found int the supporting information.

The adsorbed concentration of Cr (VI) and V(V) with respect to time was calculated by $Q = \frac{(C - Ce) * V}{W}$ where C and Ce are same as above, V is volume (mL) and, W = mass of soil used (g). The linear equations used to fit our Langmuir and Freundlich isotherms are Ceq/q Vs Ce and log Qe Vs log Ceq.

2. Kinetic experiments

The linear equations used to fit our kinetic data to pseudo first and second order reactions are given below.

$\ln(qe - qt) = \ln qe - kt$ …..Pseudo 1st order reaction

$\frac{t}{qt} = \left(\frac{1}{qe}\right) * t + (1/(k * (qe^2)))$……. Pseudo 2nd order reaction

K= rate of adsorption, qt= adsorption at time t, qe = adsorption at equilibrium

3. Single Chemical extractions (parallel)

For our oxalate extraction, a 0.2 M solution of ammonium oxalate with a pH of 3 (buffered with HCl) was added to each tube containing native and Cr- and V-loaded samples. This was to target Cr, V, Mn, and Fe associated amorphous Fe oxides. Tubes were placed on the shaker for 2 hours while wrapped in aluminum foil, then centrifuged and filtered before the step was repeated. For other samples, (sodium citrate-bicarbonate-dithionite (CBD) was added to the tubes to target Cr, V, Mn, and Fe coprecipitated with crystalline Fe(oxyhydr)oxides in our native and Cr- and V-loaded samples. Initial solutions of 0.3 M sodium citrate and 1 M sodium bicarbonate were created. Twenty mL of sodium citrate and 2.5 mL sodium bicarbonate were added prior to the tubes being heated to 80°C over a hot water bath. Once at the correct temperature, 0.5 g sodium dithionite was added. Tubes were then placed back in the hot water bath for 30 minutes at 80°C with intermittent shaking and stirring before they were centrifuged at 4200 rpm for 10 minutes. All samples were filtered with #41 Whatman filter paper, acidified with several drops of 15.8 M HNO_3 and this extraction was not repeated. Lastly, a 1 M solution of $MgCl_2$ was prepared and 50 mL aliquots were added to each test tube containing native and Cr- and V-loaded samples and equilibrated on the shaker for two hours. This step was repeated twice, and the solutions were filtered with #41 Whatman filter paper, acidified with 15.8 M HNO_3 before been stored in the refrigerator prior to ICP-MS analysis.

Table S1: Chemical extraction procedure for native and Cr and V loaded saprolites.

Extractant	Species extracted	Reaction time and solid solution ratio
Ammonium oxalate buffered to pH 3.	Cr and V sorbed on amorphous phases	2 hours (under dark conditions). 0.5 g of saprolite to 40 mL of oxalate solution
Citrate Bicarbonate Dithionite buffered to pH 8, continuously stirred in 80C water bath.	Cr and V sorbed on crystalline phases	35 minutes, 0.5 g of saprolite to 25 mL of solution.
Magnesium chloride ($MgCl_2$)	Cr and V ionically bound on surfaces	2 extractions, total of 4 hours

Table S2: Statistical analysis of goodness of fit from Langmuir and Freundlich models.

Saprolite	Adsorbate	Model	R^2	χ^2
	Cr(VI)	Langmuir	0.977	2.34
Union County		Freundlich	0.872	7.14
	V(V)	Langmuir	0.966	18.63
		Freundlich	0.965	30.90
	Cr(VI)	Langmuir	0.994	1.76
Redlair		Freundlich	0.854	5.04
	V(V)	Langmuir	0.977	11.38
		Freundlich	0.983	12.45

Table S3: Standard spectra used in the V K-edge EXAFS LCF of native Union County and Redliar observatory saprolites. Standard in bold italics were used for final fits.[4]

Sample ID
V^{5+} sorbed kaolinite (batch experiment)
V^{5+} sorbed ferrihydrite-humic substance (HS)complex at pH 6
V^{5+} sorbed ferrihydrite
V^{5+} sorbed gibbsite
V^{5+} sorbed goethite
V^{5+} sorbed humic substance (HS)
V^{5+} sorbed thiol
V^{5+} sorbed poorly ordered kaolinite (KGa2)
NH_4VO_3
$NaVO_3$
V^{4+} sorbed goethite
V^{4+} substituted ferrihydrite
V^{4+} substituted well-ordered kaolinite (KGa1b)
$VOSO_4$
VCl_3
V^{3+} substituted magnetite

Table S4: V K-edge XANES linear combination fits (LCFs) for native Union County and Redlair saprolites

Sample ID	Component	% Contribution	R-value
Native UC saprolite	V^{4+} substituted ferrihydrite	15.9 ± 2.1	0.003
	V^{3+} substituted magnetite	37.4 ± 2.7	
	V^{4+} substituted kaolinite	37.9 ± 1.5	
	$VOSO_4$	8.8 ± 5.5	
Native RL saprolite	V^{5+} sorbed Ferrihydrite-HS	19.6 ± 5.1	0.005
	$VOSO_4$	11.4 ± 4.0	
	V^{4+} substituted kaolinite	34.2 ± 4.8	
	V^{3+} substituted magnetite	35.6 ± 3.1	

Table S5: V K-edge XANES linear combination fits (LCFs) for vanadium-loaded Union County and Redlair saprolites

Sample ID	Component	% Contribution	R-value
V-loaded UC saprolite	V^{3+} substituted magnetite	17.0 ± 1.5	0.002
	V^{4+} substituted kaolinite	49.1 ± 2.4	
	V^{5+} sorbed kaolinite	33.9 ± 3.3	
V-loaded RL saprolite	V^{5+} sorbed Ferrihydrite-HS	13.2 ± 8.8	0.003
	$VOSO_4$	7.9 ± 3.7	
	V^{4+} substituted kaolinite	32.6 ± 4.1	
	V^{3+} substituted magnetite	20.9 ± 2.6	
	V^{5+} sorbed kaolinite	25.4 ± 10.8	

Table S6: Standard spectra used in the Fe K-edge EXAFS LCF for native Union County and Redliar observatory saprolite, day.[1–3] Standard in bold italics were used for final fits.

Sample ID
Hydrous ferric oxide w/Si
Chlorite
Goethite
Hematite
Nontronite
Lepidocrocite
Ferrihydrite
Magnetite
Pyrite
Siderite
Hornblende
Biotite
Fe(III)-phosphate

Table S7: Fe XANES linear combination fits (LCFs) for native Union County and Redlair saprolites.

Sample ID	Component	% Contribution	R-value
Native UC saprolite	HFO_Si	20 ± 3.7	0.0004
	Chlorite	12 ± 0.9	
	Goethite	21 ± 1.5	
	Hornblende	25 ± 1.6	
	Magnetite	22 ± 3.7	
Native RL saprolite	Ferrihydrite	61.5 ± 6.0	0.0003
	Hematite	27 ± 2.5	
	*Siderite	4.1 ± 0.8	
	*Biotite	3.8 ± 0.8	
	*Chlorite	3.6 ± 0.6	

*Standards that contributed less than 10% were only included because they significantly improved the fits.

Figure S1: X-ray diffraction pattern of Union County saprolite

Figure S2: X-ray diffraction pattern of Redlair observatory saprolite.
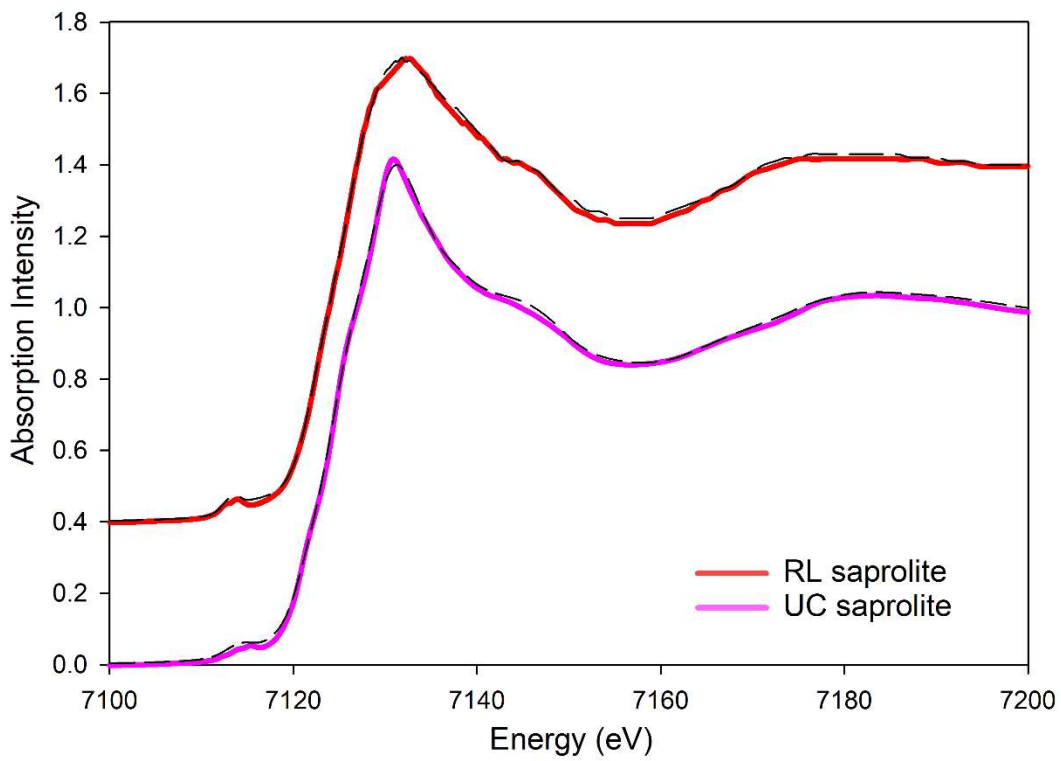
Figure S3: Iron K-edge XANES spectra of Union County and Redlair observatory saprolite spectra. Dashed lines are the LCF fits.
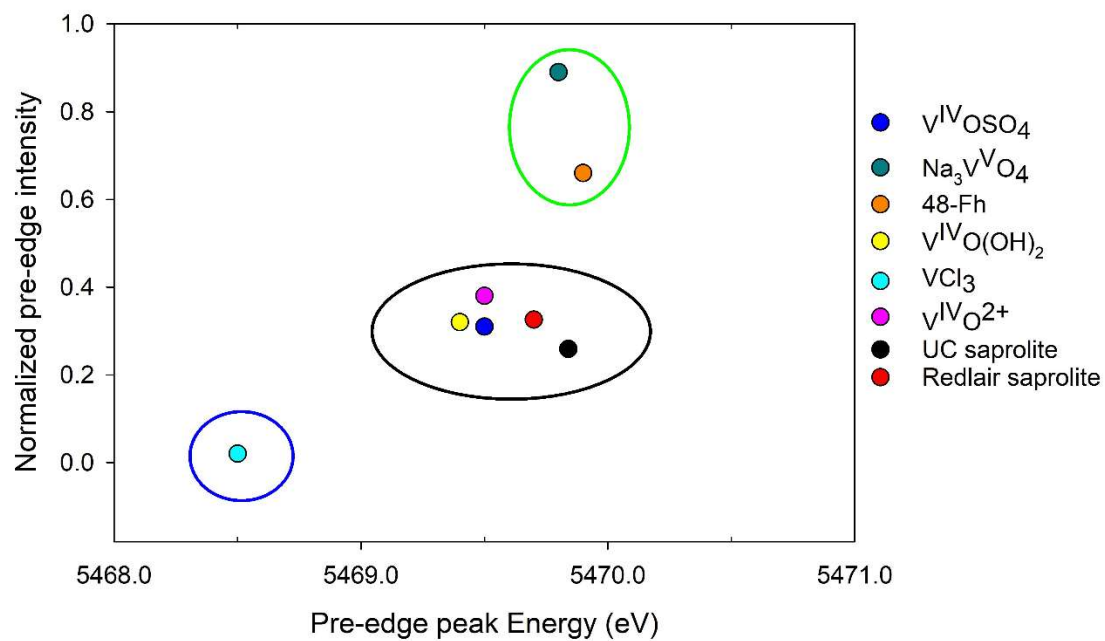
Figure S4: Normalized pre-edge peak intensity plotted against pre-edge energy position for standards and native UC and Redlair saprolites. Data was plotted using the calibration curve of Vessey and Lindsay, 2020.[6] Circled groups V(V) (green) V(IV) (black), and V(III) (blue) oxidation states.
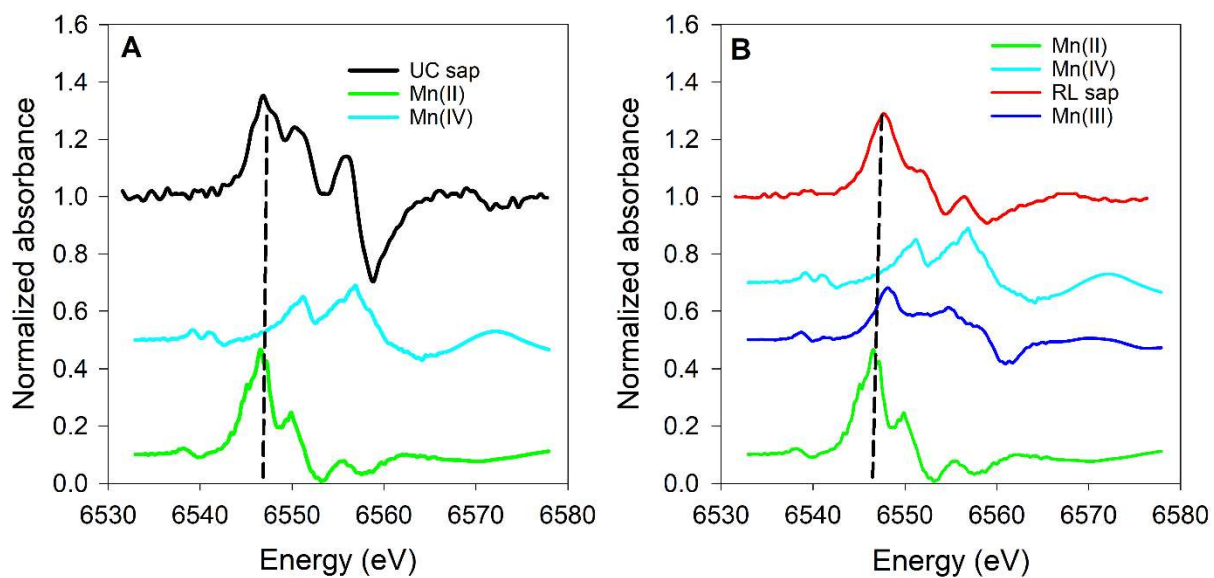
Figure S5: XANES Mn K-edge first derivatives of A) Union County saprolite B) Redlair saprolite. Mn(II), (III), and (IV) spectra of standard materials were Hureaulite. Feitknechtite, and Ramsdellite[5] respectively.
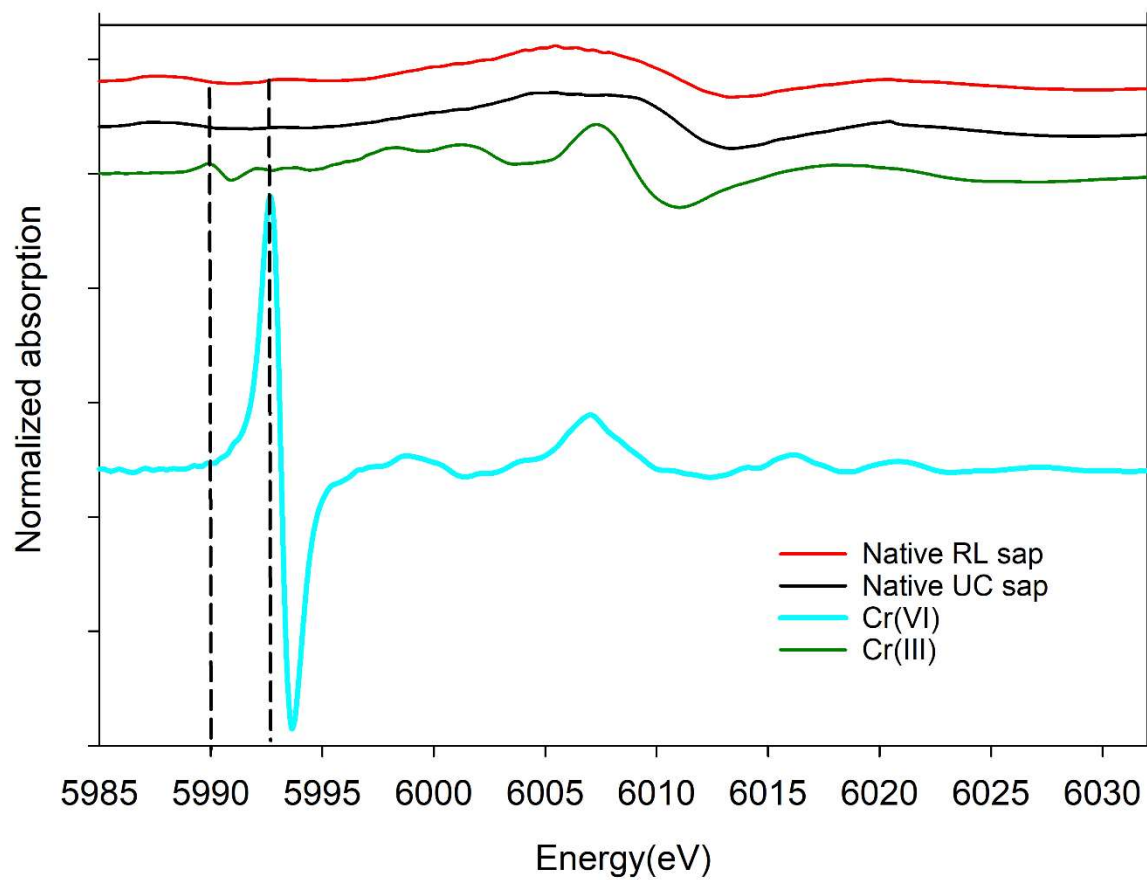
Figure S6: XANES Cr K-edge first derivatives of Union County saprolite and Redlair saprolite. Cr(III), and Cr(IV) spectra of standard materials were chromite and $K_2Cr_2O_7$ respectively.
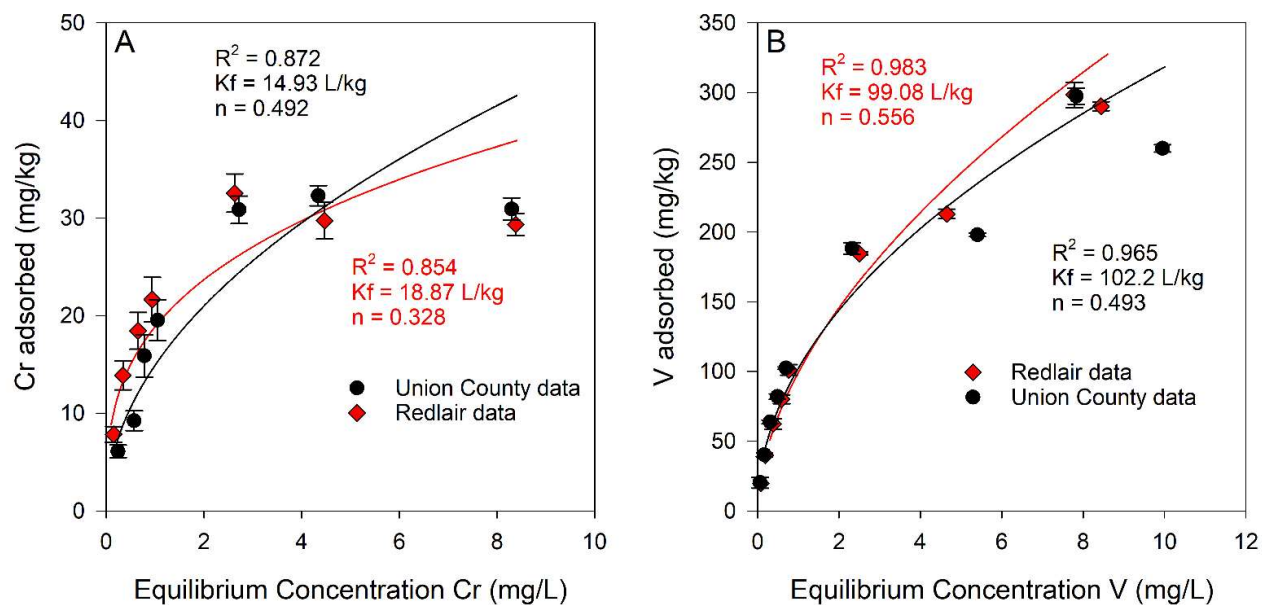
Figure S7: Freundlich isotherm models showing sorption of Cr and B) V(V) onto Union County (black line) and Redlair observatory (red line) saprolites. Reaction condition for Cr: Ionic strength (I) = 0.02 M NaCl, pH = 6.5, C_0Cr = 5 - 100 μM, C_0V = 20 - 450 μM, solid solution ration was 2g/40mL. Error bars indicate Standard error of replicates.

\
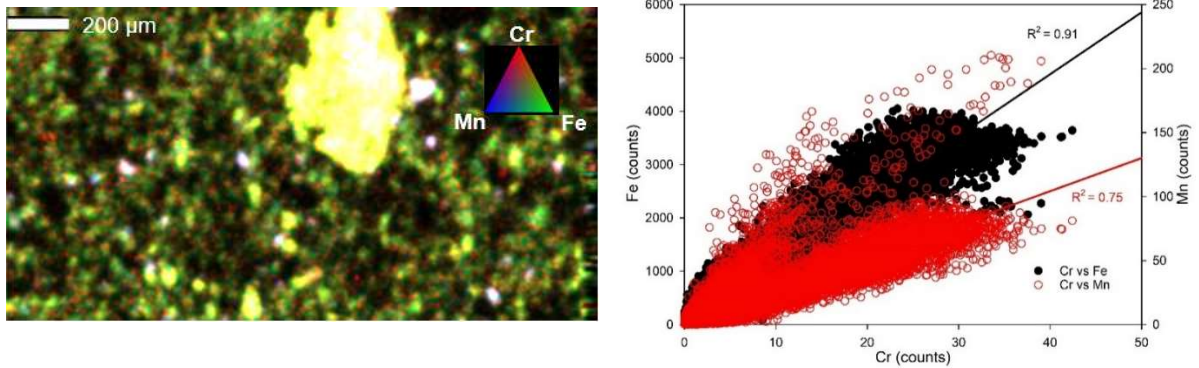
Fig S8: Solid-phase Cr, Fe and Mn spatial associations. (A) Tricolor μ-XRF maps of Cr-loaded (60 µM) Redlair saprolite (RL-1). Red, green, and blue colors represent Cr, Fe and Mn counts, respectively. (B) Correlation plot of Cr, Fe and Mn.
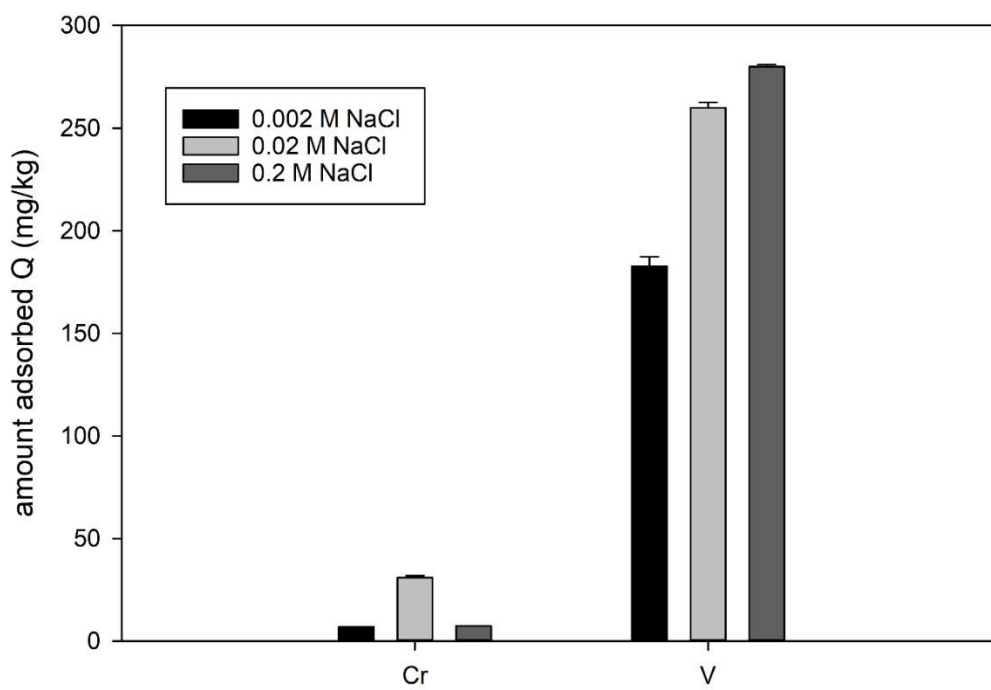
Figure S9: Effect of ionic strength on Cr and V sorption on Union County saprolite. pH = 6.6, [V] = 10 mg/L, time = 48 hours.

APPENDIX C

SUPPLEMENTAL MATERIAL FOR CHAPTER IV

Table S1: Strong acid digestion and sequential extraction data. These samples are the native Union County saprolite. The labels on the side stand for the specific digestion or extraction used. MG= Magnesium Chloride extraction. OX= Ammonium oxalate/oxalic acid extraction, CBD= Citrate bicarbonate dithionite, and SAD= Strong Acid Digestion.

Extraction	Cr (mg/kg)	Cr SE	V (mg/kg)	V SE	Fe (mg/kg)	Fe SE	Mn (mg/kg)	Mn SE
SAD	24.67	0.54	31.05	0.74	23769.52	7.11	426.28	3.07
CBD	3.68	0.30	16.44	1.13	10686.49	17.58	132.99	12.27
OX	0.91	0.00	3.23	0.15	1137.59	33.87	105.14	9.52
MG	n/a	n/a	0.24	0.02	77.28	1.31	63.64	1.31

Table S2: Strong acid digestion and sequential extraction data. These samples are the native Redlair observatory saprolite. The labels on the side stand for the specific digestion or extraction used. MG= Magnesium Chloride extraction. OX= Ammonium oxalate/oxalic acid extraction, CBD= Citrate bicarbonate dithionite, and SAD= Strong Acid Digestion.

Extraction	Cr (mg/kg)	Cr SE	V (mg/kg)	V SE	Fe (mg/kg)	Fe SE	Mn (mg/kg)	Mn SE
SAD	15.56	0.67	190.49	3.27	47211	1885	280	7
CBD	6.36	0.28	80.29	1.95	15113	329	32	1
OX	0.87	0.00	15.71	0.44	531	18	25	0.6
MG	n/a	n/a	1.34	0.02	78	1	22	0

Table S3: Standard spectra used in the Fe K-edge EXAFS LCF for unreacted/native Union County and Redliar observatory saprolite, day 14, 28, and 40 biotic and abiotic citric acid incubations for reacted Union County and Redliar observatory saprolite[1–3]. Standard in bold italics were used for final fits.

Sample ID
Hydrous ferric oxide w/Si
Chlorite
Goethite
Hematite
Nontronite
Lepidocrocite
Ferrihydrite
Magnetite
Pyrite
Siderite
Hornblende
Biotite
Fe(III)-phosphate

Table S4: Standard spectra used in Fe XANES linear combination fits (LCFs) for native Union County and Redlair.

Sample ID	Component	% Contribution	R-value
Native UC saprolite	HFO_Si	20 ± 3.7	0.0004
	Chlorite	12 ± 0.9	
	Goethite	21 ± 1.5	
	Hornblende	25 ± 1.6	
	Magnetite	22 ± 3.7	
Native RL saprolite	Ferrihydrite	61.5 ± 6.0	0.0003
	Hematite	27 ± 2.5	
	*Siderite	4.1 ± 0.8	
	*Biotite	3.8 ± 0.8	
	*Chlorite	3.6 ± 0.6	

Table S5: Fe EXAFS linear combination fits (LCFs) for native Union County saprolite and biotic and abiotic post reaction products (day 14 and 40).

Sample ID	Component	% Contribution	R-value
Native UC Saprolite	HFO_Si	32 ± 2.7	0.02
	Chlorite	20 ± 1.7	
	Goethite	24 ± 1.2	
	Hornblende	24 ± 2.7	
BHC D14	HFO_Si	29 ± 5.7	0.02
	Chlorite	42 ± 2.0	
	Goethite	18 ± 1.4	
	Hornblende	11 ± 3.4	
BHC D40	HFO_Si	24 ± 2.5	0.04
	Chlorite	10 ± 2.6	
	Goethite	28 ± 1.8	
	Hornblende	38 ± 4.1	
AHC D14	HFO_Si	30 ± 1.3	0.02
	Chlorite	47 ± 0.5	
	Goethite	23 ± 1.8	
AHC D40	HFO_Si	27 ± 2.2	0.04
	Chlorite	47 ± 0.9	
	Goethite	26 ± 3.1	

Table S6: Fe EXAFS linear combination fits (LCFs) for native Redlair observatory saprolite and biotic and abiotic post reaction products (day 14 and 28).

Sample ID	Component	% Contribution	R-value
Native RL Saprolite	HFO_Si	59 ± 2.4	0.03
	Goethite	25 ± 1.1	
	Hornblende	16 ± 1.0	
BHC D14	Ferrihydrite	33 ± 1.5	0.03
	HFO_Si	18 ± 1.5	
	Goethite	12 ± 1.5	
	Hornblende	13 ± 1.5	
	Nontronite	16 ± 1.5	
	*Hematite	8 ± 3.6	
BHC D28	Ferrihydrite	23 ± 1.6	0.03
	HFO_Si	39 ± 1.6	
	Goethite	18 ± 1.6	
	Hornblende	11 ± 1.6	
	*Nontronite	6 ± 1.6	
	*Hematite	3 ± 3.9	
AHC D14	Ferrihydrite	42 ± 2.3	0.06
	HFO_Si	20 ± 2.3	
	*Goethite	6 ± 2.3	
	*Hornblende	5 ± 2.3	
	Nontronite	14 ± 2.3	
	Hematite	13 ± 5.6	
AHC D28	Ferrihydrite	13 ± 1.5	0.03
	HFO_Si	37 ± 1.5	
	Goethite	12 ± 1.5	
	Hornblende	13 ± 1.5	
	Nontronite	16 ± 1.5	
	*Hematite	9 ± 3.7	

*Standards that contributed less than 10% were only included in biotic and abiotic RL saprolite incubations because they significantly improved the fits.
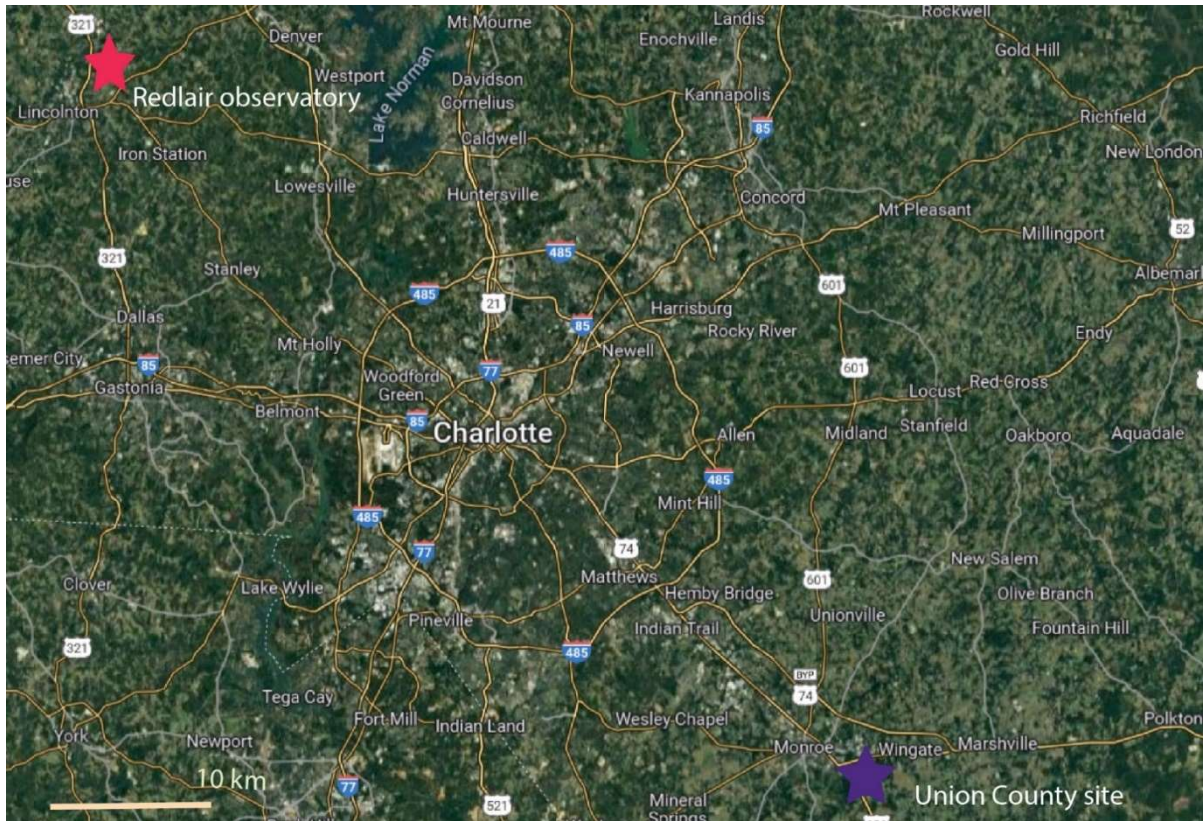
Figure S1: Map of suburban North Carolina showing sample collection sites in Union County (Red) and Redlair Observatory in Gaston County (Red).
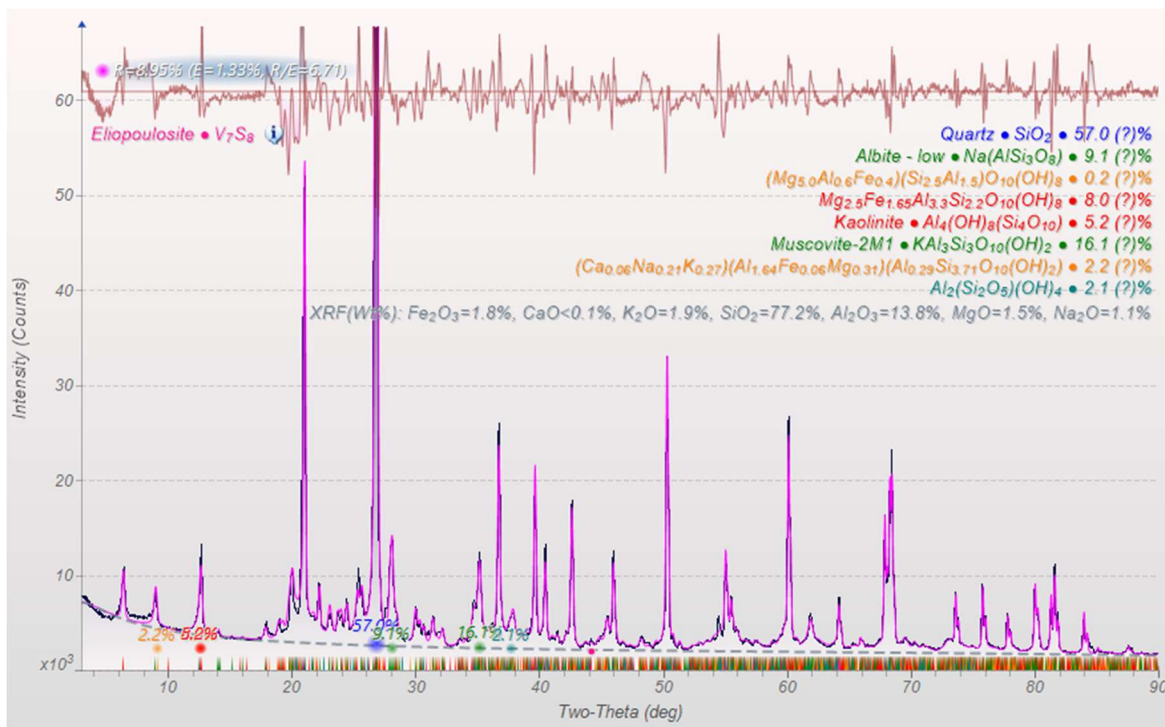
Figure S2: X-ray diffraction pattern of Union County saprolite
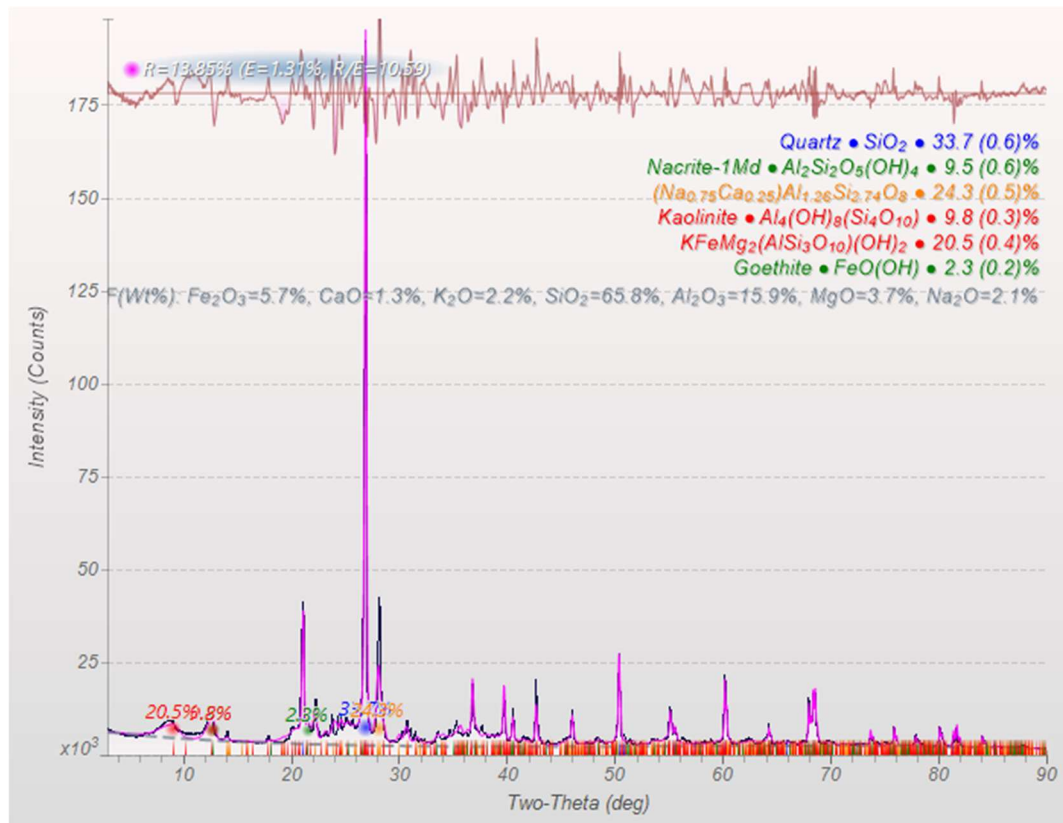
Figure S3: X-ray diffraction pattern of Redlair observatory saprolite.
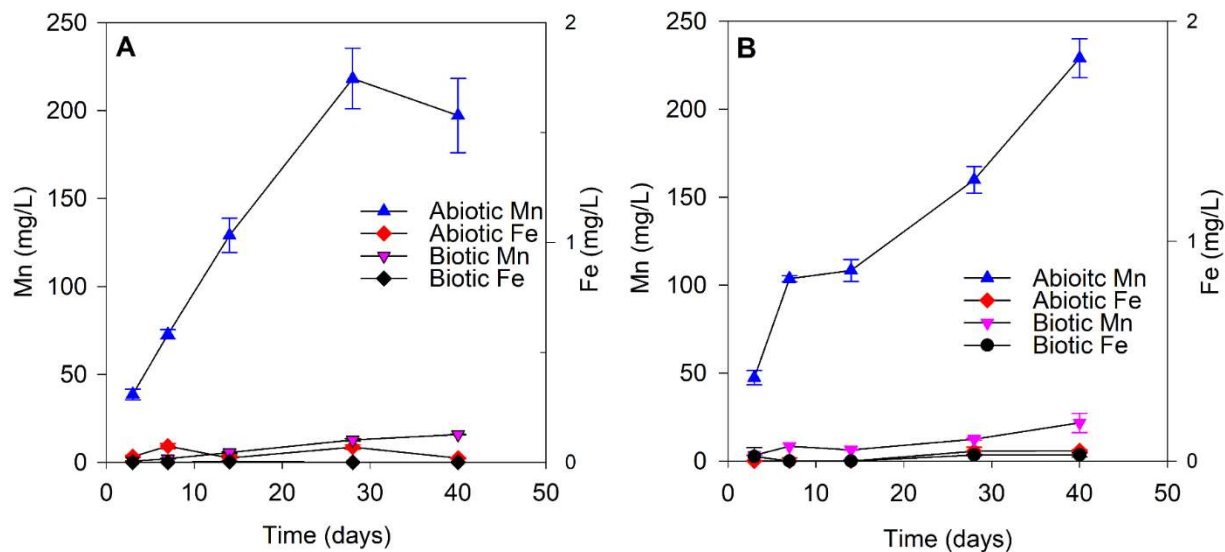
Figure S4: Dissolved concentrations of biotic and abiotic Mn and Fe from soil-free (Mn-oxide + chemical additives) control experiments in A) Union County, B) Redlair. Additives include Ionic strength (I) = 10 mM KCl, HEPES = 25 mM. For (abiotic controls) bronopol = 10 mM, pH = 6.6 ± 0.1 Error bars represent standard error of replicates.
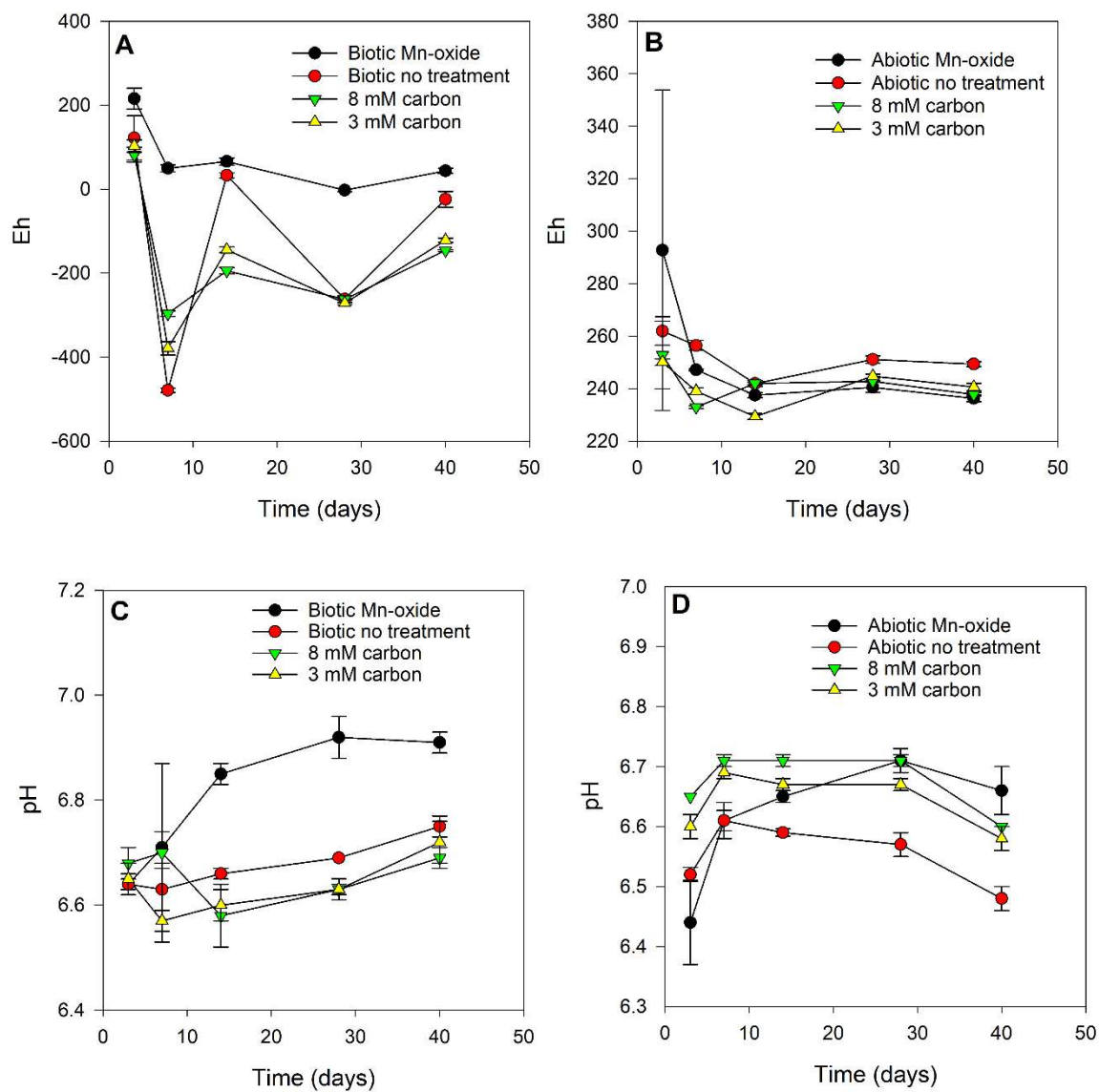
Figure S5: (A) Eh data of all biotic, **(B)** Abiotic samples, **(C)** pH data of all biotic and, **(D)** Abiotic samples in the batch incubation of Union County saprolite. Initial experimental conditions: Ionic strength (I) = 10 mM KCl, HEPES = 25 mM, pH = 6.6 ± 0.1. Error bars represent standard error of experimental triplicates.

.
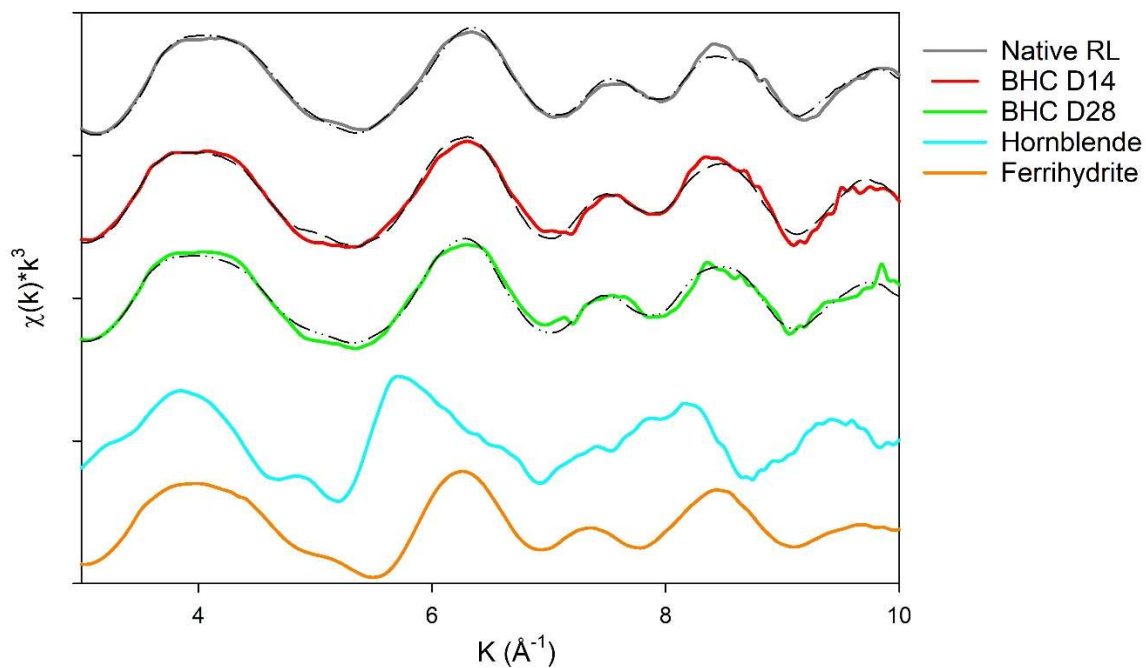
Figure S6: Fe K-edge EXAFS spectra for Redlair observatory saprolite and post reaction products at day 14 and 40 for biotic incubations. Dashed lines represent LCF fits. Fit parameters are shown in Table S5. Initial experimental conditions: Ionic strength (I) = 10 mM KCl, HEPES = 25 mM, pH = 6.6 ± 0.1.
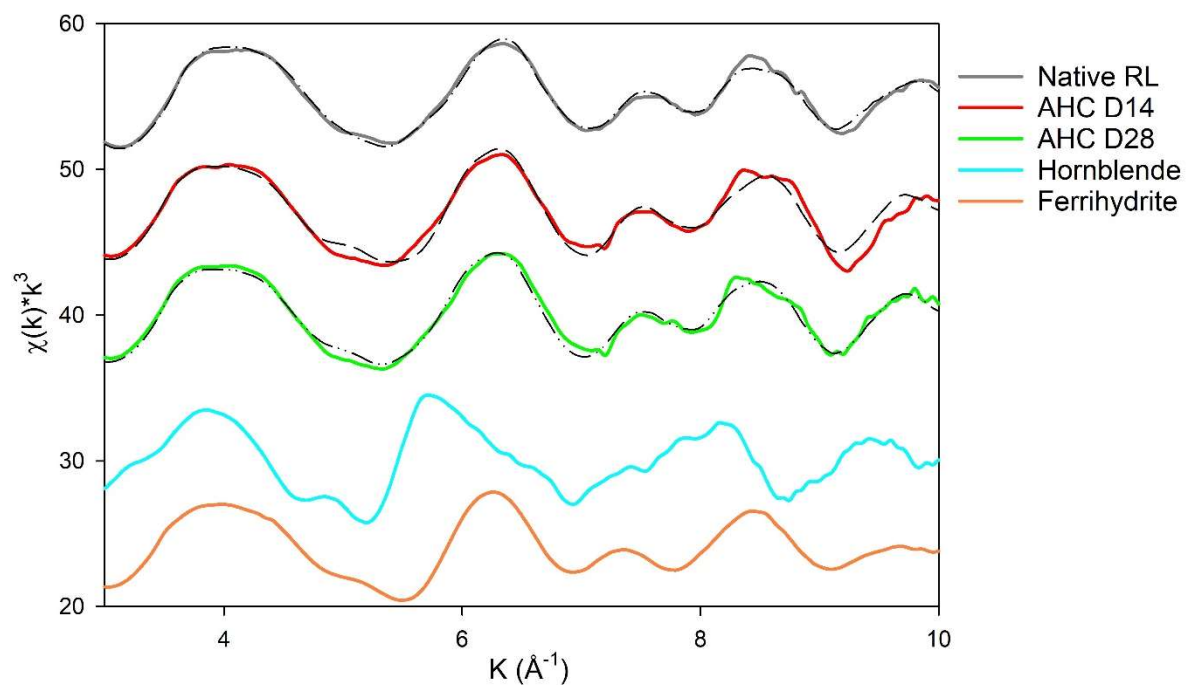
Figure S7: Fe K-edge EXAFS spectra for native Redlair observatory saprolite and post reaction products at day 14 and 28 for abiotic incubations. Dashed lines represent LCF fits. Fit parameters are shown in Table S5. Initial experimental conditions: Ionic strength (I) = 10 mM KCl, HEPES = 25 mM, pH = 6.6 ± 0.1.
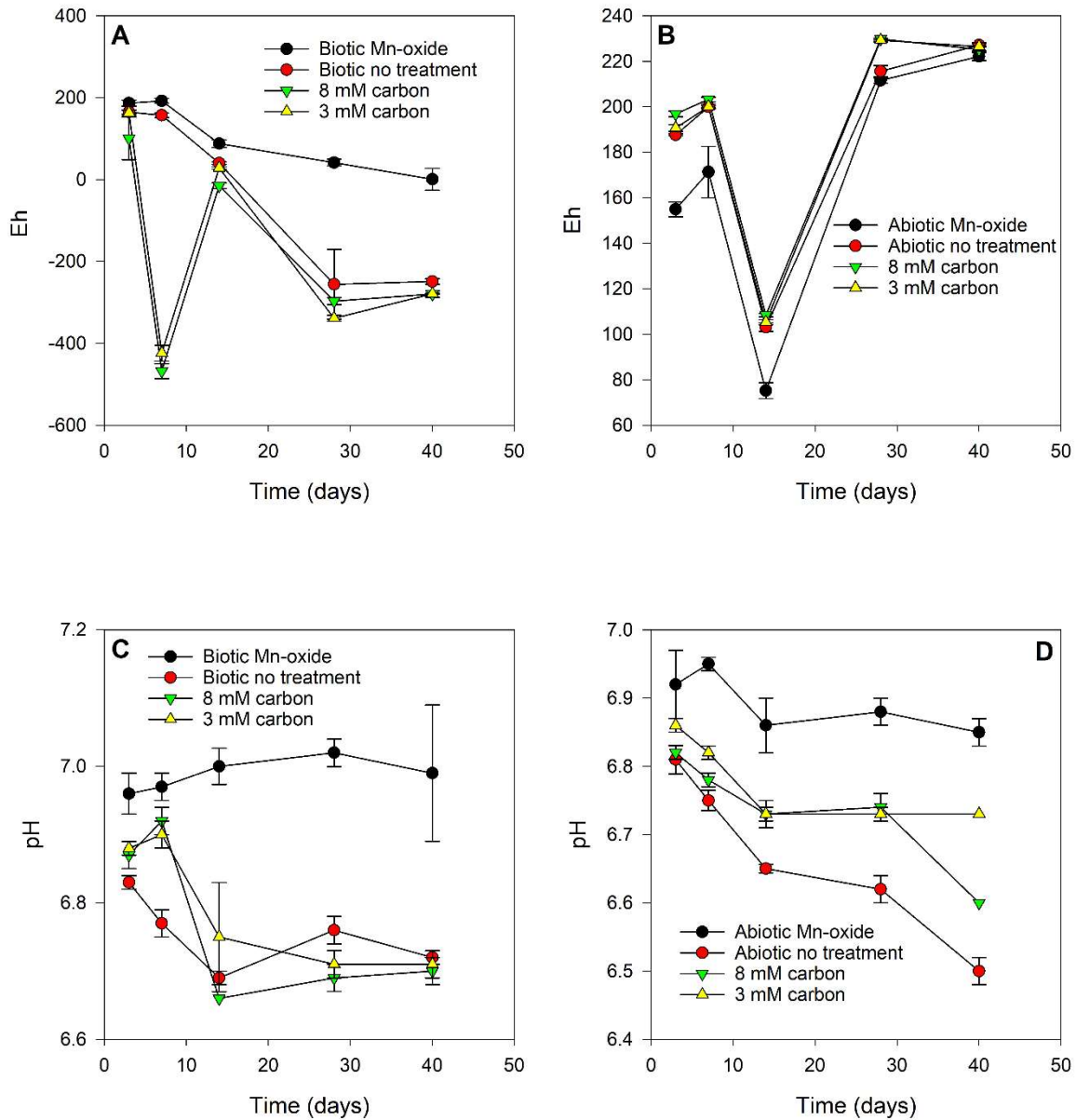
Figure S8: (A) Eh data of all biotic, **(B)** Abiotic samples, **(C)** pH data of all biotic and, **(D)** Abiotic samples in the batch incubation of Redlair Observatory saprolite. Initial experimental conditions: Ionic strength (I) = 10 mM KCl, HEPES = 25 mM, pH = 6.6 ± 0.1. Error bars represent standard error of experimental triplicates.

REFERENCES FOR SUPPLEMENTAL MATERIAL

1. Whitaker, A. H., Peña, J., Amor, M. & Duckworth, O. W. Cr(VI) uptake and reduction by biogenic iron (oxyhydr)oxides. *Environ. Sci. Process. Impacts* **20**, 1056–1068 (2018).

2. Duckworth, O. W., Akafia, M. M., Andrews, M. Y. & Bargar, J. R. *Siderophore-Promoted Dissolution of Chromium from Hydroxide Minerals*. (2014).

3. Polizzotto, M. L. *et al.* Solid-phases and desorption processes of arsenic within Bangladesh sediments. *Chem. Geol.* **228**, 97–111 (2006).

4. Wisawapipat, W. & Kretzschmar, R. Solid Phase Speciation and Solubility of Vanadium in Highly Weathered Soils. *Environ. Sci. Technol.* **51**, 8254–8262 (2017).

5. Manceau, A., Marcus, M. A. & Grangeon, S. Determination of Mn valence states in mixed-valent manganates by XANES spectroscopy. *Am. Mineral.* **97**, 816–827 (2012).

6. Vessey, C. J. & Lindsay, M. B. J. Aqueous Vanadate Removal by Iron(II)-Bearing Phases under Anoxic Conditions. *Environ. Sci. Technol.* **54**, 4006–4015 (2020).